Aus dem

Institut für Kardiovaskuläre Physiologie und Pathophysiologie im Walter-Brendel-Zentrum für Experimentelle Medizin

Institut der Ludwig-Maximilians-Universität München

The role of vacuolar protein sorting-associated protein 18 homolog (VPS18) in neutrophil biology

Dissertation
zum Erwerb des Doctor of Philosophy (Ph.D.)
an der Medizinischen Fakultät
der Ludwig-Maximilians-Universität München

vorgelegt von
Jincheng Gao

aus
Weihai (China)

Jahr
2025

Mit Genehmigung der Medizinischen Fakultät der
Ludwig-Maximilians-Universität München

Erstes Gutachten:	Prof. Dr. Barbara Walzog
Zweites Gutachten:	Prof. Dr. Christian Schulz
Drittes Gutachten:	Prof. Dr. Franziska Hartig-Vielmuth
Viertes Gutachten:	Prof. Dr. Jürgen Bernhagen

Dekan: Prof. Dr. med. Thomas Gudermann

Tag der mündlichen Prüfung: 26.02.2025

Table of content

Abstract

Neutrophils are the first responders to inflammation and an adequate number of neutrophils in the circulation is essential to maintain immune homeostasis. Congenital neutropenia is a group of rare genetic disorders of hematopoiesis characterized by diminished neutrophil counts in the circulation from birth. It is a life-threatening condition that can lead to recurrent infections. The mechanisms underlying congenital neutropenia are diverse, complex and remain incompletely understood. However, impaired intracellular vesicle trafficking has been linked to this disorder. Vacuolar protein sorting-associated protein 18 homolog (VPS18) is a core subunit of the HOPS and COVERT complexes and regulates intracellular vesicle trafficking through the endolysosomal and autophagosomal pathways. A patient with a heterozygous mutation in the *VPS18* gene showed congenital neutropenia and recurrent infections. The underlying mechanisms of the symptoms of this patient and the role of VPS18 in neutrophil biology remained exclusive. Thus, the aim of this study was to elucidate the role of VPS18 in neutrophil biology *in vitro* and *in vivo* using the hematopoietic Hoxb8 cell system and a transgenic zebrafish model.

Analysis of Hoxb8 cells as a model system for neutrophils revealed impaired maturation during differentiation in *Vps18* mutants as studied by May-Grünwald-Giemsa staining. This finding was further confirmed by quantifying different myeloid maturation stages in these cells based on stage-specific markers on the cell surface. Upon differentiation, *Vps18* mutants exhibited an increase in early and late apoptotic cells compared to CTRL Hoxb8 cells. Subsequently, an essential rescue experiment elucidated that the premature apoptosis in *Vps18* mutants was specifically caused by VPS18 deficiency. In the zebrafish model, a reduced number of neutrophils was observed in $vps18^{+/-}$ zebrafish larvae which resembles the patient's situation, compared to $vps18^{+/+}$ zebrafish larvae. The migration behavior of the residual neutrophils was analyzed *in vivo* using a spinning disk confocal microscope. Here, no differences in neutrophil migration were detectable under steady state conditions or during acute inflammation between $vps18^{+/+}$ and $vps18^{+/-}$ zebrafish larvae.

In summary, the neutrophil maturation defects *in vitro* and *in vivo* upon reduction of VPS18 expression provide evidence that VPS18 plays a fundamental role in neutrophil development.

List of figures

List of tables

List of abbreviations

3D	3-dimensional
AF	Auto-fluorescence
AGM	Aorta-gonad-mesonephros
ALPM	Anterior lateral plate mesoderm
ANOVA	Analysis of variance
ANCs	Absolute neutrophil counts
APC	Allophycocyanin
BM	Bone marrow
BSA	Bovine serum albumin
bp	Base pair
CC	Coiled-coil
CD	Cluster of differentiation
CHCR	Clathrin heavy chain repeat
CHO	Chinese hamster ovary
CHS	Chediak-Higashi syndrome
CHT	Caudal hematopoietic tissue
CN	Congenital neutropenia
CORVET	Class C core vacuole endosome tethering
CRISPR/Cas9	Clustered regularly interspaced short palindromic repeats /CRISPR-associated protein 9
CTRL	Control
CXCR 2	C-X-C motif chemokine receptor 2
CXCR 4	C-X-C motif chemokine receptor 4
dpf	Days post fertilization
DFP	Diisopropyl fluorophosphate
dHoxb8 cells	Hoxb8-SCF cell-derived neutrophils
DMSO	Dimethyl sulfoxide
Dor	*Deep orange*
dsRed	*red fluorescent protein from Discosoma*
EDTA	Ethylenediaminetetraacetic acid
EGFP	Enhanced green fluorescent protein
ELANE	Elastase, neutrophil expressed
ER	Estrogen responsive element
ER	Endoplasmic reticulum
FBS	Fetal bovine serum
FC	Flow cytometry
FITC	Fluorescein isothiocyanate
fli1	*friend leukemia integration 1*
FMO	Fluorescence minus one
FSC	Forward scatter
G6PT	Glucose-6-phosphatase catalytic subunit 1
G6PC3	Glucose-6-phosphatase catalytic subunit 3
GAPDH	Glyceraldehyde-3-phosphate dehydrogenase
G-CSF	Granulocyte colony-stimulating factor
GFP	Green fluorescence protein
GMPs	Granulocyte-monocyte progenitors

gRNA	guide ribonucleic acid
HAX1	Hematopoietic cell-specific Lyn substrate 1 associated protein X-1
HBSS	Hank's saline solution
HL-60	Human leukemia-60
Hoxb8	Homeobox protein Hox-B8
HOPS	Homotypic fusion and vacuole protein sorting
hpf	Hours post fertilization
HSCs	Hematopoietic stem cells
HSPC	Hematopoetic stem and progenitor cell
ICM	Intermediate cell mass
IgG	Immunoglobulin G
JAGN1	Jagnunal homolog 1
KD	Knock-down
KO	Knock-out
LFA-1	Lymphocyte function-associated antigen-1
LMPPs	Lymphoid-primed multipotent progenitors
lyz	*lysozyme C*
Ly6G	Lymphocyte antigen 6G
Mac-1	Macrophage-1 antigen
MFI	Mean fluorescence intensity
MGI	Mouse Genome Informatics
min	Minutes
MPPs	Multipotent progenitors
MPS	Mucopolysaccharidosis
mpx	*myeloperoxidase*
NA	Numerical aperture
NE	Neutrophil elastase
NETs	Neutrophil extracellular traps
Neu	Neutrophil
NIH	National Institutes of Health
P12	Postnatal day 12
PAGE	Polyacrylamide gel electrophoresis
PCR	Polymerase chain reaction
PE	Phycoerythrin
PBS	Phosphate buffered saline
PBST	Phosphate buffered saline with Tween®20
PBSTx	Phosphate buffered saline with Triton X-100
PerCP/Cy	Peridinin chlorophyll protein/Cyanine
PFA	Paraformaldehyde
PLB	Promyelocytic leukemia
P/S	Penicillin/streptomycin
PTU	*N*-Phenylthiourea
RFLP	Restriction fragment length polymorphism
preNeu	Premature neutrophil
proNeu	Neutrophil progenitor
rm	Recombinant murine
Rab	Ras-related protein
ROS	Reactive oxygen species

RPMI	Roswell Park Memorial Institute
RT	Room temperature
SBDS	Shwachman-Bodian-Diamond syndrome
SCF	Stem cell factor
SCN	Severe congenital neutropenia
SD	Standard deviation
SDS	Sodium dodecyl sulfate
SNAREs	Soluble N-ethylmaleimide-sensitive factor attachment protein receptors
srp	*signal recognition particle*
SSC	Side scatter
TAE	Tris base, acetic acid and EDTA
TBS	Tris buffered saline
TBST	Tris buffered saline with Tween® 20
TL	Tüpfel long fin
TMRM	Tetramethylrhodamine methyl ester
TNF-α	Tumor necrosis factors-α
TGN	*Trans*-Golgi network
UPR	Unfolded protein response
VPS	Vacuolar protein sorting-associated protein
WKM	Whole kidney marrow
wpf	Weeks post fertilization
WT	Wild type

1. Introduction

The immune system has a pivotal role in protecting the body from external threats. As professional phagocytes of the innate immune system, neutrophils are the first immune cells to arrive at the site of inflammation (1). At steady state, after their release into the circulation, most neutrophils remain inactive, age, and ultimately undergo non-inflammatory apoptosis with subsequent elimination by macrophages (2). Upon inflammation, neutrophils are recruited from the circulation to the inflamed tissue through a multi-step process, encompassing slow rolling, adhesion, adhesion strengthening, intraluminal crawling and transmigration and abluminal crawling (3). This process is mediated by leukocyte adhesion molecules of the β_2 integrin family (CD11/CD18), such as lymphocyte function-associated antigen-1 (LFA-1) and macrophage-1 antigen (Mac-1). Once neutrophils arrive at the site of inflammation, they eliminate microorganisms *via* multiple ways including phagocytosis, generation of reactive oxygen species (ROS), release of microbicidal substances from granules (degranulation) and formation of neutrophil extracellular traps (NETs) (4-6). In addition to their role in pathogen elimination, they also contribute to wound healing, tissue remodeling and immunomodulation (7). Furthermore, neutrophils have been reported to play a role in metabolic diseases, cancer, and autoimmune diseases (8-10).

In general, mature neutrophils are considered as short-lived cells which only circulate in the bloodstream for a limited time. However, it has been reported that they could survive for around 5.4 days in human circulation, 12.5 hours in mouse peripheral blood and 5 days in zebrafish tissue as resting neutrophils (11-13). Neutrophils become activated by extracellular cytokines, growth factors or bacterial products, resulting in a multifold increase in their longevity to ensure the presence of primed neutrophils at the site of inflammation (14-16). In tissues, neutrophils exhibit their defense functions, but they may also cause tissue damage.

1.1 Neutrophil development

In mammals, neutrophils are generated in the bone marrow (BM) during hematopoiesis. At steady state, a healthy adult human can produce up to 2×10^{11} neutrophils per day (17). Hematopoietic stem cells (HSCs) are the origin of neutrophils and initially differentiate into multipotent progenitors (MPPs), followed by lymphoid-primed multipotent progenitors (LMPPs) and granulocyte-monocyte progenitors (GMPs) (18, 19). Subsequently,

upon stimulation by granulocyte colony-stimulating factor (G-CSF), the GMPs terminally develop into myeloblasts, promyelocytes, and myelocytes which retain the capability of proliferation (**Figure 1A**). Continually, these cells differentiate into non-proliferative precursors, namely metamyelocytes and band cells, until differentiation into mature neutrophils is achieved.

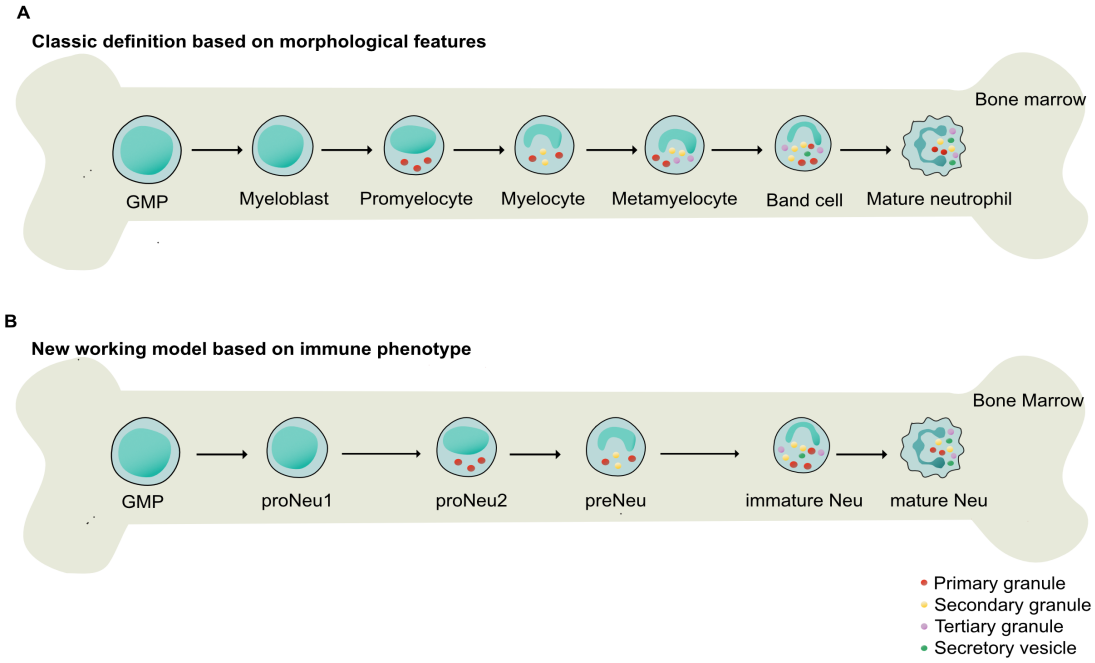

Figure 1. Schematic of neutrophil differentiation in the BM. (A) A classic definition of neutrophil maturation stages in the BM based on morphological changes. **(B)** A new working model of neutrophil maturation stages in the BM based on the immune phenotype. GMP: granulocyte-monocyte progenitor, proNeu: neutrophil progenitors, preNeu: premature neutrophils, immature Neu: immature neutrophils, mature Neu: mature neutrophils. Adapted from Lawrence et al., 2018, Evrard et al., 2018 and Kwok et al., 2020 (18, 20, 21).

The unique cell morphological features of each stage enable the distinguishment of neutrophil maturation stages during differentiation upon May-Grünwald-Giemsa staining (18, 22, 23). A promyelocyte (size: 20-25 µm) is identifiable by its large, round nucleus and peroxidase-positive primary/azurophilic granules which are reddish-purple/blue (24, 25). The cytoplasm of the promyelocyte appears light blue. In the myelocyte (size: 14-20 µm), the nucleus has an eccentric and oval shape, while secondary/specific granules (pink or lilac) are formed. Tertiary/gelatinase granules develop as the cell differentiates into a metamyelocyte (size: 10-18 µm) with an indented and kidney-shaped nucleus. The nucleus of a band cell (size: 10-16 µm) is curved but not yet segmented and secretory

vesicles are formed. A mature neutrophil (size: 10-15 μm) contains a segmented nucleus and all granules, which are critical for pathogen clearance (18, 26, 27).

The determination of neutrophil maturation stages by analyzing the distinct morphological changes is well established and used for decades. Recently, Ng's lab proposed a new working model based on the immune phenotypes (**Figure 1B**) (20, 21). In this new model, five neutrophil maturation stages were described: early committed neutrophil progenitors (proNeu1&2), a committed proliferative premature neutrophil (preNeu), a non-proliferative immature neutrophil (immature Neu), and a segmented mature neutrophil (mature Neu). Neutrophils from each maturation stage can be identified by the expression of specific cell surface markers (**Table 1**). Cell morphological analysis of these neutrophil maturation stages revealed that proNeu1 and proNeu2 might correspond to myeloblast and promyelocyte/early myelocyte, respectively. preNeu, immature Neu and mature Neu might represent metamyelocyte/early band cell, late band cell and mature neutrophil, respectively.

Table 1. Specific markers on neutrophils at different maturation stages (20, 21).

	proNeu1	proNeu2	preNeu	immature Neu	mature Neu
Mouse	Lineage$^-$, CD115$^-$, Flt3$^-$, CD81$^+$, Ly6C$^+$, CD34^{hi}, c-kit^{hi}, CD16/32^{hi}, CD11b^{lo}, CD106$^-$	Lineage$^-$, CD115$^-$, Flt3$^-$, CD81$^+$, Ly6C$^+$, CD34$^+$, c-kit^{hi}, CD16/32$^+$, CD11b^{lo}, CD106$^+$	Lineage$^-$, CD115$^-$, Siglec-F$^-$, c-kit^{int}, CD11b$^+$, CXCR4$^+$ Ly6G^{lo}	Linage$^-$, CD115$^-$, Siglec-F$^-$, c-kit$^-$, CD11b$^+$, CXCR4$^-$, Ly6G$^+$, CXCR2$^-$, CD101$^-$	Linage$^-$, CD115$^-$, Siglec-F$^-$, c-kit$^-$, CD11b$^+$, Ly6G$^+$, CXCR2$^+$, CD101$^+$
Human	Lineage$^-$, CD34$^+$, CD38$^+$, CD66b$^+$, CD71$^+$, CD11b$^-$, CD49d^{hi}, CXCR4$^+$, CD81^{hi}, CD24^{lo}, CXCR2$^-$	Lineage$^-$, CD34$^-$, CD38$^+$, CD66b$^+$, CD71$^+$, CD11b$^-$, CD49d^{int}, CXCR4$^+$, CD81^{lo}, CD24^{hi}, CXCR2$^-$	Lineage$^-$, CD15$^+$, CD33^{int}, CD34$^-$, Siglec8$^-$, CD66b$^+$, CD11b^{lo}, CD49d^{lo}, CD101$^-$, CXCR4$^+$, CXCR2$^-$	Lineage$^-$, CD15$^+$, CD33^{int}, CD66b$^+$, CD10$^-$, CD16^{int}, CD11b^{lo}, CD49d$^-$, CD101^{int}, CXCR4$^+$, CXCR2$^+$	Lineage$^-$, CD15$^+$, CD33^{int}, CD66b$^+$, CD11b^{hi}, CD49d$^-$, CD10$^+$, CD101^{int}, CD16^{hi}, CXCR4$^-$, CXCR2$^+$

The egress of neutrophils from the BM is governed by two C-X-C chemokine receptors (CXCRs), namely CXCR2 and CXCR4 (28, 29). In this context, CXCR2 transmits a mobilization signal to facilitate the release of neutrophils into the circulation, while CXCR4 contributes to retaining neutrophils within the BM. Fully matured neutrophils express more CXCR2 but less CXCR4, promoting their exit from the BM. Following daily turnover, upregulated CXCR4 on the surface of aged neutrophils enables the homing of these

cells back to the BM. Subsequently, they are eliminated by macrophages to maintain homeostasis (28).

1.1.1 Neutropenia

At a steady state, the normal range of neutrophils in a healthy adult is 1.8-8.0 $\times 10^9$/L in the peripheral blood (30). The impaired maturation of neutrophils or the reduced release of mature neutrophils into the circulation can lead to a reduction of neutrophil numbers in the peripheral blood (31). When the absolute neutrophil counts (ANCs) fall below 1.5×10^9/L in the peripheral blood for adults and children over one year of age, it is generally defined as neutropenia (31). Neutropenia can be caused by various conditions, including inherited hematopoietic disorders, autoimmune diseases, chemotherapy, and certain viral infections (32-34). Due to the reduced number of neutrophils, the patients are often at a higher risk of developing recurrent and life-threatening infections.

Congenital neutropenia (CN) is a group of rare genetic disorders of hematopoiesis characterized by diminished neutrophil counts in the circulation from birth (30). To date, mutations in several genes, including neutrophil elastase (*ELANE)*, Shwachman-Bodian-Diamond syndrome *(SBDS)*, glucose-6-phosphatase catalytic subunit 1 *(G6PT)* and hematopoietic cell-specific Lyn substrate 1 associated protein X-1 *(HAX1)* have been identified as cause of CN (**Figure 2**) (35). Here, one of the most prevalent genetic factors associated with CN is the gene *ELANE*, which encodes the neutrophil elastase (NE), a serine protease involved in multiple neutrophil functions, such as degranulation and NET formation, allowing bacterial killing (36, 37). Mutations in *ELANE* can lead to abnormal folding, cytoplasmic accumulation or impaired intracellular protein trafficking of the NE protein, activating cell stress (38-41). Persistent cell stress ultimately causes increased premature cell death in the BM of CN patients (42). Furthermore, BM morphological examinations of these patients unveil a maturation arrest in myeloid precursors during neutrophil development (43).

The severity of neutropenia in individual patients might fluctuate over time (35). Consequently, CN patients may suffer from either transient neutropenia or permanent neutropenia. In addition to neutropenia, CN patients often display severe immunodeficiency and diverse organ dysfunctions. As a treatment option and to rescue the circulating neutrophil numbers, clinicians treat CN patients with G-CSF as a stimulant for neutrophil development (44-46). Thus, the symptoms and survival chances of the majority of patients treated

with G-CSF can be improved. However, CN patients who do not respond to G-CSF treatment are at risk of developing malignant hematopoietic diseases, such as leukemia. Hematopoietic stem cell transplantation might be the last option for those patients who do not respond to G-CSF (47-52).

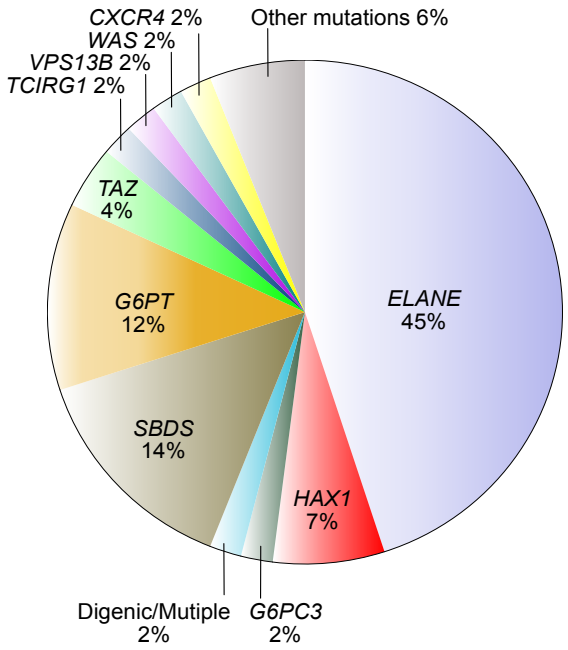

Figure 2. Mutations in known genes are responsible for CN. *ELANE*: elastase, neutrophil expressed. *HAX1*: hematopoietic cell-specific Lyn substrate 1 associated protein X-1. *G6PC3*: glucose-6-phosphatase catalytic subunit 3. *SBDS:* Shwachman-Bodian-Diamond syndrome. *G6PT*: glucose-6-phosphatase catalytic subunit 1. *TAZ*: tafazzin, phospholipid-lysophospholipid transacylase. *TCIRG1:* T cell immune regulator 1, ATPase H^+ transporting V0 subunit a3. *VPS13B:* vacuolar protein sorting 13 homolog B. *WAS*: Wiskott-Aldrich syndrome actin nucleation promoting factor. *CXCR4*: C-X-C motif chemokine receptor 4. Adapated from Skokowa et al., 2017 (35). Copyright 2017 by Springer Nature. Adapted with permission.

1.2 Intracellular vesicle trafficking

In eukaryotic cells, intracellular vesicle trafficking represents a fundamental process that is essential for a variety of cellular functions, such as the transport of nutrients, signaling, secretion of hormones, and degradation of dysfunctional proteins and organelles (53). It mainly includes three pathways: the endocytic pathway, the exocytic or biosynthetic pathway and the autophagy pathway (**Figure 3**) (54). The endocytic pathway delivers cargo from the extracellular environment into cells *via* the plasma membrane. (55). The vesicles containing the internalized cargo from the extracellular environment are transported to early endosomes through the plasma membrane. After being sorted by the early endosomes, the vesicles are either transported back to the plasma membrane *via* recycling

endosomes or to lysosomes for degradation *via* late endosomes. Additionally, the vesicles can be delivered to the Golgi apparatus *via* the retrograde pathway. The exocytic or biosynthetic pathway transports vesicles with newly synthesized proteins from the ER-Golgi to either intracellular compartments, such as endosomes or to the plasma membrane. Autophagy is a process that entails delivering cytoplasmic materials to the lysosome for degradation (56). It has the following steps: phagophore initiation and elongation, autophagosome formation and autophagosome-lysosome fusion (57).

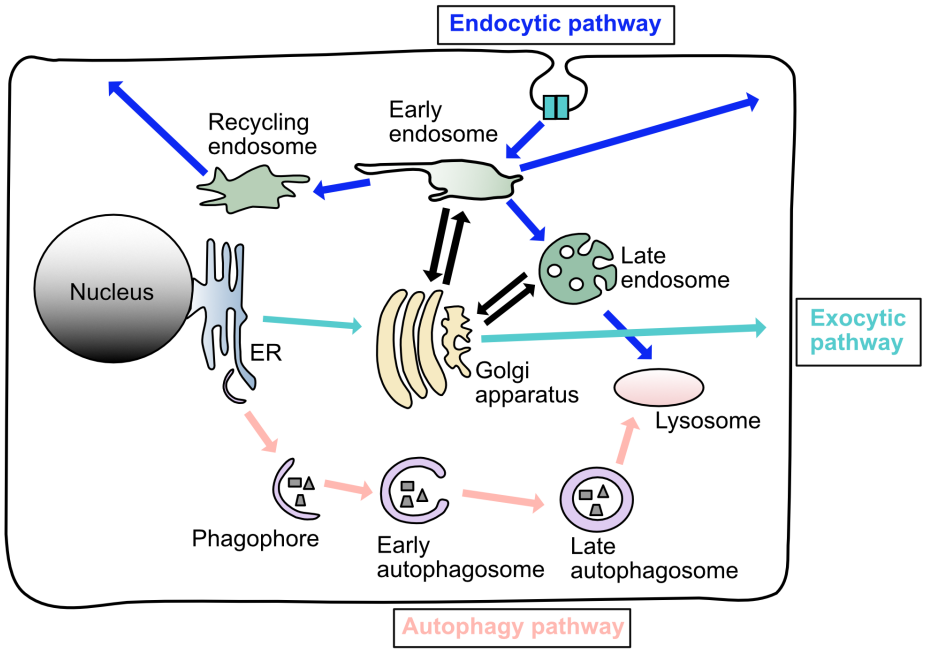

Figure 3. Intracellular vesicle trafficking pathways. Three major intracellular vesicle trafficking pathways: endocytic pathway (blue), exocytic pathway (cyan) and autophagy pathway (pink). Adapted from Kawauchi et al., 2012 (58).

Vesicles containing soluble cargo or transmembrane proteins are first formed and budded from the donor organelles (**Figure 4**) (53). During this phase, coat proteins are recruited by the Ras-related protein (Rab) GTPases to the donor organelle membrane, leading to the deformation of the flat membrane and resulting in the release of coated vesicles (scission) (53, 59). The uncoating process happens shortly after the vesicle release. Subsequently, the vesicles are transported close to the target organelles along cytoskeletal tracks. Prior to fusion, the initial interaction between the vesicles and their target membranes is mediated by the tethering factors, which are recruited by the Rab GTPases. Vesicle fusion with the target membrane is mediated by the paring of soluble N-ethylmaleimide-sensitive factor attachment protein receptors (SNAREs).

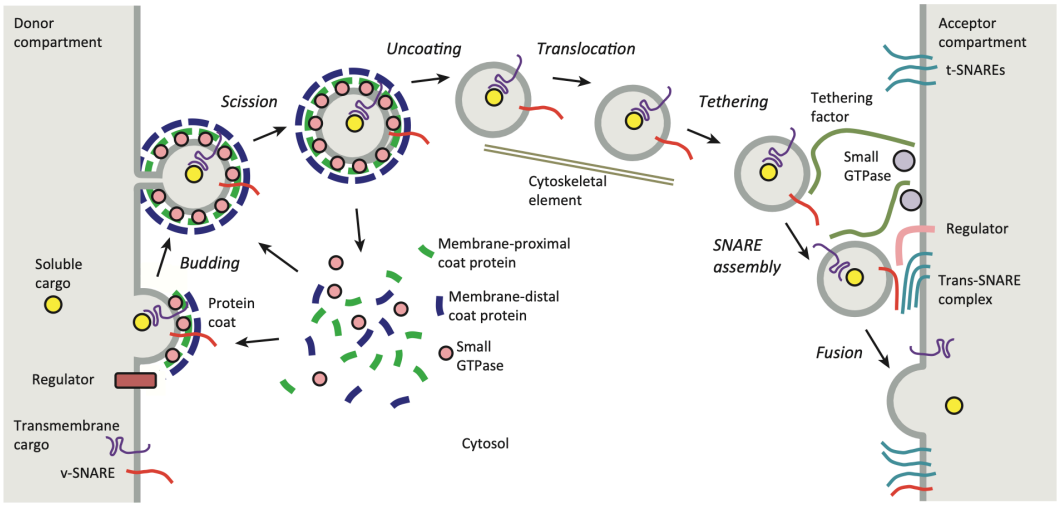

Figure 4. Vesicle transport system. The budding of vesicles carrying specific cargo from the donor organelles is initiated by the interaction between coat protein and membrane-associated GTPase. During the scission process, the connection between vesicles and donor organelles is severed by the coat proteins. Subsequently, after the uncoating process, the vesicles are transported close to the proper target organelles, where they are tethered to the target membranes by binding between tethering factors and Rab GTPases. Following the docking process, where the SNAREs assemble into a four-helix bundle, the vesicles are fused with the target membranes which is mediated by the SNARE complexes. Adapted from Bonifacino et al., 2004 (60). Copyright 2004 by Elsevier. Adapted with permission.

1.2.1 Tethering factors

Despite the name, tethering factors are not only required for vesicle capture. They are also involved in uncoating, recognition of a vesicle to the target membrane, assembly of SNARE complexes, as well as promoting SNARE-mediated membrane fusion (61). To date, two groups of tethering factors have been identified: long putative coiled-coil proteins and multi-subunit complexes (MTCs) (53, 62, 63). The structure of each tethering factor is diverse, challenging to define a common mechanism for their function. Nevertheless, all tethering factors are involved in nearly all vesicle fusion events by interacting with Rab GTPases (53). The coiled-coil proteins are predominantly involved in vesicle fusion at the Golgi apparatus and early endosomes (63). In the past, several coiled-coil proteins have been identified which predominantly regulate vesicle fusion at the Golgi apparatus and endosomes (64). For instance, early embryonic antigen 1 (EEA1), one of the well-studied coiled-coil proteins, is located in early endosomes. It interacts with the lipid phosphoinositol-3-phosphate (PI3P), Rab5 and SNAREs to mediate the fusion of early endosomes. MTCs are divided into three groups: exocytic complexes associated with tethering containing helical rods (CATCHR), endolysosomal class C VPS

complexes and transport protein particle (TRAPP) complexes (53, 62). Exocytic CATCHR includes the Golgi-associated retrograde protein (GARP), endosome-associated recycling protein (EARP), conserved oligomeric Golgi (COG), exocyst and DSL1 complexes. GARP is involved in retrograde trafficking from endosomes to the *tans*-Golgi network (TGN) (65). EARP regulates vesicle trafficking from endosomes to recycling endosomes (66). COG binds to SNAREs on the Golgi to regulate the vesicle trafficking from the endosome to the Golgi apparatus (67). Excyst facilitates vesicle tethering at post-Golgi and plasma membrane (68). DSL1 mediates vesicle transport from the Golgi to the ER by binding to ER-localized SNAREs (69). Endolysosomal class C VPS complexes comprise class C core vacuole/ endosome tethering (CORVET) and homotypic fusion and vacuole protein sorting (HOPS) complexes. CORVET is involved in the fusion of early endosomes, whereas HOPS promotes the fusion of late endosomes and autophagosomes with lysosomes (53, 62). TRAPP complexes are required for tethering of ER-derived vesicles to the Golgi apparatus, vesicle trafficking within TGN and from early endosome to the late Golgi. Notably, except for the TRAPP complexes, all of the tethering factors are Rab effectors (53).

1.2.2 CORVET and HOPS tethering complexes

Both CORVET and HOPS tethering complexes comprise six subunits (**Figure 5A**) (70). Among the six subunits, four subunits, namely vacuolar protein sorting-associated protein 11 homolog (VPS11), VPS16, VPS18 and VPS33A are shared. These four subunits are conserved across species. VPS3 and VPS8 are exclusive subunits of the CORVET complex. They bind to Rab5 in human cells and in yeast VPS21 (the homolog of Rab5) to mediate the tethering and docking of early endosomes (**Figure 5B**) (71, 72). The two unique subunits of the HOPS complex are VPS39 and VPS41. They facilitate the docking and fusion of late endosomes and autophagosomes with lysosomes by binding to Rab7 (73). Notably, defects in subunits of CORVET/HOPS complexes are associated with a range of disorders, such as neurodegeneration, pigmentation disorders, neutropenia, and cancer. Patients with homozygous mutations in *VPS11* suffer from central nervous system diseases, including cognitive impairment, hypotonia, seizure and cortical blindness or optic atrophy (74, 75). Patients with homozygous mutations in *VPS16* have been documented to exhibit so-called mucopolysaccharidosis (MPS)-like features including the growth retardation and multiple organ dysfunction. (76, 77). Notably, the patients also suffered from neutropenia. Likewise, the clinical symptoms of the patients harboring

homozygous mutations in *VPS33A* were anemia, neutropenia, infections, and MPS-plus disease (78).

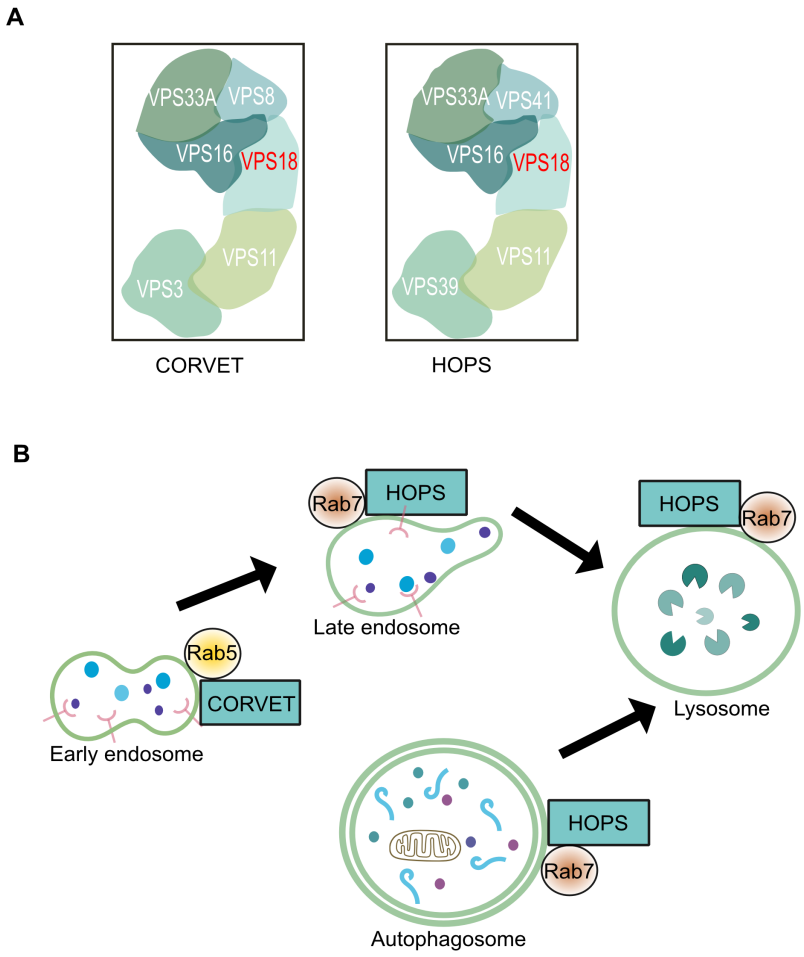

Figure 5. CORVET and HOPS tethering complexes facilitate the fusion of vesicles in the endolysosomal system. (A) The subunits of HOPS and CORVET complexes. **(B)** CORVET binds to Rab5 to mediate the fusion of early endosomes. HOPS binds to Rab7 enabling the fusion of late endosomes or autophagosomes with lysosomes. Adapted from Balderhaar et al., 2013 (79). Copyright 2013 by The Company of Biologists. Adapted with permission.

1.2.3 Vacuolar protein sorting-associated protein 18 homolog (VPS18)

VPS18 is a 973 amino acid long protein which is ubiquitously expressed and highly conserved across eukaryotic species (80-86). It possesses a seven-bladed β-propeller domain at the N-terminus, two coiled-coil (CC) domains, and one clathrin heavy chain repeat (CHCR) domain, as well as a RING finger domain at the C-terminus (**Figure 6**) (80). In yeast cells, the β-propeller domain is required for keeping HOPS structural stability and function (87). Moreover, VPS18 can interact with VPS11 *via* their β-propeller domains.

It has been suggested that the CHCR domain is required for homo-oligomerization (88). Interestingly, among the CORVET and HOPS subunits, only VPS8, VPS11, VPS18 and VPS41 have RING domains (89). The RING domain is required for protein-protein interactions (85, 90, 91). The interaction between VPS18 and VPS41 *via* their RING domains is required for the HOPS complex formation (85). In addition, due to the RING domain, VPS18 can act as an E3 ubiquitin ligase which can recognize specific proteins and attach ubiquitin molecules to them for degradation (84, 92, 93). To date, the exact function of CC domains in VPS18 remains unclear.

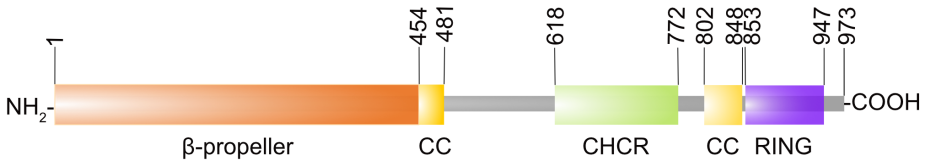

Figure 6. Schematic of the domain structure of human VPS18. VPS18 consists of a seven-bladed β-propeller domain (orange), two coiled-coil (CC) domains (yellow), a clathrin heavy chain repeat (CHCR) domain (green), and a RING finger domain (purple). Numbers indicate the amino acid positions in the protein. Adapted from Simon-Vecsei et al., 2021 (80). Copyright 2021 by Elsevier. Adapted with permission.

Functions of VPS18 are conserved across different species. In yeast, Vps18 deficiency resulted in defects in biosynthetic, endocytic and autophagic pathways (90, 94, 95). In *Drosophila melanogaster*, mutations in *Deep orange* (*Dor*), the *Vps18* homologue, induced a block in melanosome biogenesis, resulting in pigmentation defects (96-98). Additionally, accumulation of autophagosomes was observed in the *Dor* mutant larval fat body due to impaired fusion between autophagosome and lysosome. Zebrafish with mutations in *vps18* showed decreased pigmentation in eyes and skin, as well as degeneration of the retinal pigmented epithelium due to the reduction of melanosomes in the retinal pigment epithelium and accumulation of immature melanosomes (86, 99). Additionally, it has been observed that the hepatocytes of these zebrafish were filled with enlarged endosomal-like vesicles. Interestingly, the complete knock-out (KO) of *Vps18* in mice causes embryonic or early postnatal lethality (100). Neural-specific *Vps18* KO mice exhibited serious growth retardation and died before the postnatal day 12 (P12). Here, ablation of VPS18 in neural cells blocked early endosome maturation and late endosome and autophagosome degradation, resulting in severe neurodegeneration. Additionally, the depletion of *Vps18* in neural cells increased the expression of β1 integrins on the cell surface, leading to impaired neural cell migration.

Interestingly, Prof. Dr. Christoph Klein and his team identified a patient (ID: patient 1) bearing a heterozygous mutation in *VPS18* (personal communication by Prof. Dr. Christoph Klein). This mutation resulted in a premature stop codon at amino acid position 234 (Arg234*). At the time of diagnosis, the female patient 1 was 2.8 years old and suffered from severe recurrent infections, fever, recurrent aphthous ulcers and severe diaper rash. The ANCs were < 500/µL and thus, she was diagnosed with severe congenital neutropenia (SCN). Her bone marrow cytology also suggested a late maturation arrest in granulocytes.

1.3 Hoxb8-stem cell factor (SCF) cell line

Neutrophils are terminally differentiated and non-proliferative cells, presenting a challenge for *in vitro* expansion and genetic manipulation. To address this limitation, several *in vitro* models have emerged: myeloid leukemia cell lines, such as human leukemia (HL)-60 cells and its subclone promyelocytic leukemia (PLB)-985 cells, which can undergo differentiation into neutrophil-like cells through exposure to different stimuli (101, 102). In contrast to primary neutrophils which have to be freshly isolated from donors, these cells are easily accessible. Moreover, they are amenable to transduction, allowing for genetic and molecular studies. Therefore, these cells have been extensively utilized in neutrophil research (4). Nonetheless, these models still have shortcomings (103, 104). The process of differentiating these cells into neutrophil-like cells may vary across studies due to different stimuli being applied, leading to inconsistencies in the characteristics of the resulting cells. Differentiated HL-60 cells lack crucial characteristics of mature neutrophils, specifically the absence of secondary/tertiary granules leading to compromised bacterial eradication. To further overcome these limitations, Wang et al. established an immortalized estrogen-regulated (ER) of Hoxb8 cell line (Hoxb8 cells) (105). Hoxb8 is a transcription factor that can block myeloid progenitor cell differentiation (106). These myeloid progenitors were transduced with retroviral vectors encoding an ER-Hoxb8 fusion protein, which enables the indefinitely expanding progenitors *in vitro* in the presence of estrogen and stem cell factor (SCF) (**Figure 7**) (107). Hoxb8 cells can easily be generated from mouse BM and modified using genome editing techniques such as CRISPR/Cas9. Upon estrogen withdrawal and the addition of G-CSF, Hoxb8 cells differentiate into mature neutrophils within 4 days. These Hoxb8 cell-derived neutrophils

(dHoxb8 cells) closely resemble mature murine neutrophils compared to other myeloid leukemia cell lines (108).

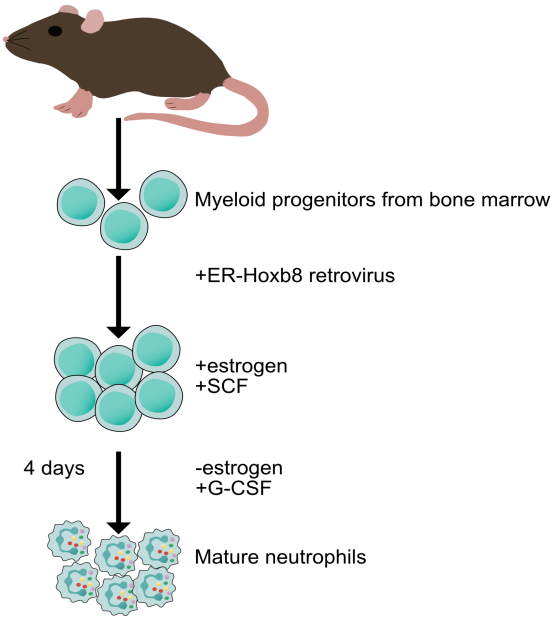

Figure 7. Generation and differentiation of immortalized Hoxb8-SCF cells into mature neutrophils. Myeloid progenitor cells were collected from the mouse BM and infected with a retrovirus encoding ER-Hoxb8 fusion protein. To culture those cells *in vivo*, SCF and estrogen were added to the medium. Upon estrogen withdrawal and addition of G-CSF, the Hoxb8 cells are able to differentiate into mature neutrophils. Adapted from Liebermann et al., 2006 (109). Copyright 2006 by Springer Nature. Adapted with permission.

To date, different research groups have validated that Hoxb8 cells can develop into mature neutrophils and that dHoxb8 cells can phenotypically and functionally mimic primary mature neutrophils. The maturation process of Hoxb8 cells can emulate *in vitro* the development of neutrophil progenitors to mature neutrophils in the BM (110, 111). Moreover, dHoxb8 cells have been demonstrated as a valid *in vitro* model for studying neutrophil trafficking, as these cells exhibit a similar capability of rolling, adhesion and migration as murine neutrophils (112, 113). The functional activities of dHoxb8 cells, including ROS production, phagocytosis, NET formation, degranulation and cytokine production have been confirmed to be similar to those of murine neutrophils (112, 114-118). Interestingly, by injecting the Hoxb8 cells in living mice, Gran et al. and Orosz et al. demonstrated that these cells were capable of engrafting into live mice allowing their analysis *in vivo* (119, 120).

1.4 Zebrafish (*Danio rerio*) model

The zebrafish is a teleost fish, a member of the *Cyprinidae* family which is originally from South and Southeastern Asia (121). As an invaluable model organism in biomedical research, zebrafish possess numerous unique characteristics, including prolific reproduction (generating up to 300 eggs per mating pair per week) and external embryonic development (122, 123). The optical transparency of zebrafish larvae allows them to be studied through non-invasive imaging techniques in the situation *in vivo* (124). The zebrafish genome has been completely sequenced, revealing that at least 70% of the human coding genes have direct equivalents in zebrafish (125). Moreover, zebrafish provide the possibility to study gene function through overexpression, temporary depletion, or genome editing by multiple techniques, including CRISPR/Cas9 (126, 127). Owing to these advantages, zebrafish have been extensively used in diverse areas of biomedical research, such as studies on embryonic development, hematopoietic development and tissue repair and regeneration, as well as drug discovery and toxicology studies.

Importantly, the immune systems are highly conserved in zebrafish, making them an extremely versatile model for studying neutrophil biology (128, 129). The morphological and functional features of zebrafish neutrophils resemble those of mammalian neutrophils (130-132). Zebrafish neutrophils have polymorphic nuclei and primary and secondary granules. They can be mobilized to the inflamed site and fulfill their functions, such as killing bacteria. Additionally, in zebrafish the adaptive immune system becomes fully mature a few weeks after the innate immune system, which is barely accessible in classical vertebrate models, allowing for the independent study of neutrophil biology in zebrafish larvae (133, 134).

1.4.1 Immune system ontogeny in zebrafish

The immune system of zebrafish develops in two waves of hematopoiesis (**Figure 8**) (135, 136). As early as around 12 hours post fertilization (hpf), the initial primitive hematopoiesis takes place in intermediate cell mass (ICM) and anterior lateral plate mesoderm (ALPM) (137). The ICM, equivalent to the extra-embryonic yolk sac blood islands of mammals, exclusively gives rise to erythroid cells, while myeloid progenitor cells first develop in the ALPM (138). These myeloid progenitor cells further differentiate into primitive macrophages, embryonic microglia, and neutrophilic granulocytes. At

approximately 24 hpf, ALPM-derived granulocyte progenitors start to differentiate into neutrophils (139). From around 30 hpf onwards, the emergence of multipotential HSCs in the aorta-gonad-mesonephros (AGM) indicates the start of the final definitive wave of hematopoiesis (140). During this stage, HSCs migrate to the caudal hematopoietic tissue (CHT) and give rise to all lineages, including neutrophils. At approximately 48 hpf, neutrophils are abundant in the CHT (141, 142).

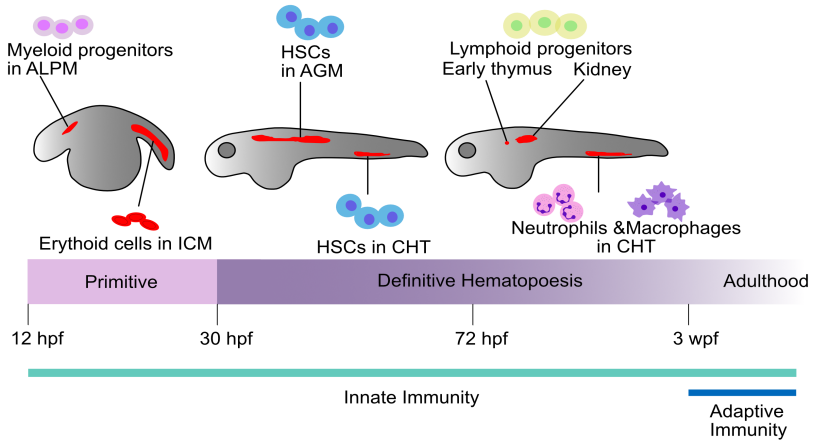

Figure 8. Development of the immune system in zebrafish. The innate immune system starts at 12 hpf when myeloid progenitor cells and erythroid cells develop in ALPM and ICM, respectively. Definitive hematopoiesis starts at 30 hpf when HSCs appear in AGM and CHT. Starting from around 72 hpf onwards, lymphoid progenitors emerge in the early thymus and kidney. The adaptive immune system is fully developed at around 3 wpf. ALPM: anterior lateral plate mesoderm, ICM: intermediate cell mass, HSC: Hematopoietic stem cells, AGM: aorta-gonad-mesonephros, CHT: caudal hematopoietic tissue. Adapted from Miao et al., 2021 (135). Copyright 2021 by Miao, Kim, Meara, Qin and Feng. Adapted with permission.

By 72 hpf, HSCs migrate to the early thymus, where the lymphoid progenitors are produced (143). Meanwhile, the kidney marrow begins to develop and eventually becomes the site of definitive hematopoiesis in adult zebrafish (144). Notably, the innate immunity remains predominant in zebrafish until 3 weeks post fertilization (wpf), when the adaptive immunity becomes fully functional.

To visualize neutrophils in zebrafish larvae, Sudan black B staining was initially employed to label the myeloperoxidase-positive granules of neutrophils (145). Subsequently, with the emergence of transgenic reporter lines, neutrophils have been monitored by expressing fluorescent reporter proteins under the control of neutrophil-specific promoters, including *myeloid peroxidase (mpx)* (130, 144) and *lysosome C* (*lyz*) (146, 147). *mpx* has been widely used as a specific marker for neutrophils, while a weak fluorescent signal

was also reported in macrophages in 3 dpf zebrafish larvae (147, 148). *lyz* labels neutrophils and macrophages at 32 hpf. However, starting from 48 hpf onwards, *lyz* becomes a primary marker for neutrophils (146, 149, 150). In the present study, we employed the transgenic zebrafish line Tg(*fli1:gfp;lyz:dsRed*) expressing red fluorescent protein from *Discosoma* (dsRed) under the control of the *lyz* promoter to specifically label neutrophils (**Figure 9**) (146, 147). Additionally, the endothelial cells of this zebrafish line express green fluorescent protein (GFP) under the control of the *friend leukemia integration 1* (*fli1)* promoter (151).

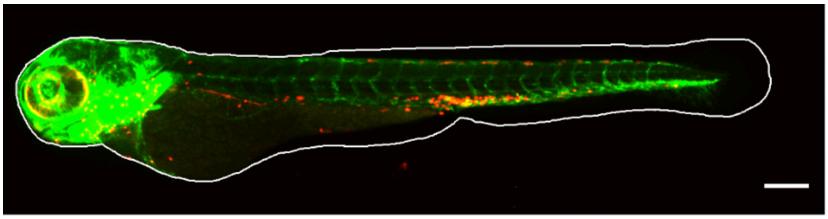

Figure 9. Representative image of Tg(*fli1:gfp;lyz:dsRed*) zebrafish larva at 3 dpf. Endothelial cells, green. Neutrophils, red. Scale bar, 200 µm. Adapted from Bader et al., 2021 (152).

The zebrafish model, like any other model system, possesses potential drawbacks (153). The limited availability of antibodies for zebrafish constrains research into the molecular functions of several proteins.

1.5 Aim of the study

VPS18 is one of the core subunits of CORVET and HOPS complexes which are involved in endolysosomal and autophagosomal pathways. Interestingly, Prof. Dr. Christoph Klein and his group identified a patient (patient 1) with a heterozygous mutation in *VPS18* suffering from neutropenia and recurrent infections. Deficiency of other core subunits of CORVET and HOPS complexes (VPS16 and VPS33A) causes neutropenia in patients as well. Likewise, patients with mutations in *VPS13B* and *VPS45* were reported to suffer from neutropenia due to impaired vesicle trafficking (154, 155). However, the function of VPS18 in neutrophil biology has not been studied to date.

Therefore, the first aim of this study was to verify whether mutations in *VPS18* can cause neutrophil maturation defects by characterizing neutrophil maturation stages in Hoxb8 cells during differentiation. The second aim of this study was to decipher the kind of cell death that *Vps18* mutant neutrophil progenitors underwent during the differentiation process. The third aim of this study was to verify whether the phenotypes were specifically caused by the mutations in *Vps18* by performing essential rescue experiments. The fourth aim of this study was to verify whether mutations in *VPS18* led to a reduction of neutrophil numbers *in vivo* using the zebrafish model. The last aim of this study was to characterize the migration behavior of the remaining viable neutrophils in *vps18* mutant zebrafish lines.

In summary, this study was undertaken to provide a significant advance in understanding the role of VPS18 in neutrophil biology, which may help to provide insights into the mechanisms of a potentially novel congenital neutropenia syndrome in humans.

2. Materials and methods

2.1 Materials

2.1.1 Experimental models

Name	Source
SCF-producing Chinese hamster ovary (CHO) cells	Prof. Dr. Hans Häcker, University of Utah School of Medicine, Salt Lake City, USA (113)
Hoxb8-SCF cells	Generated in our lab (113)
AB or Tüpfel long fin (TL) wild type (WT) zebrafish	Zebrafish Facility of Deutsches Zentrum für Neurodegenerative Erkrankungen (DZNE, Munich) (156)
C57BL/6NCrl mice	Core Facility Animal Models of the Biomedical Center Munich of the Ludwig-Maximilians-Universität München (157)
Vps18$^{flox/flox}$ mice	The Centre for Phenogenomics in Toronto, Canada. Mouse Genome Informatics (MGI) ID: MGI: 6316269
Vav-iCre$^{+/-}$ mice	The Jackson Laboratory. Stock No. 018968[179]

2.1.2 Reagents and kits

Name	Source	Catalog No.
Agarose	Genaxxon, Germany	M3044-0500
Annexin V Binding Buffer	Biolegend, USA	422201
BD FACS™ lysing solution	BD Biosciences, USA	349202
Bovine serum albumin (BSA)	Sigma-Aldrich, USA	A6003
BlueStar plus prestained protein marker	Nippon Genetics, Japan	MWP04
Bromphenol blue	AppliChem, Germany	A2331
Calcium chloride ($CaCl_2$)	AppliChem, Germany	A4088
Diisopropyl fluorophosphate (DFP)	Sigma-Aldrich, USA	55-91-4
Dimethyl sulfoxide (DMSO)	Sigma-Aldrich, USA	D8418
β-Estradiol	Sigma-Aldrich, USA	E2758
Ethanol absolute	Th. Geyer, Germany	5054.1
Ethylenediaminetetraacetic acid (EDTA)	AppliChem, Germany	181670.1211
Eukitt® Quick-hardening mounting medium	Sigma-Aldrich, USA	03989
Fetal bovine serum (FBS)	Sigma-Aldrich, USA	F7524
Fixation/Permeabilization Kit	BD Biosciences, USA	554714
Formaldehyde solution 37%	Carl Roth, Germany	7398.1
FlexAble CoraLite®488 Antibody Labeling Kit for Rabbit Immunoglobulin G (IgG)	Proteintech, USA	KFA001
FlexAble CoraLite® Plus 647 Antibody Labeling Kit for Rabbit IgG	Proteintech, USA	KFA003
FastGene 100 bp DNA marker	Nippon Genetics, Japan	MWD100

Giemsa solution	Carl Roth, Germany	T862.2
Glycerol	AppliChem, Germany	A3552
Glycine	AppliChem, Germany	A1067
HEPES	AppliChem, Germany	A3724
Hank's saline solution (HBSS)	Biochrom, Germany	L2045
Hygiene cleaner	REWE, Germany	8079152
LICOR blocking buffer	LICOR Biosciences, USA	927-6000
MetaPhor™ Agarose	Lonza Bioscience, USA	50181
Midori Green Advance	Nippon Genetics, Japan	MG04
Methanol	Th. Geyer, Germany	1462
Methylene blue	Sigma-Aldrich, USA	61734
β-Mercaptoethanol	AppliChem, Germany	A1108
May-Grünwald solution	Carl Roth, Germany	T863.2
Magnesium sulfate ($MgSO_4$)	AppliChem, Germany	A4101
M-PER™ Mammalian Protein Extraction Reagent	Thermo Fisher Scientific, Germany	78501
Mini-PROTEAN® TGX Stain-Free Precast Gel	BIO-RAD, USA	456-8095
Puromycin	Sigma-Aldrich, USA	P8833
N-Phenylthiourea (PTU)	Sigma-Aldrich, USA	103-85-5
Phosphate-buffered saline (PBS)	Biowest, USA	L0615
PCRBIO Rapid Extract PCR kit	PCR Biosystems, UK	PB10.24-08
PCRBIO HS Taq Mix Red	PCR Biosystems, UK	PB10.13-02
Phenol red	Sigma-Aldrich, USA	143-74-8
Penicillin/streptomycin (P/S)	Sigma-Aldrich, USA	P0781
Pierce™ BCA Protein Assay Kit	Thermo Fisher Scientific, Germany	23225
Ponceau S solution	AppliChem, Germany	A2935
Pronase	Roche, Switzerland	11459643001
Protease inhibitor cocktail	Sigma-Aldrich, USA	P8340
Proteinase K	Invitek Molecular, Germany	39450-01-6
RPMI 1640 medium	Sigma-Aldrich, USA	R8758
rmTNF-α	R&D systems, USA	410-MT
rmTNF-α	PeproTech, Germany	315-01A
Recombinant mouse granulocyte colony stimulating factor (rmG-CSF)	PeproTech, Germany	250-05
Sodium dodecyl sulfate (SDS)	AppliChem, Germany	132363.1209
Select agar	Thermo Fisher Scientific, Germany	30391023
Sodium chloride (NaCl)	AppliChem, Germany	A2942
Sodium fluoride (NaF)	Sigma-Aldrich, USA	7681-49-4
Sodium orthovanadate (Na_3O_4)	Sigma-Aldrich, USA	13721-39-6
Tris-Acetate-EDTA (TAE)	Nippon Genetics, Japan	ID1521
5× Trans-Blot® Turbo™ transfer buffer	BIO-RAD, USA	#10026938
0.25% Trypsin-EDTA	Gibco, Germany	#25200-056
Tricaine	Pharmaq, UK	MS-222

Trypan blue	Gibco, Germany	#15250061
Tris	AppliChem, Germany	A1087
Tween 20	Sigma-Aldrich, USA	9005-64-5
Tunicamycin	Sigma-Aldrich, USA	11089-65-9
TritonX-100	AppliChem, Germany	69227-22-1
UltraComp eBeads™ Compensation Beads	Thermo Fisher Scientific, Germany	01-2222-42

2.1.3 Buffers

Name	**Ingredients**
Blocking buffer for western blot	50% (v/v) Tris buffered saline with Tween® 20 (TBST) 50% (v/v) LICOR blocking buffer
Bleaching solution	0.8% (v/v) Hygiene cleaner dH_2O
Cell freezing medium	90% (v/v) FBS 10% (v/v) DMSO
CHO cell culture medium	RPMI 1640 10% (v/v) FBS 1% (v/v) P/S
E3 medium (60×)	5 mM NaCl 0.17 mM KCl 0.33 mM $CaCl_2$ 0.33 mM $MgSO_4$ dH_2O
Flow cytometry (FC) staining buffer	PBS 5% (v/v) FBS
Formaldehyde solution (4%, pH 7.4)	PBS 37% (v/v) Formaldehyde solution
Hoxb8 cell culture medium	RPMI 1640 10% (v/v) FBS 4% (v/v) supernatant from SCF-producing CHO cells 1% (v/v) P/S 30 µM β-mercaptoethanol 1 µM β-estradiol
Hobx8 cell differentiation medium	RPMI 1640 10% (v/v) FBS 4% (v/v) supernatant from SCF-producing CHO cells 1% (v/v) P/S 20 ng/ml rmG-CSF
Hank's buffer (pH 7.4)	HBSS 0.6% BSA 0.6 mM EDTA
Laemmli buffer (4×)	10 mL tris (1M, pH 6.8) 4 g SDS 20 mL glycerol

	10 mL β-mercaptoethanol 0.1 g bromophenol blue 50 mL dH_2O
PBST (1×)	1×PBS 0.1% (v/v) Tween-20
PDT	1×PBST 0.3% (v/v) Triton-X 100 1% (v/v) DMSO
PTU (10×)	5 mM 1-phenyl-2-thiourea dH_2O
Protein isolation buffer	M-PER™ Mammalian Protein Extraction Reagent 1×Protease inhibitor cocktail 1 mM DFP 20 mM NaF 2 mM Na_3VO_4
TBST	20 mM tris 137.2 mM NaCl 0.1% (v/v) Tween-20 dH_2O
TE buffer	1 mM EDTA 10 mM tris-Cl dH_2O
Transfer buffer (1×)	200 ml 5× Trans-Blot® Turbo™ transfer buffer 200 ml ethanol 600 ml dH_2O
Running buffer (10×)	2 M glycine 250 mM tris 1% (v/v) SDS

2.1.4 Restriction enzymes

Enzyme	**Source**
AcuI	New England Biolabs (R0641L), USA
BtgI	New England Biolabs (R0608S), USA

2.1.5 Antibodies

Primary antibody	**Conjugate**	**Source**	**Catalog No.**
Anti-mouse CD11b (Clone M1/70)	Brilliant Ultraviolet 496	BD Biosciences, USA	749864
Anti-mouse CD16/CD32 (Clone Ab93)	Brilliant Ultraviolet 615	BD Biosciences, USA	751701
Anti-mouse CD24 (Clone M1/69)	Alexa Fluor 700	Biolegend, USA	101836
Anti-mouse CD34 (Clone HM34)	Alexa Fluor 647	Biolegend, USA	128606

Anti-mouse CD49d (Clone 9C10)	Brilliant Ultraviolet 563	BD Biosciences, USA	741243
Anti-mouse CD62L (Clone MEL-14)	Brilliant Violet 480	BD Biosciences, USA	746726
Anti-mouse CD81 (Clone Eat-2)	Peridinin chlorophyll protein/Cyanine (PerCP/Cy) 5.5	Biolegend, USA	104912
Anti-mouse CD101 (Clone Moushi101)	Allophycocyanin (APC)	Thermo Fisher Scientific, Germany	17-1011-82
Anti-mouse CD106 (Clone 429)	Brilliant Violet 605	BD Biosciences, USA	745193
Anti-mouse CD115 (Clone AFS97)	Brilliant Ultraviolet 737	BD Biosciences, USA	750948
Anti-mouse c-kit (Clone 2B8)	Brilliant Violet 421	Biolegend, USA	105828
Anti-mouse CXCR2 (Clone SA044G4)	Phycoerythrin (PE)	Biolegend, USA	149304
Anti-mouse CXCR4 (Clone L276F12)	Brilliant Violet 711	Biolegend, USA	146517
Anti-mouse Ly6A/E (Clone D7)	Brilliant Ultraviolet 661	BD Biosciences, USA	741466
Anti-mouse Ly6C (Clone HK1.4)	Brilliant Violet 785	Biolegend, USA	128041
Anti-mouse Ly6G (Clone 1A8)	Brilliant Ultraviolet 395	BD Biosciences, USA	565964
Anti-glyceraldehyde-3-phosphate dehydrogenase (GAPDH) (Clone 6C5)	-	Merck Millipore, Germany	MAB374
Purified anti-active caspase 3	-	BD Biosciences, USA	559565
Rabbit anti-mouse VPS18 (Clone EPR13378)	-	Abcam, UK	ab178416
Rabbit anti-active caspase-3 (Clone C92-605)	Alexa Fluor 647	BD Biosciences, USA	560626
Rabbit anti-active caspase-3 (Clone C92-605)	PE	BD Biosciences, USA	550821

Isotype control	**Conjugate**	**Source**	**Catalog No.**
Rabbit IgG antibody	PE	R&D systems, USA	IC1051P

Rabbit IgG antibody	Alexa Fluor 405	R&D systems, USA	IC1051V
Rabbit mAb IgG XP® isotype control (Clone DA1E)	-	Cell Signaling Technology, USA	3900
Rabbit IgG, polyclonal isotype control	-	Abcam, UK	ab37415
Recombinant Rabbit IgG, monoclonal isotype control (Clone EPR25A)	-	Abcam, UK	ab172730
Recombinant Rabbit IgG, monoclonal isotype control (Clone EPR25A)	Alexa Fluor 488	Abcam, UK	ab199091
Recombinant Rabbit IgG, monoclonal isotype control (Clone EPR25A)	Alexa Fluor 647	Abcam, UK	ab199093

Secondary antibody	**Conjugate**	**Source**	**Catalog No.**
Goat anti-rabbit F(ab')2-IgG (H+L) cross-adsorbed secondary antibody	Alexa Fluor 488	Jackson ImmunoResearch, USA	111-547-008
Goat anti-rabbit F(ab')2-IgG (H+L) cross-adsorbed secondary antibody	Alexa Fluor 647	Jackson ImmunoResearch, USA	111-607-008
Donkey anti-rabbit IgG (H+L) high cross-absorbed secondary antibody	Alexa Fluor 647	Thermo Fisher Scientific, Germany	A31573
Goat anti-rabbit F(ab')2-IgG (H+L) cross-adsorbed secondary antibody	Alexa Fluor 488	Thermo Fisher Scientific, Germany	A-11070
Goat anti-rabbit F(ab')2-IgG (H+L) cross-adsorbed secondary antibody	Alexa Fluor 647	Thermo Fisher Scientific, Germany	A-21246
Goat anti-rabbit IgG (H+L) high cross-absorbed secondary antibody	Alexa Fluor 488	Thermo Fisher Scientific, Germany	A11034
Donkey anti-mouse secondary antibody	IRDye 680RD	LICOR Biosciences, USA	926-68072
Donkey anti-rabbit secondary antibody	IRDye 800CW	LICOR Biosciences, USA	926-32213

2.1.6 Fluorescent dyes

Dye	Em/Ex (nm)	Source	Catalog No.
Fluorescein isothiocyanate (FITC) Annexin V	488/519	Biolegend, USA	640906
LIVE/DEAD™ Fixable Yellow Dead Cell Stain kit	400/575	Thermo Fisher Scientific, Germany	L34968
LIVE/DEAD™ Fixable Near-IR Dead Cell Stain kit	633/775	Thermo Fisher Scientific, Germany	L34976
Pacific Blue™ Annexin V	405/455	Biolegend, USA	640918
Sytox™ Red dead cell stain	640/658	Thermo Fisher Scientific, Germany	S34859
Tetramethylrhodamine methyl ester (TMRM)	561/574	Thermo Fisher Scientific, Germany	T668
Zombie UV™ Fixable Viability Kit	450/459	Biolegend, USA	423107

2.1.7 Software

Software	Source
Affinity Designer	Serif, UK
EndNote X9	Clarivate Analytics, USA
FACS Diva	BD Biosciences, USA
FlowJo v.10	BD Biosciences, USA
FIJI	National Institutes of Health (NIH), USA
GraphPad Prism v.9	GraphPad Software, USA
Image Studio Lite v.5.2	LI-COR Biosciences, USA
Inkscape	GitLab, USA
Leica Application Suite X	Leica, Germany
Microsoft Office	Microsoft, USA
Slidebook 6.0.13	3i, USA

2.1.8 Equipment

Equipment	Source
5418R centrifuge	Eppendorf, Germany
Bright-field microscope with color camera	Leica, Germany
Cytospin® III cytocentrifuge	Tharmac, Germany

CytoFLEX S	Beckman Coulter, USA
Cell culture incubator Galaxy 170s	Eppendorf, Germany
Cytek® Aurora Spectrum Cytometry	Cytek Biosciences, USA
Examiner Spinning Disk Confocal Microscope	Zeiss, Germany
FemtoJet® 4×	Eppendorf, Germany
Leica M205 fluorescence stereo microscope	Leica, Germany
Leica DM2500 bright field microscope with color camera	Leica, Germany
Multifuge™ X3R centrifuge	Thermo Fisher Scientific, Germany
NanoDrop™ 2000	Thermo Fisher Scientific, Germany
Odyssey® CLx imaging system	LI-COR Biosciences, USA
peqSTAR thermocycler	PEQLAB, Germany
SevenCompact™ pH meter S210	Mettler Toledo, USA
Trans-Blot® Turbo™ transfer system	BIO-RAD, USA
Thermomixer	Eppendorf, Germany

2.1.9 Consumables

Consumable	**Source**
Cell strainer (40 µm)	Th. Geyer, Germany
Cell strainer (70 µm)	Greiner, Germany
Cover slide	Paul Marienfeld, Germany
Cryotube	SARSTEDT, Germany
Glass slide for microscopy	Paul Marienfeld, Germany
Centrifuge tubes (15 ml and 50 ml)	Greiner, Germany
0.2 µm filter	SARSTEDT, Germany
Fast read® 102 cell counting chamber	Kova International, USA
Multiwell plates (12-well and 96-well)	Greiner, Germany
Micro tubes (1.5 ml and 2 ml)	SARSTEDT, Germany
Pipette tips (10 µl, 100 µl, 300 µl and 1 ml)	Greiner, Germany
Petri dishes (35 mm)	Greiner, Germany
Round bottom tubes (5 ml)	Greiner, Germany
Syringe (20 ml)	B. Braun, Germany
Suspension cell culture flask (75 cm^2)	Greiner, Germany
Serological pipettes (5 ml, 10 ml, 25 ml)	SARSTEDT, Germany
Transfer pipette (3.5 ml)	SARSTEDT, Germany

2.2 Methods

2.2.1 Alignments

Protein sequences of human (*Homo sapiens*), murine (*Mus musculus*), and zebrafish (*Danio rerio*) VPS18 were acquired from the UniProt database (https://www.uniprot.org/). (158, 159). Subsequently, sequence alignments were performed using Clustal Omega (https://www.ebi.ac.uk/Tools/msa/clustalo/). Identity and similarity analysis was performed with the Sequence Manipulation Suite (https://www.bioinformatics.org/sms2/ident_sim.html): Identity and Similarity, using default settings.

2.2.2 Zebrafish husbandry and breeding

Zebrafish were maintained and bred at the zebrafish facility of Deutsches Zentrum für Neurodegenerative Erkrankungen (DZNE, Munich). They were kept at standard conditions at 28.5 °C under a light/dark cycle of 14 h/10 h (160). The wild type (WT) zebrafish strains AB or Tüpfel long fin (TL) were used in the present study (156).

For breeding the zebrafish, pairwise male and female adult zebrafish were placed in a mating tank in the late afternoon. The eggs were collected the next morning and transferred into a sterile petri dish. Zebrafish eggs and larvae were maintained in 1× E3 medium supplemented with 0.3 µg/ml of methylene blue at 28.5 °C until 5 dpf (161). To eliminate potential contamination, bleaching of the embryos was performed at 24 hpf by bathing the embryos in the bleaching solution for 5 min, followed by a 5 min rinse in tap water (162). After repeating this step twice, the embryos were finally rinsed twice in tap water. Afterwards, embryos were transferred into a new peri dish with 10 ml E3 medium supplemented with 0.3 µg/ml of methylene blue. One mg/ml pronase was added to the medium to allow the embryos to hatch from the denatured chorion. In addition, 0.003% *N*-Phenylthiourea (PTU) was added into the medium to prevent pigmentation (163). For analysis, zebrafish larvae were anesthetized with 0.08 mg/ml tricaine in E3 medium or euthanized by an overdose of tricaine (0.3 mg/ml).

2.2.3 Generation of *vps18* mutant zebrafish lines

In the present study, *vps18* mutant zebrafish lines were used which were generated and generously provided by Dr. Daniela Maier-Begandt. Two *vps18* mutant zebrafish lines

were generated using CRISPR/Cas9 technique with the transgenic zebrafish line Tg(*fli1:gfp;lyz:dsRed*) (**Figure 10**). Notably, both *vps18* mutant zebrafish lines carried heterozygous mutations in *vps18*. The first *vps18* mutant zebrafish line (referred to as *vps18*$^{+/-}$ G26Δ) harbored a mutation in the exon 1 of *vps18* leading to a deletion of 22 base pairs (bp) resulting in a premature stop codon at amino acid position 26 (Gly26*). The second *vps18* mutant zebrafish line (referred to as *vps18*$^{+/-}$ K464Δ) harbored a mutation in the exon 4 of *vps18* leading to a deletion of 32 bp resulting in a premature stop codon at amino acid position 464 (Lys464*). The zebrafish embryos were injected at a one-cell stage with corresponding guide RNAs and Cas9 protein. Zebrafish of the F_0 generation were raised and outcrossed with Tg(*fli1:gfp;lyz:dsRed*) zebrafish. Genotyping and sequencing were then performed with the F_1 generation.

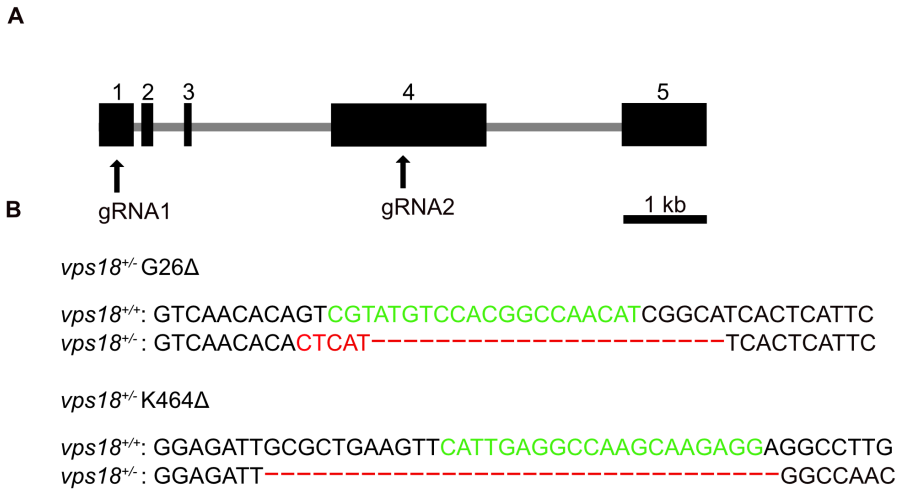

Figure 10. Generation of *vps18*$^{+/-}$ zebrafish by CRISPR/Cas9 technique. (A) Schematic of the *vps18* gene and target exon 1 of gRNA1 and exon 4 of gRNA2. **(B)** Partial genomic sequence of zebrafish lines *vps18*$^{+/-}$ G26Δ and *vps18*$^{+/-}$ K464Δ. The target sequence of the gRNA (green) and deletions (-, red).

2.2.4 Mouse husbandry and breeding

C57BL/6NCrl mice were bred in the Core Facility Animal Models of the Biomedical Center Munich of the Ludwig-Maximilians-Universität München. The *Vps18*$^{flox/flox}$ mice with C57BL/6NCrl background were purchased from The Centre for Phenogenomics in Toronto, Canada. The *Vav-iCre*$^{+/-}$ female mice (stock No. 018968[179], The Jackson Laboratory) were crossed with *Vps18*$^{flox/flox}$ male mice. *Vav-iCre*$^{+/-}$/*Vps18*$^{wt/flox}$ (*Vav-iCre*$^{+}$/*Vps18*$^{wt/flox}$) mice were used as target animals, and *Vav-iCre*$^{-/-}$/*Vps18*$^{wt/flox}$ (*Vav-iCre*$^{-}$/*Vps18*$^{wt/flox}$) mice were used as controls. All animal experiments in this study were carried out following the animal protection standards of the DZNE and LMU which were

approved by the government of Upper Bavaria (Regierung von Oberbayern, Munich, Germany).

2.2.5 Genotyping

To determine the genotypes of mice and zebrafish, genomic DNA was extracted from tail biopsies of mice or clippings of the caudal fin from adult zebrafish or whole zebrafish larvae by using PCRBio Rapid Extract PCR Kit (PCR Biosystems) according to the manufacturer's protocol. Extracted DNA was used as a template and added to the PCR reaction mix (**Table 2**). The primers used for genotyping are listed in **Table 3**. *vps18*-1 (for gRNA 1) and *vps18*-2 (for gRNA 2) primers were used for zebrafish genotyping. *Vps18-wt, distal loxP,* target mutation *(tm)1c,* and *Vav-iCre* primers were employed for mouse genotyping. The PCR reaction conditions are shown in **Table 4**.

Table 2. Master mix for the PCR reaction.

Component	25 µl reaction volume (per sample)
2× Taq master mix	12.5 µl
Forward primer (1:20 dilution)	1 µl
Reverse primer (1:20 dilution)	1 µl
Template DNA	2-4 µl
PCR grade dH_2O	to 25 µl

Table 3. Primers used for genotyping.

Name	Forward primer (5'-3')	Reverse primer (5'-3')	Expected band size of PCR product (bp)
vps18-1	AAGACAGA-CATGCAACCAACAC	AATGGGTTTTTCTTC CTCCAAT	524
vps18-2	TAGTCCTCACCCAG-TTCCACTT	AATAAATGTTGCTT-GCCTTCGT	565
Vav-iCre	GCCTGCCCTCCCTGTG GATGCCACCT	GTGGCAGAAGGGG-CAGCCACACCATT	800
Vps18-wt	TGTAGGAGAGCAGCG-CAGGGTTAC	GAAGTTATCTCGAC-GAAGTTCC	261
distal loxP	GCGCAAC-GCAATTAATGATAAC	TCGTGCTGGGAT-TCATCCTTGTGGG	166
tm1c	TGCAGCGGAC-TATCGAGAAAGCAAC	GGGATTGGTTCTCTG TGCCTGAGATG	255

Table 4. PCR reaction conditions.

Step		Temperature	Time
Initial denaturation		94 °C	2 min
35-45 cycles	Denaturation	94 °C	30 s
	Annealing	60 or 65 °C	30 s
	Extension	72 °C	30 s
Final extension		72 °C	10 min

The cycling conditions were adjusted to different primers. For *vps18*, *Vps18-wt, distal loxP,* and *tm1c* primers, the annealing temperature was 60 °C. For *Vav-iCre* primers, the annealing temperature was 65 °C. The cycle number for *Vps18-wt, distal loxP, tm1c,* and *Vav-iCre* primers was 35.

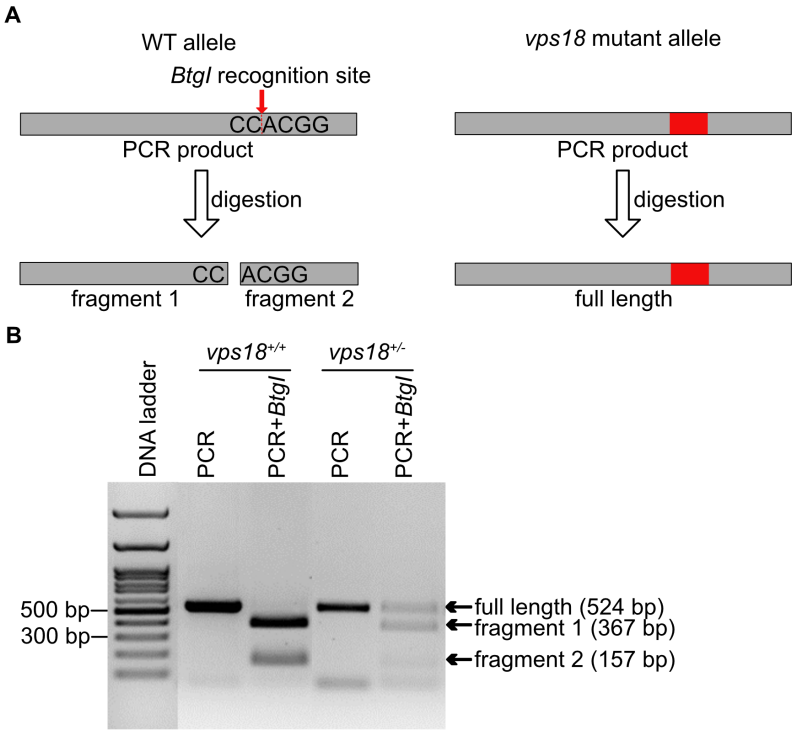

Figure 11. RFLP analysis of zebrafish genotype. (A) Left panel: schematic representation of recognition site of enzyme *BtgI* in PCR product of WT allele. Right panel: schematic representation of *vps18* mutant allele containing a mutated site (red box). **(B)** Representative image of gel electrophoresis of PCR products of $vps18^{+/+}$ and $vps18^{+/-}$ zebrafish larvae as indicated. PCR products undigested (PCR) or with *BtgI* digestion (PCR+*BtgI*) are shown. The numbers on the left indicate the size of the DNA ladder (lane 1). Lanes 2-3 show $vps18^{+/+}$ zebrafish larvae, whereas $vps18^{+/-}$ zebrafish larvae are shown in lanes 4-5. Arrows indicate different sizes of bands. Results are representative of n=4 independent experiments.

The PCR with *vps18* primer pairs resulted in PCR products with the same size for $vps18^{+/+}$ or $vps18^{+/-}$ zebrafish. To further distinguish the $vps18^{+/+}$ or $vps18^{+/-}$ zebrafish, a

restriction fragment length polymorphism (RFLP) assay was performed (127). The PCR products were digested with the restriction enzyme *AcuI* (restriction site: CTGAAG[16/14]) or *BtgI* (restriction site: C/CRYGG) for 2 h at 37 °C. The digested and undigested PCR products were separated on 1.5% agarose gel along with the FastGene 100 bp DNA marker. Agarose gels were imaged with a Peqlab gel documentation imaging system with UV light. The PCR with the specific primer pair resulted in a PCR product size of 524 bp for both *vps18*$^{+/+}$ and *vps18*$^{+/-}$ zebrafish larvae. In *vps18*$^{+/-}$ zebrafish, the restriction site for *BtgI* was mutated, as a result of CRISPR/Cas9 genome editing (**Figure 11A**). Therefore, the PCR product of the mutated *vps18* gene was not digested by *BtgI.* Thus, the PCR products of *vps18*$^{+/+}$ zebrafish larvae were cleaved into 2 fragments (size: 367 bp, fragment 1 and 157 bp, fragment 2) upon *BtgI* (PCR+ *BtgI*) digestion (**Figure 11B**). The PCR products of *vps18*$^{+/-}$ zebrafish larvae were digested into 2 fragments (size: 367 bp and 157 bp) and additionally showed the undigestible PCR product with 524 bp, full length.

2.2.6 Generation of *Vps18* mutant Hoxb8 cells

The immortalized Hoxb8 cell line was generated and generously provided by Dr. Annette Zehrer according to Wang et al., 2006 (107) and Zehrer et al., 2018 (113). In the present study, two heterozygous *Vps18* mutant Hoxb8 cells were generated and generously provided by Dr. Annette Zehrer using WT Hoxb8 cells treated with CRISPR/Cas9 gene editing technique. Both clones (clone 1 and 2, *Vps18*$^{+/-}$ mutants) harbored one WT allele and one mutated allele (**Figure 12**).

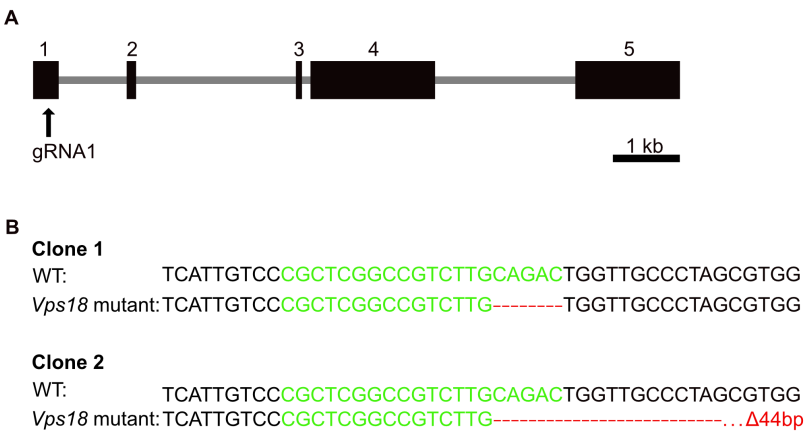

Figure 12. Generation of CTRL and *Vps18* mutant Hoxb8 cells by CRISPR/Cas9 technique. (A) Schematic of the *Vps18* gene and target exon 1 of gRNA1 **(B)** Partial genomic sequence of clone 1 and clone 2. gRNA target sequence (green) and deletions (-, red).

Clone 1 harbored a deletion of 8 bp that resulted in a frame shift inducing a premature stop codon at amino acid position 21 of VPS18. Similarly, 44 bp were deleted in clone 2 resulting in a premature stop codon at amino acid position 35 of VPS18. WT Hoxb8 cells received the same viral transduction but without gRNA and were used as controls (*Vps18*$^{+/+}$, CTRL Hoxb8 cells).

2.2.7 Generation of VPS18-EGFP expressing Hoxb8 cells

To rescue the VPS18 expression in *Vps18* mutant Hoxb8 cells, VPS18-enhanced green fluorescent protein (EGFP) expressing Hoxb8 cells (referred to as VPS18 rescue) were generated and generously provided by Dr. Annette Zehrer. Here, Clone 1 cells were transduced with pMSCV-*Puro-hVPS18- EGFP*. Additionally, WT Hoxb8 cells were transduced with EGFP alone as a control (referred to as WT-EGFP). A flow cytometric analysis was subsequently conducted to validate the successful transduction, as evidenced by a marked elevation in the EGFP signal in WT-EGFP and VPS18 rescue cells (**Figure 13**).

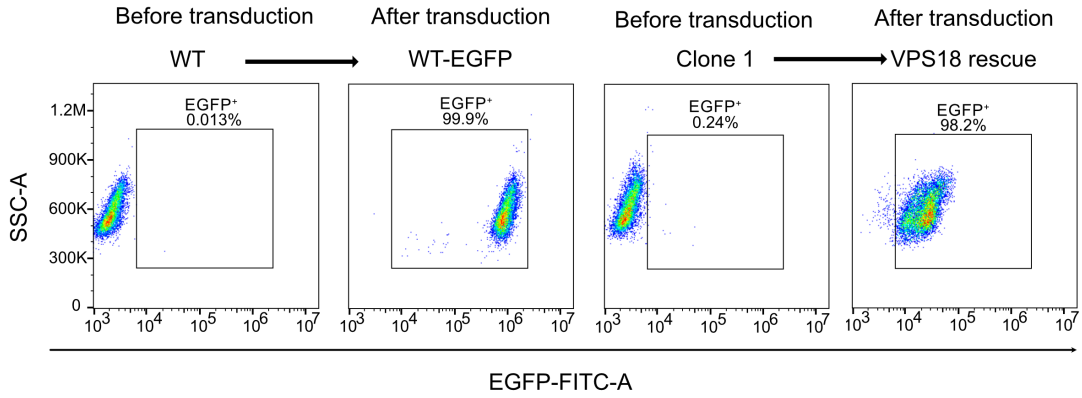

Figure 13. Verification of successful VPS18 rescue cell generation. EGFP fluorescence intensity in WT, WT-EGFP, clone 1 and VPS18 rescue Hoxb8 cells was measured with flow cytometry. Numbers indicate EGFP$^+$ cells in the percent of total single living cells (100%).

2.2.8 Cell culture and differentiation

WT-EGFP Hoxb8 cells were cultured in Hoxb8 cell culture medium, whereas CTRL, *Vps18* mutant and VPS18 rescue Hoxb8 cells were cultured in the Hoxb8 cell culture medium supplemented with 5 µg/ml puromycin. All cell lines were maintained at 37 °C, 5% CO_2, and 95% air humidity. The medium was changed every 2 days. Differentiation was induced by culturing the cells in Hoxb8 differentiation medium supplemented with 20 ng/ml rmG-CSF for 4 days. For long-term storage, cells were washed once with PBS

at 300 × g for 5 min and resuspended in cell freezing medium. Cells were stored in cryotubes at -80 °C and transferred to liquid nitrogen the next day. To thaw cells, the cryotubes containing the frozen cells were quickly placed in a 37 °C water bath until the cells were thawed. Cell suspensions were transferred into fresh Hoxb8 cell culture medium and washed once with PBS by centrifugation at 300 × g for 5 min to eliminate residual DMSO. The cell pellet was resuspended in fresh Hoxb8 cell culture medium and transferred into a new cell culture flask. To determine cell numbers, cells were counted in a Fast read® 102 cell counting chamber and 0.5% trypan blue was used to exclude dead cells.

2.2.9 Western blot

To detect the expression of VPS18 from the BM of mice, mice femurs were flushed using a 20 G needle in ice-cold PBS containing 2 mM EDTA and 5% FBS and passed through a 70 µm cell strainer. After washing once with ice-cold PBS, BM cells were lysed in protein isolation buffer on a rotator for 30 min at 4 °C and centrifuged at 1600 × g at 4 °C for 15 min. The supernatant was transferred into a new tube and the protein concentration was determined with a Pierce™ BCA Protein Assay Kit. Cell lysates were mixed with 4 × Laemmli buffer and heated at 95 °C for 5 min to denature the proteins. Cell lysates (30 µg per lane) and marker (8 µL) were loaded on Mini-PROTEAN TGX Stain-Free Gel and proteins were separated by electrophoresis at 220 V for 30 min. After separation, proteins were transferred onto nitrocellulose membranes by using the Trans-Blot® Turbo™ Transfer System. Membranes were incubated with blocking buffer for at least 1 hour at room temperature (RT) with gentle rocking. After blocking, membranes were incubated with anti-VPS18 (1:1000 dilution in blocking buffer) and anti-GAPDH (1:5000 dilution in blocking buffer) primary antibodies at 4 °C overnight. Following three times of washing with TBST, membranes were incubated with secondary antibodies (1:10,000 dilution in blocking buffer) for 2 h at RT. The membranes were imaged at the Odyssey® CLx imaging system and analyzed with Image Studio Lite software.

2.2.10 Flow cytometry

The Beckman Coulter CytoFLEX S was used for analyzing the expression of VPS18 and active caspase 3, cell apoptosis and whole kidney marrow (WKM) of adult zebrafish. Cytek® Aurora Spectrum Cytometry was used for analyzing neutrophil maturation. All

data were subsequently analyzed using FlowJo software after excluding debris, doublets and dead cells.

2.2.10.1 Intracellular staining of VPS18 and active caspase 3

To analyze the expression of VPS18 and active caspase 3 by flow cytometry, intracellular staining was performed. CTRL and *Vps18* mutant Hoxb8 cells (5×10^5 cells per sample) were first stained with LIVE/DEAD™ Fixable Yellow Dead Cell Stain Kit (1:1000 dilution in PBS) according to the manufacturer's instructions. Subsequently, cells were fixed in 100 µl 1 × BD fixation/permeabilization buffer on ice for 20 min. After washing twice with 500 µl 1 × BD permeabilization/washing buffer, the cells were stained with recombinant anti-VPS18 primary antibody (1:50 dilution in 1 × BD permeabilization/washing buffer) on ice for 45 min. Subsequently, cells were washed twice with 500 µl 1 × BD permeabilization/washing buffer followed by staining with Alexa Fluor 488-conjugated goat anti-rabbit IgG secondary antibody (1:300 dilution in 1 × BD permeabilization/washing buffer) on ice for 45 min in the dark. Cells were then washed twice with 500 µl 1 × BD permeabilization/washing buffer and resuspended in 200 µl 1 × BD permeabilization/washing buffer before analyzing with the CytoFLEX S. As a negative control, cells were incubated with a corresponding isotype control antibody instead of the primary antibody. The mean fluorescence intensity (MFI) of the signal was quantified by FlowJo software.

To detect the activation of caspase 3, CTRL and *Vps18* mutant Hoxb8 cells at day 3 of differentiation were stained with PE-conjugated anti-active caspase 3 antibody. Cells were first fixed with 1 × BD fixation/permeabilization buffer on ice for 20 min. After washing twice with 1 × BD permeabilization/washing buffer, cells were stained with PE-conjugated anti-active caspase 3 antibody (1:20 dilution in 1 × BD permeabilization/washing buffer) on ice for 30 min in the dark. Samples were then analyzed with the CytoFLEX S. As a negative control, cells were incubated with a corresponding isotype control antibody instead of the primary antibody. The Percentage of active caspase 3 positive cells was quantified by FlowJo software.

2.2.10.2 Cell apoptosis assay

To analyze the type of cell death, we employed tetramethylrhodamine methyl ester (TMRM), FITC Annexin V, and Sytox red dead cell stain. TMRM accumulates in the

inner mitochondrial membrane of healthy cells and indicates viable cells. Annexin V binds to phosphatidylserine on the surface of cells when cells undergo apoptosis. Sytox red binds to nucleic acids of cells with compromised plasma membranes. Here, $TMRM^+$ cells were defined as viable cells, Annexin V^+ Sytox red^- cells as early apoptotic cells, and Annexin V^+ Sytox red^+ cells as late apoptotic cells. CTRL and *Vps18* mutant Hoxb8 cells (5×10^5 cells per sample) were washed once in PBS and once in Annexin V-binding buffer. Subsequently, cells were incubated with 200 nM TMRM, 3.6µg/ml FITC Annexin V and 10 nM Sytox red dead cell stain at 37 °C for 15 min in the dark. The fluorescence intensity of TMRM, Annexin V, and Sytox red was detected using the CytoFLEX S. Fluorescence minus one (FMO) controls were used to determine the negative cell population. Cells incubated at 75 °C for 5 min were used as a positive control for Annexin V and Sytox red double positive cells.

2.2.10.3 Neutrophil maturation assay

Neutrophils from different maturation stages encompassing GMP-like cell ($CD34^+$c-$kit^{hi}$$CD16/CD32^+Ly6C^-$), proNeu ($CD34^+$c-$kit^{hi}CD16/CD32^+Ly6C^+$), preNeu ($CD34^-$c-$kit^{int}CD49d^+$), immature Neu (c-$kit^-CD49d^-CXCR2^+CD101^-$) and mature Neu (c-$kit^-CD49d^-CXCR2^+CD101^+$) were analyzed according to Ng et al. (20, 21). By employing this protocol, CTRL and *Vps18* mutant Hoxb8 cells during differentiation (day 0, 1, 2, 3 and 4) were analyzed with flow cytometry. Cells (5×10^5 cells per sample) were collected by centrifugation. After washing once with Hank's buffer, cells were stained with the mixture of primary antibodies (**Table 5**) for 20 min on ice and subsequently fixed with 4% formaldehyde solution in PBS for 15 min at RT in the dark. The samples were washed once with Hank's buffer prior to analysis. Data acquisition was performed on a Cytek® Aurora and data were analyzed using FlowJo. Dead cells were distinguished by auto-fluorescence (AF) signal.

Table 5. Primary antibodies are used for neutrophil maturation assay.

Primary antibody	Conjugate	Clone	Dilution in FC staining buffer
CD11b	Brilliant Ultraviolet 496	M1/70	1:200
CD16/CD32	Brilliant Ultraviolet 615	Ab93	1:50
CD24	Alexa Fluor 700	M1/69	1:200

CD34	Alexa Fluor 647	HM34	1:75
CD49d	Brilliant Ultraviolet 563	9C10	1:100
CD62L	Brilliant Violet 480	MEL-14	1:200
CD81	PerCP/Cy 5.5	Eat-2	1:50
CD101	APC	Moushi101	1:50
CD106	Brilliant Violet 605	429	1:100
CD115	Brilliant Ultraviolet 737	AFS97	1:100
c-kit	Brilliant Violet 421	2B8	1:50
CXCR2	PE	SA044G4	1:50
CXCR4	Brilliant Violet 711	L276F12	1:50
Ly6A/E	Brilliant Ultraviolet 661	D7	1:50
Ly6C	Brilliant Violet 785	HK1.4	1:300
Ly6G	Brilliant Ultraviolet 395	1A8	1:300

2.2.10.4 Analysis of WKM in adult zebrafish

Two-year-old *vps18*$^{+/+}$ and *vps18*$^{+/-}$ adult zebrafish were euthanized with 0.3 mg/ml tricaine in E3 medium. The WKM was isolated according to Gerlach et al. and subsequently resuspended in ice-cold FC staining buffer (164). Briefly, single-cell suspensions were generated by passing the kidney tissue through a 40 µm cell strainer using a 1-mL syringe plunger handle. Sytox red was added to exclude dead cells. The samples were then measured using the CytoFLEX S and the data were analyzed using FlowJo. Granulocytic cells were distinguished based on their side scatter (SSC) and forward scatter (FSC) profiles (165). Neutrophils were identified as dsRed^{+} cells.

2.2.11 Microscopy

2.2.11.1 May-Grünwald-Giemsa staining

For morphological analysis, CTRL and *Vps18* mutant Hoxb8 cells (5×10^4 cells per sample) were collected each day during differentiation. Cytospins were prepared on glass slides using a Cytospin® III cytocentrifuge (Tharmac) at 970 × g for 10 min. The slides

were air-dried and stained with May-Grünwald working solution for 5 min and with 12% Giemsa working solution for 15 min. After drying, images were obtained from stained samples using a bright field Leica DM2500 microscope equipped with a DMC2900 CMOS camera. An HCX PL FLUOTAR 63 × /1.25 oil immersion objective was used for phase contrast, resulting in an image pixel size of 92 nm. Cells at different stages of neutrophil development were characterized according to their nuclear morphology and cytoplasmic granules at least 100 cells manually from at least five different fields of view of one slide (22).

2.2.11.2 Total neutrophil counts in zebrafish larvae

For counting total neutrophil numbers, zebrafish larvae at 3 dpf were euthanized with 0.3 mg/ml tricaine in E3 medium and fixed with 4% formaldehyde solution in PBS at 4 °C overnight. After removing the formaldehyde solution, the zebrafish larvae were washed with PBS twice and mounted in 1.5% low melting agarose. The zebrafish larvae were visualized with a spinning disk confocal laser microscope (Examiner, Zeiss) equipped with a 5 × /0.15NA objective and Slidebook software or under a Leica M205 FA stereo microscope equipped with a DFC7000 T camera and Leica Application Suite X software. Fluorescence for GFP (endothelial cells) was acquired using an excitation wavelength of 488nm. Fluorescence for dsRed (neutrophils) was acquired using an excitation wavelength of 561nm. Neutrophil numbers were counted manually by using Leica Application Suite X software or FIJI software (166).

2.2.11.3 Neutrophil trafficking at steady state and during sterile inflammation

For analysis of spontaneous neutrophil migration, living zebrafish larvae at 5 dpf were analyzed at steady state as described elsewhere (152). Zebrafish larvae at 5 dpf were anesthetized with 0.08 mg/ml tricaine in E3 medium and subsequently mounted in 1.5% low-melting agar in E3 medium containing 0.08 mg/ml tricaine to retain a proper position (**Figure 14A)**. Time-lapse imaging was performed with a spinning disk confocal laser microscope (Examiner, Zeiss) equipped with a 10 × /0.3NA water immersion objective. Neutrophils in the head area indicated by the red rectangle were imaged and recorded for 15 min with a time interval of 1 min (**Figure 14B**). Maximum intensity projections were generated. Two-dimensional (2D) migration velocity and Euclidean distance were quantified with FIJI software with the Manual Tracking and the Chemotaxis Tool plugins

(ibidi). Analysis of neutrophil trafficking upon sterile inflammation was performed upon tail fin transection in zebrafish larvae as described previously (152). Briefly, the zebrafish larvae at 5 dpf were anesthetized with 0.08 mg/ml tricaine in E3 medium and subsequently the tail fins were removed by using a scalpel blade under a microscope (**Figure 14C**). After cutting the tail fins, the zebrafish larvae were placed in fresh E3 medium and incubated at 28.5 °C. They were euthanized with 0.3 mg/ml tricaine in E3 medium and fixed with 4% formaldehyde solution in PBS at 0, 1, 3, or 6 hours post wounding (hpw), respectively. Fixed zebrafish larvae were then incubated at 4 °C overnight. Images were acquired with the Leica M205 FA stereo microscope mentioned above. The number of recruited neutrophils within a 200 µm distance to the wound was quantified manually.

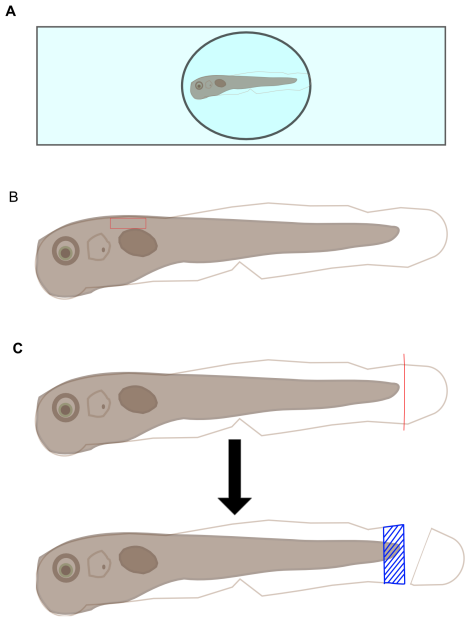

Figure 14. Analysis of neutrophil trafficking in zebrafish larvae. **(A)** Schematic of mounting of zebrafish larvae for imaging. **(B)** Schematic of a zebrafish larva for analyzing neutrophil spontaneous migration at steady state. The red rectangle indicates the location of the imaging area. **(C)** Schematic of a zebrafish larva for analyzing neutrophil trafficking upon sterile inflammation. The red line in the upper panel indicates the region where the tail fin transection was performed to initiate sterile inflammation. The blue shaded area in the lower panel indicates the area where the recruited neutrophils were quantified (200 µm away from the wound).

2.2.12 Statistical analysis

GraphPad Prism software was used for statistical analysis. Data is shown as mean ± standard deviation (SD). At least 3 independent experiments were performed for each experiment. Unpaired student's t-test or one-way ANOVA with Tukey's multiple comparison

test or two-way ANOVA with Tukey's multiple comparison was applied to determine the statistical significance for the experimental group and control group. Statistically significance was evaluated as * $p < 0.05$, ** $p < 0.01$, *** $p < 0.001$ and **** $p < 0.0001$.

3. Results

3.1 VPS18 is conserved in humans, mice and zebrafish

To better understand the functional similarity of VPS18 in different species, sequence alignments of human, murine and zebrafish amino acid sequences of VPS18 were performed. Here, identity and similarity values were calculated. Identity is defined as the exact identical amino acids in the compared sequences. Similarity is defined as amino acids with similar structural and chemical characteristics. Human and murine VPS18 showed a high amino acid identity of 95.7% (**Table 6**). Zebrafish Vps18 shared 65.8% identity and 78.5% similarity with humans. These data suggest that VPS18 may share similar functions among humans, mice and zebrafish.

Table 6. Amino acid identity and similarity of murine and zebrafish VPS18 in percent aligned to the human VPS18 (100%).

% to *Homo sapiens*	*Mus musculus*		*Danio rerio*	
	identity	similarity	identity	similarity
VPS18	95.8	97.4	65.8	78.5
β-propeller domain	94.3	95.9	63.3	76.9
CC domain (close to the N-terminal)	96.4	96.4	75.0	89.2
CC domain (close to the C-terminal)	100	100	70.2	78.7
CHCR domain	98.1	98.7	73.7	80.1
RING domain	92.6	96.8	58.3	76.0

The identity and similarity of each domain of VPS18 were compared among the three species (**Table 6 & Figure 15**). The β-propeller domain of human VPS18 was 94.3% identical and 95.9% similar to murine VPS18, and 63.3% identical and 76.9% similar to zebrafish Vps18. The CC domain close to the β-propeller domain showed 96.4% identity and 96.4% similarity between human and mouse, and 75.0% identity and 89.2% similarity between human and zebrafish. The second CC domain close to the RING domain showed 100% identity and 100% similarity between human and mouse, and 70.2% identity and 78.7% similarity between human and zebrafish. The CHCR domain of human VPS18 was 98.1% identical and 98.7% similar to murine VPS18, and 73.7% identical and 80.13% similar to zebrafish Vps18. The RING domain of human VPS18 was 92.6% identical and 96.8% similar to murine VPS18, and 58.3% identical and 76.0% similar to zebrafish Vps18.

Taken together, these data show that VPS18 and specifically the functional domains are highly conserved among men, mice and zebrafish, and thus further emphasize that the zebrafish is a suitable model to study VPS18.

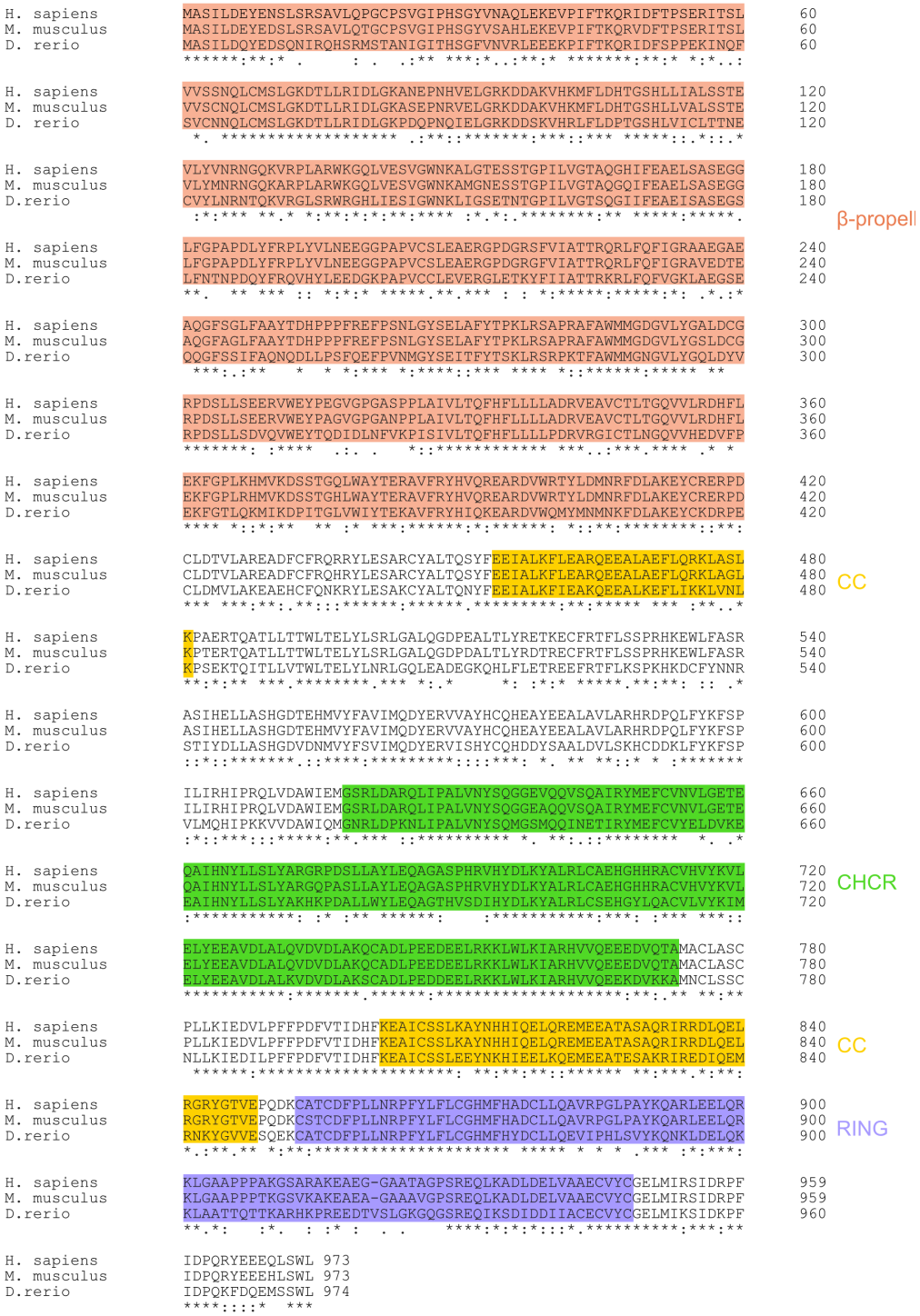

Figure 15. Sequence alignment of human, murine and zebrafish VPS18. The β-propeller (orange), CC (yellow), CHCR (green) and RING (purple) domains are highlighted in the indicated colors. Fully conserved (*), strongly similar (:) and weakly similar (.) amino acid residues are indicated below the alignment.

3.2 Residual expression of VPS18 in *Vps18* mutant Hoxb8 cells

To characterize CTRL and *Vps18* mutant Hoxb8 cells, the residual VPS18 expression was analyzed using flow cytometry at day 0 (undifferentiated) and day 4 (differentiated).

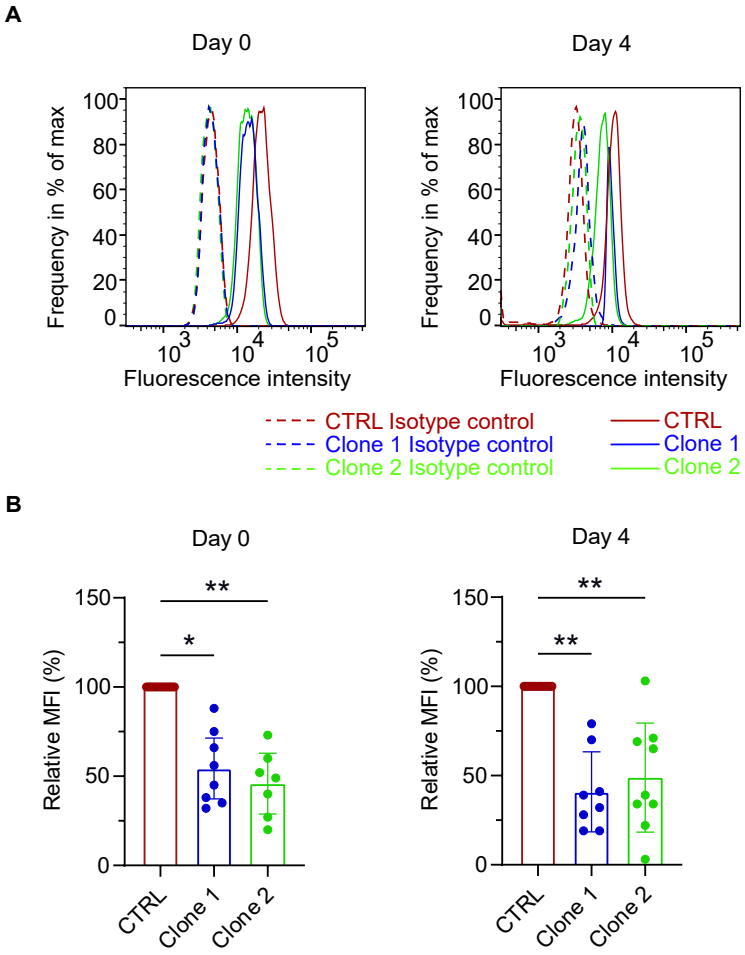

Figure 16. Flow cytometric analysis of VPS18 expression in CTRL and *Vps18* mutant Hoxb8 cells at day 0 (undifferentiated) and day 4 (differentiated). (A) Flow cytometry histograms of intracellular VPS18 staining in CTRL and *Vps18* mutant Hoxb8 cells at day 0 and day 4 of differentiation. Dashed lines indicate isotype controls. **(B)** Quantitative analysis of VPS18 expression. The mean fluorescence intensity (MFI) of VPS18 was normalized to CTRL (100%). Corresponding isotype control was used as a negative control. $n \geq 7$, Mean ± SD, One-way ANOVA with Tukey's multiple comparison test, * $p < 0.05$, ** $p < 0.01$.

Quantification of the relative MFI of VPS18 revealed that at day 0, the expression of VPS18 in both *Vps18* mutant Hoxb8 cells was downregulated to 54.4% in clone 1 and 45.9% in clone 2 compared to CTRL cells (100%) (**Figure 16**). At day 4, the expression of VPS18 also diminished to 54.4% and 48.9% in clone 1 and clone 2, respectively, compared to CTRL cells (100%). Taken together, these data indicate that the presence of one

WT allele of *Vps18* resulted in a residual VPS18 expression of approximately 50% as expected. Thus, the heterozygous *Vps18* mutant Hoxb8 cells with the reduced protein expression present a suitable model to study the patient's situation.

3.3 Mutations in *Vps18* led to impaired neutrophil maturation

To study whether heterozygous mutations in *Vps18* cause a neutrophil maturation arrest similar to the patient's situation (patient 1, personal communication by Prof. Dr. Christoph Klein), we quantified the different neutrophil maturation stages based on the morphological changes of neutrophils upon differentiation in a classic way by microscopic inspection. Here, cytospins of CTRL and *Vps18* mutant Hoxb8 cells before (day 0) and during differentiation (day 1 to day 4) were stained using May-Grünwald-Giemsa. Cells from different maturation stages (promyelocytes, myelocytes, metamyelocytes, band cells and mature neutrophils) were assessed based on their morphological profiles.

As described elsewhere, the majority of Hoxb8 cells at day 0 are at the stage of promyelocytes (**Figure 17A**) (110, 111, 167). On day 1 of differentiation, most of the CTRL and *Vps18* mutant Hoxb8 cells developed into myelocytes, suggesting that CTRL and *Vps18* mutant Hoxb8 cells developed similarly at the initial stages of neutrophil maturation (from day 0 to day 1) (**Figure 17B**). On day 2 of differentiation, 90.3% of CTRL cells were viable and differentiated further into metamyelocytes. However, the viability of clone 1 cells dropped to 81.6%. Compared to CTRL cells, the viability of clone 2 cells did not show a difference, but 46.3% of them remained at the myelocyte stage. Moreover, on day 3 of differentiation, most CTRL cells were still viable (83.8%) and progressed further into the late stages of neutrophil maturation with a combination of band cells (47.9%) and mature neutrophils (30.9%). In contrast, the cell viability of clone 1 and clone 2 dropped further to 54.1% and 76.2%, respectively. Most of the living cells in clone 1 and clone 2 were band cells. Additionally, the percentage of mature neutrophils in clone 1 and clone 2 was 7.6% and 2.1%, respectively, exhibiting a significant decrease compared to the CTRL cells. Consistent with this trend, on day 4 of differentiation when 83.6% of CTRL cells remained viable, clone 1 and clone 2 showed a significantly higher percentage of dead cells, at 71.8% and 65.4%, respectively. In contrast to 71.7% of CTRL cells were fully matured, only 15.4% of clone 1 and 16.4% of clone 2 were matured neutrophils. These results show that heterozygous mutations in *Vps18* induced a neutrophil maturation defect similar to the patient 1's situation.

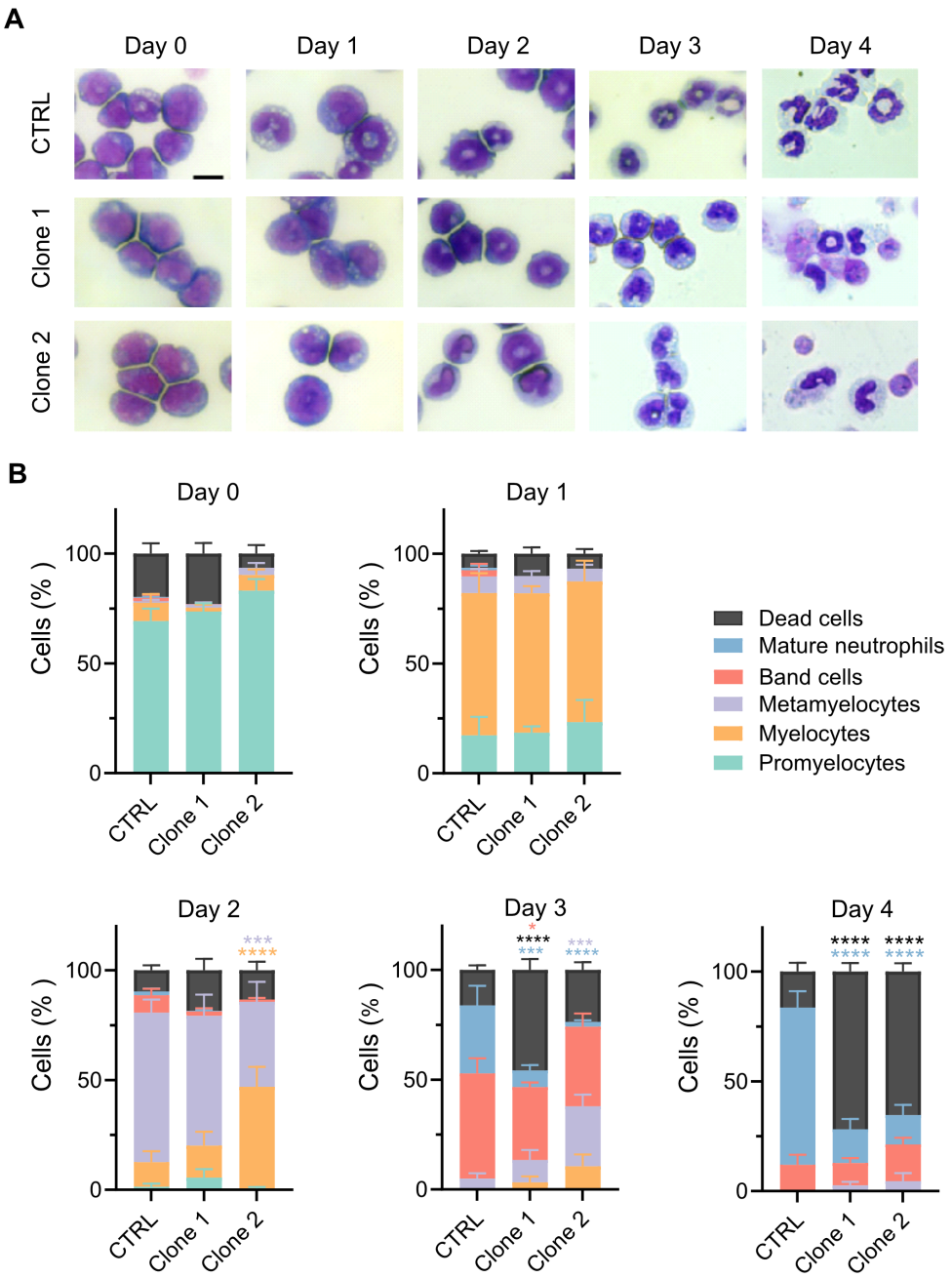

Figure 17. Neutrophil maturation analysis of CTRL and *Vps18* mutant Hoxb8 cells during differentiation based on morphological changes. (A) Representative microscopic images of CTRL and *Vps18* mutant Hoxb8 cells stained with May-Grünwald-Giemsa stain during differentiation (day 0 to day 4). Scale bar, 10µm. **(B)** Quantification of neutrophil maturation stages in CTRL and *Vps18* mutant Hoxb8 cells during differentiation (day 0 to day 4). Promyelocytes, myelocytes, metamyelocytes, band cells, mature neutrophils and dead cells were shown as a percentage of all single cells (100%). n = 5, Mean ± SD. Two-way ANOVA with Tukey's multiple comparison test. * $p < 0.05$, *** $p < 0.001$, **** $p < 0.0001$ compared to CTRL.

In order to validate our findings above, the neutrophil maturation stages were characterized using a novel classification model based on distinct cell surface markers at different

neutrophil maturation stages (20, 21). The gating strategy has been described previously **(Figure 18A)** (20, 21).

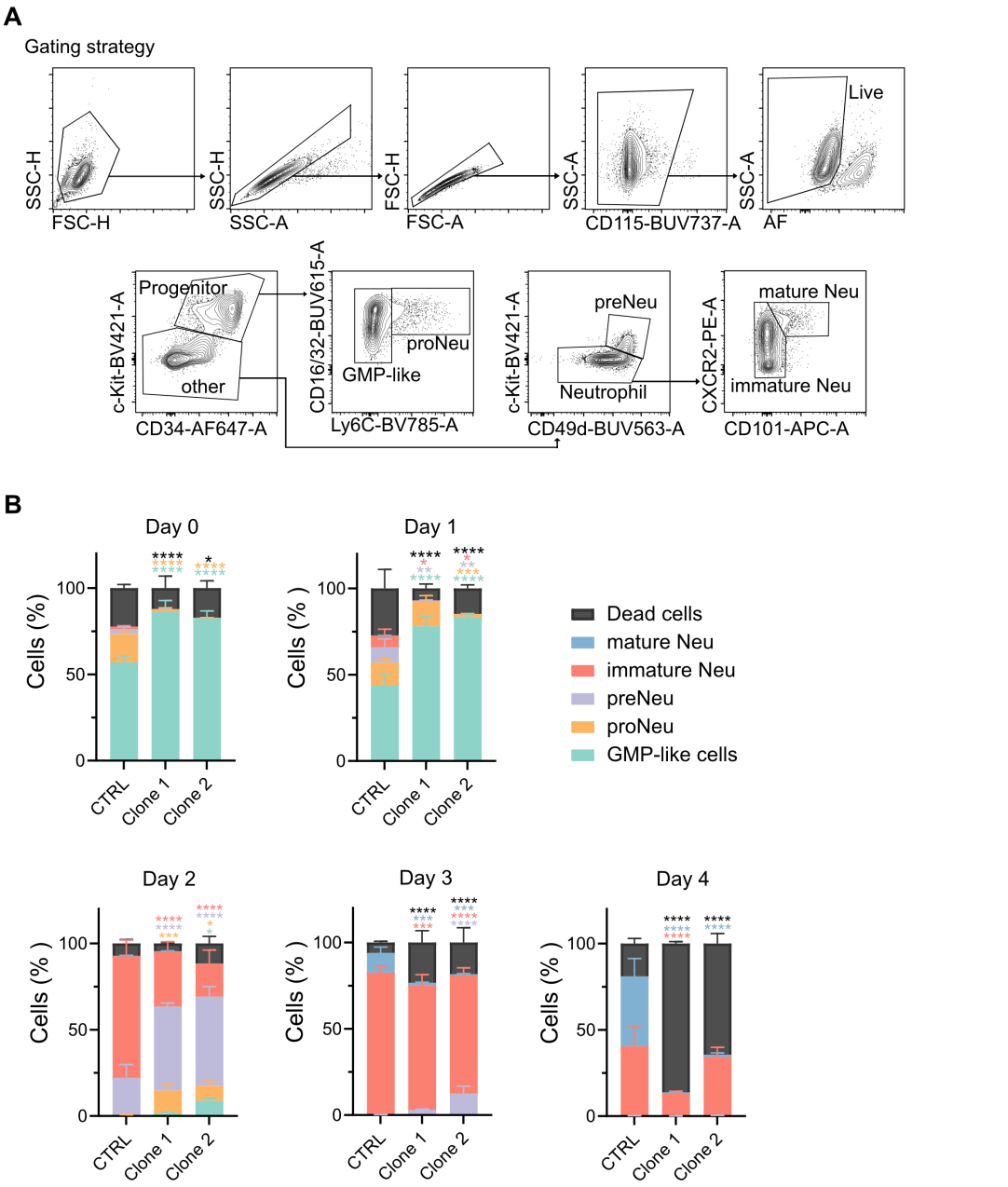

Figure 18. Neutrophil maturation analysis of CTRL and *Vps18* mutant Hoxb8 cells during differentiation based on immune phenotypes. (A) Gating strategy used to define neutrophils under different maturation stages in CTRL and *Vps18* mutant Hoxb8 cells. GMP-like cells: $CD34^{+}$c-$kit^{hi}CD16/CD32^{+}Ly6C^{-}$, proNeu: $CD34^{+}$c-$kit^{h-i}CD16/CD32^{+}Ly6C^{+}$, preNeu: $CD34^{-}$c-$kit^{int}CD49d^{+}$, immature Neu: c-$kit^{-}CD49d^{-}CXCR2^{+}CD101^{-}$, mature Neu: c-$kit^{-}CD49d^{-}CXCR2^{+}CD101^{+}$ and dead cells: AF^{+}. **(B)** Quantification of neutrophil maturation stages in CTRL and *Vps18* mutant Hoxb8 cells during differentiation (day 0 to day 4). GMP-like cells, proNeu, preNeu, immature Neu, mature Neu and dead cells were shown as percentage of all single $CD115^{-}$ cells (100%). n = 4, Mean ± SD. Two-way ANOVA with Tukey's multiple comparison test. * $p < 0.05$, ** $p < 0.01$,*** $p < 0.001$, **** $p < 0.0001$ compared to CTRL.

The debris and doublets were excluded based on their forward and side scatter properties. The AF^+ cells were determined as dead cells. The GMP-like cells were defined as $CD34^+$c-$kit^{hi}CD16/CD32^+Ly6C^-$, proNeu as $CD34^+$c-$kit^{hi}CD16/CD32^+Ly6C^+$, preNeu as $CD34^-$c-$kit^{int}CD49d^+$, immature Neu as c-$kit^-CD49d^-CXCR2^+CD101^-$ and mature Neu as c-$kit^-CD49d^-CXCR2^+CD101^+$.

At day 0 of differentiation, the majority of CRTL Hoxb8 cells were GMP-like cells and proNeus, while there was a higher presence of GMP-like cells in both *Vps18* mutant Hoxb8 cells (**Figure 18B**). On day 1 of differentiation, while the number of GMP-like cells in CTRL Hoxb8 cells was reduced to 43.9%, most of clone 1 and clone 2 remained at the GMP-like stage. The percentage of GMP-like cells in clone 1 and clone 2 was 78.0% and 83.4%, respectively. By day 2 of differentiation, when 70.5% of the CTRL cells were further developed into immature Neus, the majority of *Vps18* mutants were still at preNeu stage. Only 31.7% of clone 1 and 19.0% of clone 2 were at immature Neu stage. Whereas 11.5% of CTRL cells developed into mature Neus at day 3 of differentiation, mature Neus were barely visible in *Vps18* mutants. Compared to CTRL cells which did not contain any preNeus at day 3, 2.9% of clone 1 and 12.5% of clone 2 cells were still at preNeu stage. Additionally, in contrast to the CTRL cells containing only 6.0% of dead cells, the percentage of dead cells in clone 1 and clone 2 was 23.4% and 19.2%, respectively. At day 4 of differentiation, the CTRL cells were predominantly composed of mature Neu and immature Neu. However, the proportion of dead cells was dramatically elevated in both *Vps18* mutants, while mature Neus were almost absent in both *Vps18* mutants. These data further confirm that heterozygous mutations in *Vps18* induced a neutrophil maturation defect, leading to cell death.

3.4 Mutations in *Vps18* induced neutrophil premature apoptosis

The previous findings indicated that at the late stage of neutrophil differentiation, increased numbers of dead cell were observed in *Vps18* mutant Hoxb8 cells in comparison to CTRL cells. To further distinguish the type of cell death these *Vps18* mutants underwent, we analyzed the CTRL and *Vps18* mutant Hoxb8 cells during differentiation using a cell death panel. Here, the cell death panel comprised three different dyes: TMRM, Annexin V and SYTOX red. $TMRM^+$/Annexin V^-/SYTOX red^- cells were defined as viable cells, $TMRM^-$/Annexin V^+/SYTOX red^- cells as early apoptotic cells, and $TMRM^-$/Annexin V^+/SYTOX red^+ cells as late apoptotic cells. At day 0, both CTRL and

Vps18 mutant Hoxb8 cells showed similar proportions of viable, early and late apoptotic cells (**Figure 19A-B**).

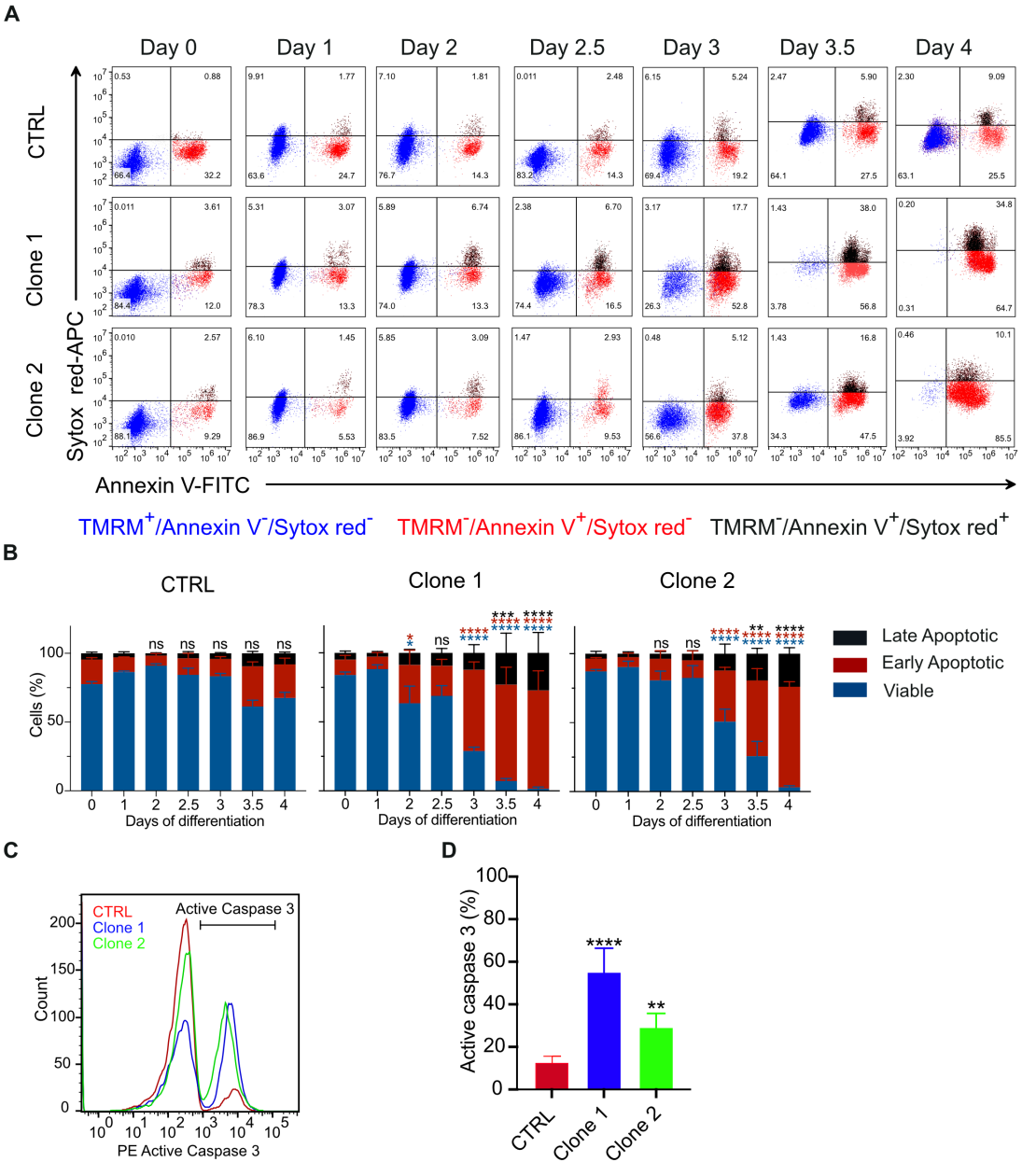

Figure 19. Cell death analysis of CTRL and *Vps18* mutant Hoxb8 cells during differentiation. **(A)** Representative dot plots of viable ($TMRM^+$/Annexin V^-/SYTOX red^-), early apoptotic ($TMRM^-$/Annexin V^+/SYTOX red^-) and late apoptotic ($TMRM^-$/Annexin V^+/SYTOX red^+) cells during differentiation (from day 0 to day 4). **(B)** of viable, early apoptotic and late apoptotic cells of all single cells (100%) during differentiation. n ≥ 3, Mean ± SD. One-way ANOVA with Tukey's multiple comparison test. * $p < 0.05$, ** $p < 0.01$, *** $p<0.001$, **** $p < 0.0001$ compared to day 0, ns = not significant. **(C)** Representative flow cytometry histogram and **(D)** quantification of active caspase 3 positive Hoxb8 cells at day 3 of differentiation in % of all single cells (100%). n = 6, Mean ± SD. One-way ANOVA with Tukey's multiple comparison test. ** $p < 0.01$, **** $p < 0.0001$ compared to CTRL.

From day 1 to day 3.5, the percentage of early apoptotic cells in CTRL Hoxb8 cells changed from 10.7% to 29.2%, while the percentage of late apoptotic cells in CTRL Hoxb8 cells changed from 2.0% to 9.5%. By day 4 of differentiation, 67.5% of CTRL Hoxb8 cells were still viable, while 24.5% of the cells underwent early apoptosis and 8.0% of the cells underwent late apoptosis. During the early stages of differentiation (from day 0 to day 2.5), the majority of both *Vps18* mutant Hoxb8 cells were viable. The percentages of early apoptotic cells were changed from 11.2% to 21.8% in clone 1 and 9.3% to 12.8% in clone 2, respectively, similar to CTRL Hoxb8 cells. However, from day 3 of differentiation onwards, the percentages of viable cells in *Vps18* mutant Hoxb8 cells were dramatically reduced, accompanied by an increase in early and late apoptotic cells. At day 4 of differentiation, the percentages of early apoptotic cells in clone 1 and clone 2 were increased to 71.3% and 73.0%, respectively. The percentage of late apoptotic cells in clone 1 and clone 2 was increased to 27.2% and 23.9%, respectively. These data show that *Vps18* mutant Hoxb8 cells die during differentiation before they are mature which we defined as premature apoptosis.

As the executioner caspase of the cell apoptosis pathway, activation of caspase 3 has been widely used as an indicator for cell apoptosis (168). To further confirm that *Vps18* mutant Hoxb8 cells underwent apoptosis, active caspase 3 in Hoxb8 cells at day 3 of differentiation was determined using flow cytometry. Here, the fraction of active caspase 3 in both *Vps18* mutants increased significantly compared to CTRL (**Figure 19C-D**). These data indicate that mutations in *Vps18* led to premature apoptosis during neutrophil maturation.

To confirm that premature apoptosis was due to mutations in *Vps18* specifically, VPS18 rescue Hoxb8 cells were analyzed using the cell death panel described above. Additionally, the presence of active caspase 3 was detected. Notably, 79.8% of VPS18 rescue Hoxb8 cells were viable at day 4 of differentiation (**Figure 20A-B**). Furthermore, in comparison to clone 1, the elevation in active caspase 3 was absent in VPS18 rescue Hoxb8 cells (**Figure 20C-D**). The level of active caspase 3 was comparable in the CTRL and VPS18 rescue Hoxb8 cells. These findings indicate that the neutrophil premature apoptosis in *Vps18* mutants was specifically caused by the mutations in *Vps18*.

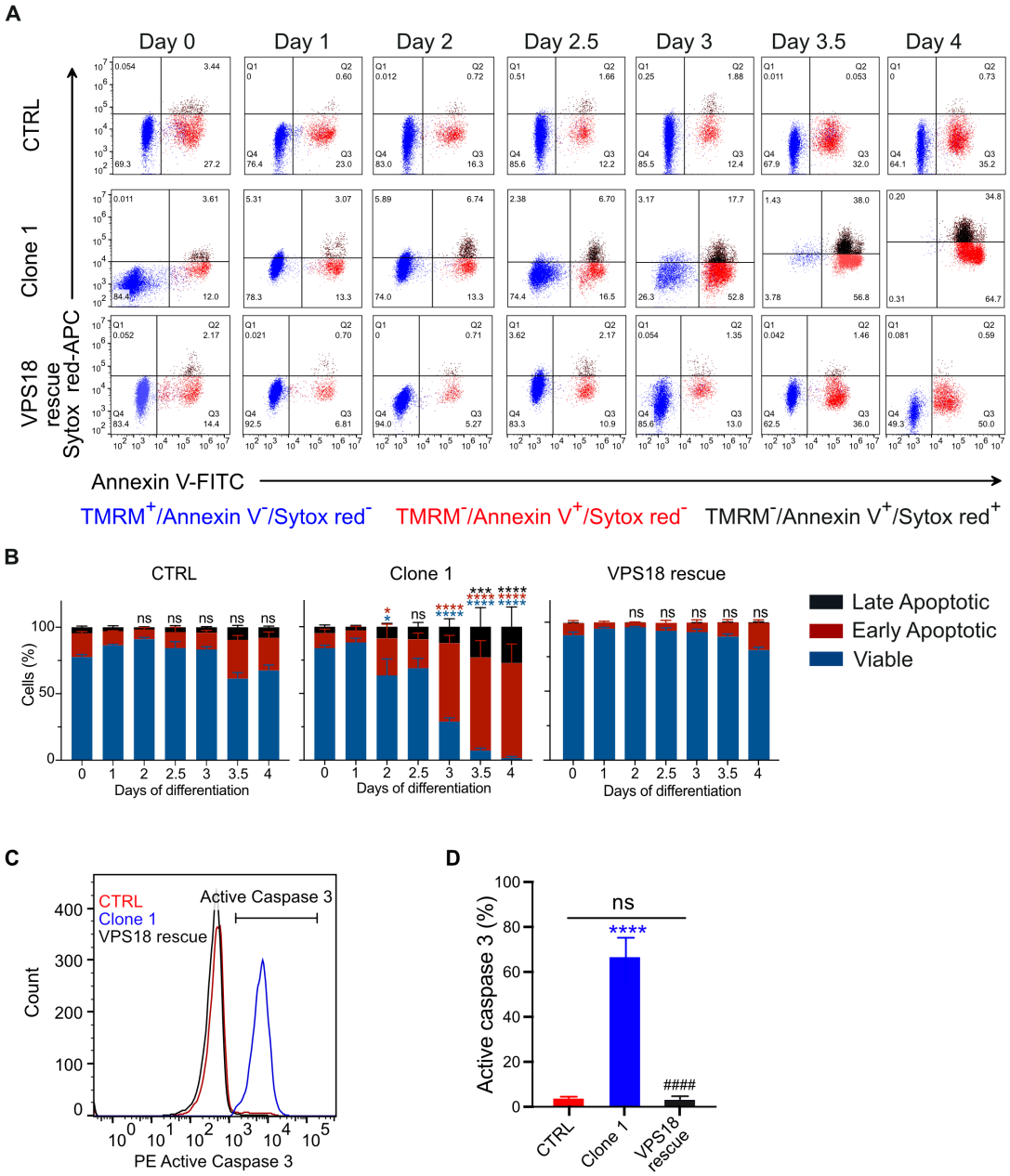

Figure 20. Cell death analysis of CTRL, clone 1 and VPS18 rescue Hoxb8 cells during differentiation. **(A)** Representative dot plots of viable ($TMRM^+$/Annexin V^-/SYTOX red^-), early apoptotic ($TMRM^-$/Annexin V^+/SYTOX red^-) and late apoptotic ($TMRM^-$/Annexin V^+/SYTOX red^+) cells during differentiation (from day 0 to day 4). **(B)** Percentage of viable, early apoptotic, and late apoptotic cells of all single cells (100%) during differentiation. n = 4, Mean ± SD. One-way ANOVA with Tukey's multiple comparison test. * $p < 0.05$, *** $p < 0.001$, **** $p < 0.0001$ compared to day 0, ns = not significant. **(C)** Representative flow cytometry histogram and **(D)** quantification of active caspase 3 positive Hoxb8 cells at day 3 of differentiation in % of all single cells (100%). n = 6, Mean ± SD. One-way ANOVA with Tukey's multiple comparison test. **** $p < 0.0001$ compared to CTRL, #### $p < 0.0001$ compared to clone 1, ns = not significant.

3.5 Inefficient reduction of VPS18 in conditional KD mouse model

To further study the role of VPS18 in neutrophil biology, a mouse line with a conditional knockdown (KD) of *Vps18* in the hematopoietic system was generated by crossing *Vav-iCre*$^{+/-}$ mice with *Vps18*$^{flox/flox}$ mice.

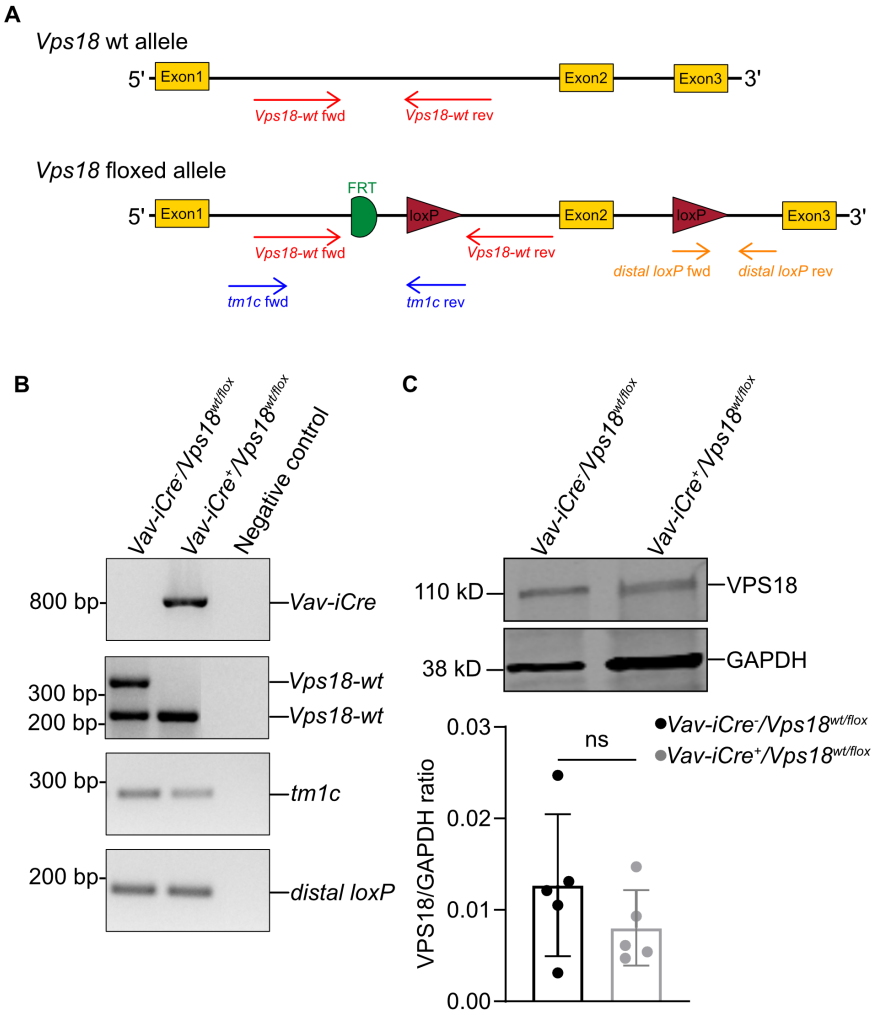

Figure 21. VPS18 expression in the conditional KD mouse model. (A) Schematic representation of *Vps18* wt and the *Vps18* floxed alleles. Yellow boxes indicate exons 1-3 of *Vps18*. Arrows represent the location of *Vps18-wt* (red), *tm1c* (blue), and *distal loxP* (orange) primer binding sites. Flippase recognition target (FRT) site: green symbol. LoxP sites: red triangles. **(B)** Representative images of gel electrophoresis of PCR products of *Vav-iCre*$^{-}$*/Vps18*$^{wt/flox}$, *Vav-iCre*$^{+}$*/Vps18* $^{wt/flox}$ and negative control with primer pairs *Vav-iCre*, *Vps18-wt*, *tm1c* and *distal loxP*, respectively. Expected band sizes are 800 bp for *Vav-iCre*, 261 bp and 409 bp for *Vps18-wt,* 255 bp for *tm1c* and 166 bp for *distal loxP*. **(C)** Representative Western blot of VPS18 and GAPDH expression (upper panel) and quantitative analysis (lower panel) of VPS18 expression in BM lysates from *Vav-iCre*$^{-}$*/Vps18*$^{wt/flox}$ and *Vav-iCre*$^{+}$*/Vps18*$^{wt/flox}$ mice. The ratio of VPS18/GAPDH was calculated and presented as a relative protein amount. Mean ± SD, n = 5. Unpaired t-test. ns = not significant.

The *Vps18* floxed allele contains a flippase recognition target (FRT) site and a loxP site before exon 2, and a second loxP site after exon 2 (**Figure 21A**). The *Vav-iCre*$^{+/-}$*/Vps18*$^{wt/flox}$ mice (*Vav-iCre*$^{+}$*/Vps18*$^{wt/flox}$) were used as target animals and *Vav-iCre*$^{-/-}$*/Vps18*$^{wt/flox}$ mice (*Vav-iCre*$^{-}$*/Vps18*$^{wt/flox}$) were used as control animals. Genotyping analysis was performed with *Vav-iCre*, *Vps18-wt*, *tm1c* and *distal loxP* primer pairs (**Table 4**). The primers *Vav-iCre* were applied to distinguish between *Vav-iCre*$^{+}$ and *Vav-iCre*$^{-}$ mice. The primers *Vps18-wt* were applied to confirm the presence of the *Vps18* wt allele (261 bp) and the *Vps18* floxed allele (409 bp) in *Vps18*$^{wt/flox}$ mice. The primers *tm1c* and *distal loxP* were applied to confirm the presence of the *Vps18* floxed allele in *Vps18*$^{wt/flox}$ mice. Here, an 800 bp band for *Vav-iCre* in *Vav-iCre*$^{+}$*/Vps18*$^{wt/flox}$ mice was observed but no band in *Vav-iCre*$^{-}$*/Vps18*$^{wt/flox}$ mice. Two bands (261 bp and 409 bp) for *Vps18-wt* were observed in *Vav-iCre*$^{-}$*/Vps18*$^{wt/flox}$ mice and one band (261 bp) in *Vav-iCre*$^{+}$*/Vps18*$^{wt/flox}$. In both *Vav-iCre*$^{-}$*/Vps18*$^{wt/flox}$ and *Vav-iCre*$^{+}$*/Vps18*$^{wt/flox}$ mice, a 255 bp band for *tm1c* and a 166 bp band for *distal loxP* were observed, suggesting a successful generation of *Vps18* KD in *Vav-iCre*$^{+}$*/Vps18*$^{wt/flox}$ mice (**Figure 21B**). To validate the VPS18 reduction in hematopoietic cells of *Vav-iCre*$^{+}$*/Vps18*$^{wt/flox}$ mice, a Western blotting analysis was performed. Unexpectedly, the expression of VPS18 in BM cells of *Vav-iCre*$^{+}$*/Vps18*$^{wt/flox}$ mice was not changed compared to *Vav-iCre*$^{-}$*/Vps18*$^{wt/flox}$ mice (**Figure 21C**). Thus, these data suggest that the Vav-iCre mouse model seemed not to be a suitable model to study the impact of *Vps18* mutations on neutrophil differentiation.

3.6 Mutations in *vps18* led to reduced neutrophil numbers in zebrafish larvae

To further investigate whether heterozygous mutations in *vps18* impair neutrophil development *in vivo*, total neutrophil numbers were quantified at 3 dpf in both *vps18* mutant Tg(*lyz:dsRed*, *vps18*$^{+/-}$ G26Δ) and Tg(*lyz:dsRed*, *vps18*$^{+/-}$ K464Δ) zebrafish lines. In these transgenic lines, neutrophils were labelled with dsRed allowing the visualization of neutrophils using a fluorescent microscope. Strikingly, the total neutrophil number in *vps18*$^{+/+}$ zebrafish larvae was 106.2, but there were only 69.8 neutrophils in *vps18*$^{+/-}$ G26Δ zebrafish larvae. (**Figure 22**). Similarly, the total neutrophil number in *vps18*$^{+/-}$ K464Δ was reduced to 88.6, compared to 110.0 neutrophils in *vps18*$^{+/+}$ zebrafish larvae. These results indicate that heterozygous mutations in *vps18* lead to a reduction in neutrophil numbers in zebrafish larvae, which is consistent with the findings in the patient 1 and *Vps18* mutant Hoxb8 cells.

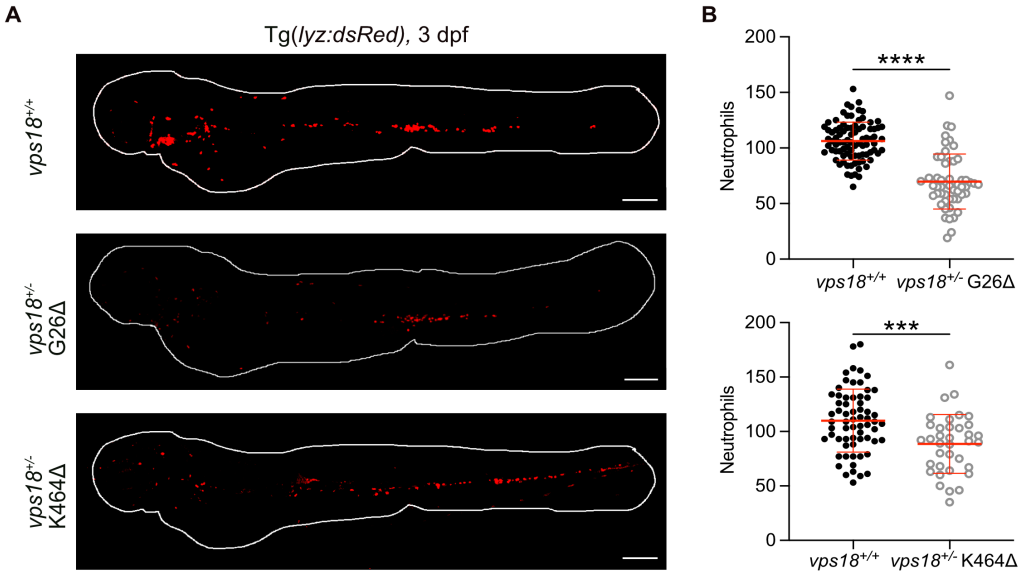

Figure 22. Total neutrophil numbers in *vps18*$^{+/+}$ and *vps18*$^{+/-}$ zebrafish larvae at 3 dpf. **(A)** Representative microscopic images of *vps*18$^{+/+}$ and *vps18*$^{+/-}$ zebrafish larvae at 3 dpf. Upper panel: *vps18*$^{+/+}$ zebrafish larva. Middle panel: *vps18*$^{+/-}$ G26Δ zebrafish larva. Lower panel: *vps18*$^{+/-}$ K464Δ zebrafish larva. Neutrophils, red. Scale bars, 200 µm. **(B)** Quantification of total neutrophil numbers in *vps*18$^{+/+}$ and *vps*18$^{+/-}$ zebrafish larvae at 3 dpf. Upper panel: total neutrophil counts in *vps*18$^{+/+}$ and *vps*18$^{+/-}$ G26Δ zebrafish larvae. Lower panel: total neutrophil counts in *vps*18$^{+/+}$ and *vps*18$^{+/-}$ K464Δ zebrafish larvae. Each dot represents one individual larva. Mean ± SD of ≥ 36 individual larvae of ≥ 5 independent experiments. Unpaired t-test. *** $p < 0.001$, **** $p < 0.0001$.

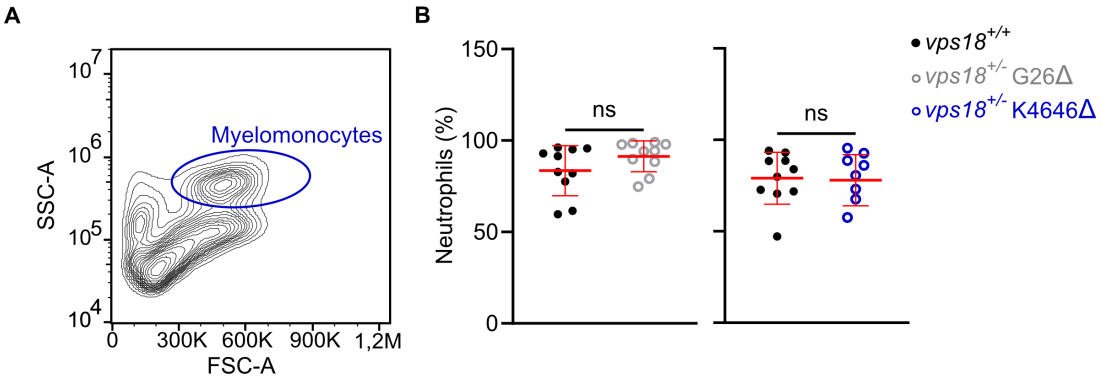

Figure 23. Flow cytometric analysis of WKM cells in two-year-old *vps18*$^{+/+}$ and *vps18*$^{+/-}$ zebrafish. **(A)** Gating strategy to define myelomonocytes from WKM cells by SSC and FSC profiles. **(B)** Percentage of neutrophils (dsRed^{+} cells) of myelomonocytes (100%) from the WKM cells of adult zebrafish. Left panel: percentage of neutrophils in *vps18*$^{+/+}$ and *vps18*$^{+/-}$ G26Δ zebrafish. Right panel: percentage of neutrophils in *vps*18$^{+/+}$ and *vps*18$^{+/-}$ K464Δ zebrafish. Mean ± SD ≥ 8 individual adult zebrafish of ≥ 2 independent experiments. Unpaired t-test.

According to the clinical information (personal communication by Prof. Dr. Christoph Klein), the patient 1's father carries the same mutation in *VPS18* but exhibits normal neutrophil counts. To elucidate whether neutrophil counts can normalize with age, akin to what has been shown in transient neutropenia, neutrophil counts of adult zebrafish were analyzed. Remarkably, flow cytometric analysis of the WKM in two-year-old adult zebrafish revealed that the percentage of neutrophils from all myelomonocytes in *vps18*$^{+/-}$ G26Δ zebrafish (91.4%) was comparable to that in *vps18*$^{+/+}$ zebrafish (83.5%). The *vps18*$^{+/-}$ K464Δ zebrafish (77.9%) also showed similar neutrophil amounts as *vps18*$^{+/+}$ zebrafish (79.0%) (**Figure 23**). Taken together, these data suggest that the patient 1 might suffer from transient neutropenia which is characterized by resolving neutrophil counts during childhood and adolescence.

3.7 Vps18 was dispensable for neutrophil migration in zebrafish larvae

To decipher whether the mutations in *vps18* impact the recruitment of residual neutrophils, I next evaluated the neutrophil migration behavior during steady state and sterile inflammation in *vps18* mutant Tg(*fli1:gfp;lyz:dsRed*, *vps18*$^{+/-}$ G26Δ) zebrafish larvae at 5 dpf. Here, GFP expression is under control of the *fli1* promoter to specifically label endothelial cells and dsRed expression is under the control of *lyz* promoter to specifically label neutrophils. Therefore, endothelial cells and neutrophils were visualized as green and red, respectively with a fluorescent microscope.

3.7.1 Residual Vps18 was sufficient to sustain normal neutrophil migration during steady state

Live imaging of non-injured zebrafish larvae was performed with a confocal microscope. Individual neutrophil in the head region was tracked and recorded for 15 min (**Figure 24A**). Within the 15 min tracking period, neutrophils in vps18+/+ zebrafish larvae showed a spontaneous migration velocity of 3.3 ± 0.2 μm/min and a Euclidean migration distance of 28.9 ± 3.0 μm (**Figure 24B**). Neutrophils of vps18+/- G26Δ zebrafish showed a similar spontaneous migration velocity of 3.9 ± 0.3 μm/min and a Euclidean migration distance of 31.4 ± 5.0 μm. Thus, these data suggest that the residual Vps18 was sufficient for neutrophil migration at steady state.

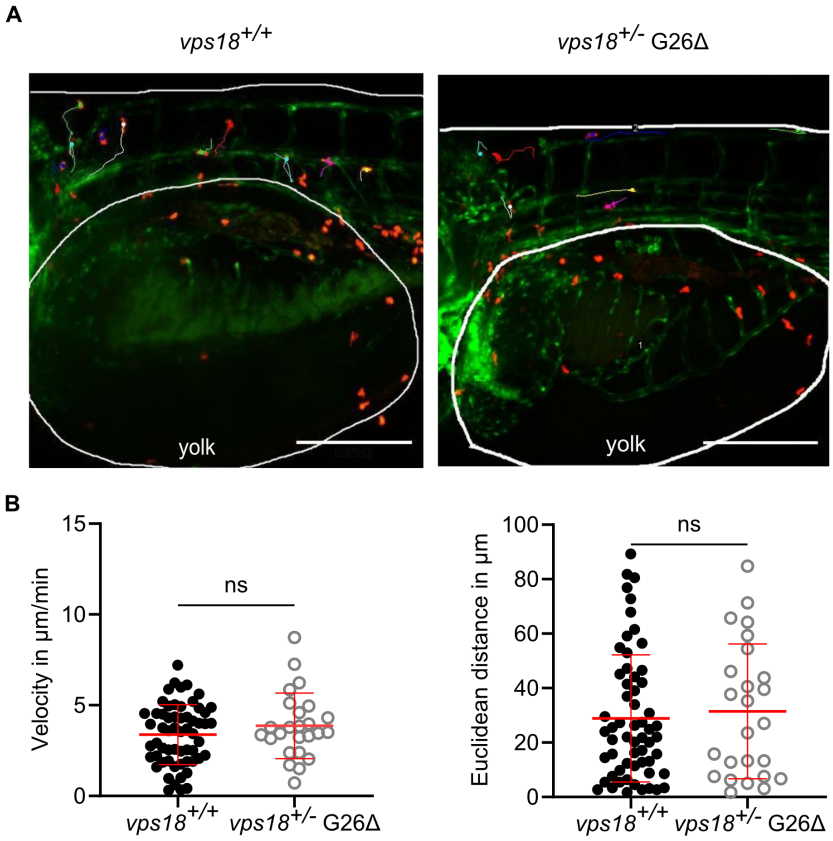

Figure 24. Neutrophil spontaneous migration at steady state in *vps18*$^{+/+}$ and *vps18*$^{+/-}$ G26Δ zebrafish larvae at 5 dpf. (A) Representative images of neutrophil spontaneous migration tracked in the head area of *vps18*$^{+/+}$ and *vps18*$^{+/-}$ G26Δ zebrafish larvae at 5 dpf. The lines indicate tracking of individual neutrophils within 15 min. Neutrophils, red. Endothelial cells, green. Scale bar, 200 µm. **(B)** Quantification of mean migration velocity and Euclidean migration distance of individual neutrophils within 15 min. Mean ± SD of ≥ 25 individual neutrophils of ≥ 9 zebrafish larvae of 4 independent experiments. Unpaired t-test. ns = not significant.

3.7.2 Residual Vps18 was sufficient to sustain efficient neutrophil migration to sites of injury

To further elucidate the impact of *vps18* mutations in neutrophil migration during inflammation in zebrafish larvae, sterile inflammation was induced by a tail fin transection in *vps18*$^{+/+}$ and *vps18*$^{+/-}$ G26Δ zebrafish larvae. The numbers of recruited neutrophils at the wound site were counted manually at 0, 1, 3 and 6 hpw, respectively (**Figure 25A**). At 0 hpw, the numbers of residual neutrophils at the wound in *vps18*$^{+/+}$ and *vps18*$^{+/-}$ G26Δ zebrafish larvae were 2.0 ± 0.4 and 1.8 ± 0.3, respectively (**Figure 25B**). From 1 hpw onwards, the number of neutrophils recruited to the wound site increased in both *vps18*$^{+/+}$ and *vps18*$^{+/-}$ G26Δ zebrafish larvae. In *vps18*$^{+/+}$ zebrafish larvae, 5.8 ± 0.6 neutrophils were found at the wound site at 1 hpw, 12.2 ± 1.3 at 3 hpw, and 21.8 ± 2.1 at 6 hpw,

respectively. However, at all-time points fewer neutrophils were present at the wound site in *vps18*$^{+/-}$ G26Δ zebrafish larvae (4.0 ± 0.6 at 1 hpw, 8.6 ± 0.9 at 3 hpw and 16.4 ± 1.6 at 6 hpw, respectively) compared to *vps18*$^{+/+}$ zebrafish larvae. Given the differences in total neutrophil counts in *vps18*$^{+/+}$ and *vps18*$^{+/-}$ G26Δ zebrafish larvae, the neutrophil recruitment efficiency was analyzed by calculating the ratio of recruited neutrophils to total neutrophils. Both *vps18*$^{+/+}$ and *vps18*$^{+/-}$ G26Δ zebrafish larvae showed a similar neutrophil recruitment efficiency over time (**Figure 25B**), indicating that the reduced neutrophil numbers at the wound site were due to the neutropenia in the *vps18*$^{+/-}$ G26Δ zebrafish larvae. These data suggest that residual Vps18 was sufficient for neutrophil migration to the sites of injury. Taken together, these data suggest that mutations in *vps18* are dispensable for neutrophil migration both during steady state and sterile inflammation. Furthermore, these data indicate that mutations in *vps18* cause premature apoptosis in neutrophils during differentiation and that the residual neutrophils are functionally normal.

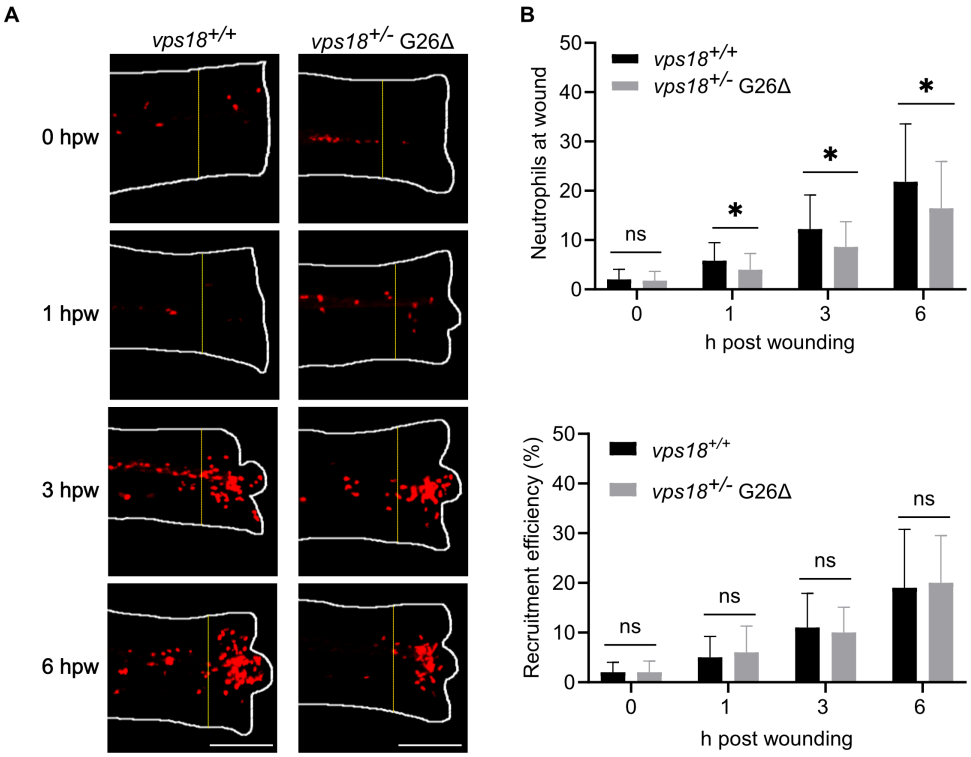

Figure 25. Neutrophil recruitment after tail fin transection in *vps18*$^{+/+}$ and *vps18*$^{+/-}$ G26Δ zebrafish larvae at 5 dpf. **(A)** Representative images of exemplary maximum intensity projections of neutrophils recruited to the wound at 0, 1, 3 and 6 hpw. Neutrophils, red. Scale bar, 200 µm. Yellow dashed lines indicate the area of recruited neutrophils analyzed (200 µm away from the wound). **(B)** Quantification of neutrophil numbers at the wound (upper panel) and recruitment efficiency (%) (lower panel) in *vps18*$^{+/+}$ and *vps18*$^{+/-}$ G26Δ zebrafish larvae upon sterile injury at 0, 1, 3 and 6 hpw. Mean ± SD of ≥ 26 individual larvae of ≥ 3 independent experiments. One-way ANOVA with Tukey's multiple comparison test. * $p < 0.05$, ns = not significant.

4. Discussion

An adequate number of mature neutrophils in the circulation is critical for innate immune homeostasis (31). CN patients typically suffer from recurrent and life-threatening infections due to insufficient neutrophil numbers in peripheral blood (35). Until now, the global prevalence of CN remains unknown. However, it is estimated to be 2 cases per million individuals in Europe (169-173). To date, mutations in several genes have been identified as the underlying cause of CN (35, 174-178). It is estimated that 45% of CN cases are caused by mutations in *ELANE*, 14% by mutations in *SBDS*, 12% by mutations in *G6PT* and 7% by mutations in *HAX1* (35). The mechanisms of these mutations have been well investigated. Here, impaired intracellular vesicle trafficking has been identified as one of the underlying mechanisms (41, 154, 179-182). The function of VPS18 in intracellular vesicle trafficking have been elucidated (90, 94, 95). Patient 1 carrying a heterozygous mutation in *VPS18* was suffering from neutropenia and recurrent infections (personal communication by Prof. Dr. Christoph Klein). However, the function of VPS18 in neutrophil biology remained exclusive. In the present study, the functional importance of VPS18 for neutrophil biology with an emphasis on neutrophil development was analyzed in detail.

4.1 Ortholog of VPS18 among humans, mice and zebrafish

In the first part of the study, the identity and similarity of the sequences of VPS18 protein and its five main domains were compared among men, mice and zebrafish. Both mice and zebrafish VPS18 showed high identity and similarity with human VPS18. Within VPS18, the β-propeller, CC, CHCR and RING domains are conserved across humans, mice and zebrafish, suggesting that also the function of VPS18 is conserved across species and that mouse and zebrafish are suitable models for studying the function of VPS18. Indeed, neural-specific *Vps18* KO mice showed disturbances in the endolysosomal pathway (100). Similar phenotypes were observed in morpholino-induced *vps18* KD zebrafish larvae, which showed a reduced number of lysosomes, accompanied by the accumulation of endosomal cargo (86). Moreover, a decreased count of pigment granules in the pigmented epithelia of the epidermis and retina was observed in these zebrafish larvae. In line with this, neural cells of CRISPR/Cas9-induced *vps18* mutant zebrafish larvae were characterized by an increased number and size of autophagosomes compared to *vps18*

WT zebrafish (183). Taken together, these findings suggest that the function of VPS18 for intracellular trafficking might be conserved across species.

4.2 VPS18 downregulation in heterozygous *Vps18* mutants

In the present study, CTRL Hoxb8 cells and two heterozygous *Vps18* mutant Hoxb8 cell lines were used as an *in vitro* model. Both mutant cell lines harbored heterozygous mutations in *Vps18* which mimic the genotype of the *VPS18* mutant neutropenic patient 1 (compare chapter 1.2.3). Interestingly, during the generation of *Vps18* mutants, no homozygous *Vps18* mutant cells were obtained (personal communication by Dr. Daniela Maier-Begandt), suggesting that a complete loss of *Vps18* is lethal. In the heterozygous *Vps18* mutants with one allele absent, a reduction of VPS18 to 50% was expected. Indeed, the expression of VPS18 in both *Vps18* mutants was reduced by approximately 50% compared to CTRL Hoxb8 cells. The *Vps18* mutant Hoxb8 progenitor cells were viable with half amount of VPS18 expression, leading to the theory that the residual amount of VPS18 was sufficient for the survival of myeloid progenitors. Similar theories have been reported previously for other proteins. For instance, mice with a complete absence of myosin heavy chain (Myh9) in their hematopoietic system were lethal (113). Likewise, Klapproth et al. reported that a certain amount of kindlin-3 in mouse hematopoietic cells is necessary for embryonic and postnatal development (184). *In vivo*, our homozygous *vps18* mutant zebrafish cannot reach adulthood (personal communication by Dr. Daniela Maier-Begandt). Similarly, zebrafish larvae with homozygous mutations in *vps18* generated by others also died after 5 dpf (99, 183). Further, *vps18* KD zebrafish embryos that were generated with high morpholino concentrations were unable to develop properly (86). In mice, Peng et al. reported that a complete deletion of *Vps18* resulted in embryonic or early postnatal lethality (100). Moreover, mice with neural-specific *Vps18* KO cannot survive beyond P12 and suffered from severe postnatal growth retardation. Based on these data, our findings suggest the necessity of a critical threshold level of VPS18 expression for cell survival.

4.3 Effect of *VPS18* mutations on neutrophil maturation

The BM maturation arrest in CN patients has been elucidated as a cause for the diminished neutrophil counts in peripheral blood (35). In the present study, analysis of neutrophil maturation in CTRL and *Vps18* mutant Hoxb8 cells during differentiation was

performed to verify the neutrophil maturation defect which has been observed in the patient 1. Here, two classification systems were employed to determine the neutrophil maturation stages during differentiation. The classic determination model is based on the morphological alterations during neutrophil development (18, 22, 23). Here, neutrophil progenitors from different maturation stages are defined based on the distinctive morphology of the nucleus, nuclear-to-cytoplasmic ratio and granule content (23). Using this approach, *Vps18* mutant Hoxb8 cells were shown to have a delayed neutrophil maturation compared to CTRL Hoxb8 cells. Moreover, an increased number of dead cells was observed in *Vps18* mutant Hoxb8 cells during the later stage of neutrophil maturation. However, this classical approach has some limitations. The morphological and histochemical observations are subjective. Moreover, the manual quantification of a limited number of cells rendered it imprecise. Recently, a new classification system was proposed which is based on the immune phenotypes of neutrophils during differentiation (20, 21). Stage-specific markers expressed on the surface of neutrophil progenitors during development enabled us to distinguish neutrophil progenitors from different maturation stages. Analysis of the CTRL and *Vps18* mutant Hoxb8 cells using this novel classification system further validated our previous finding that *Vps18* mutant Hoxb8 cells showed a neutrophil maturation defect. Based on published data, there are several explanations for this phenotype. A possible explanation as to why mutations in *Vps18* led to impaired neutrophil maturation might be that the mutations in *Vps18* impaired the autophagy pathway. Previous studies in mice neurons suggested that mutations in *Vps18* led to impaired fusion between autophagosomes and lysosomes, resulting in an accumulation of autophagosomes (100). Moreover, Riffelmacher et al. demonstrated that autophagy is essential for neutrophil metabolism during differentiation (185). Here, free fatty acids are generated by autophagy, subsequently degraded and utilized for energy production by mitochondrial respiration. Thus, a lack of VPS18 which was reported to impair the autophagosomal degradation pathway might lead to a lack of energy. Therefore, a disturbance of the autophagy pathway might account for impaired neutrophil maturation in *Vps18* mutant Hoxb8 cells during differentiation.

Of note, it has been documented CN patients often suffer from a neutrophil maturation arrest at the promyelocyte stage (177, 186). However, in our case, mutations in *VPS18* seem to block neutrophil maturation at the metamyelocyte or band cell stage (non-proliferative stage). A possible explanation is that the residual amount of VPS18 protein might be sufficient for efficient neutrophil maturation at the early stage of differentiation. At the

late maturation stages, the metamyelocytes or band cells might have an increased requirement of vesicle trafficking for further maturation (154, 179, 180, 182), indicating that more VPS18 protein might be needed for this process. Thus, the residual expression of VPS18 protein in *Vps18* mutants might not be sufficient for further differentiation, resulting in a maturation arrest at the metamyelocyte or band cell stage.

4.4 Impact of *Vps18* mutations on neutrophil survival during maturation

Upon differentiation, a higher number of dead cells was observed in *Vps18* mutant Hoxb8 cells compared to CTRL cells. To further determine the type of cell death experienced by *Vps18* mutant Hoxb8 cells, a cell death analysis was conducted using flow cytometry. During the late stage of neutrophil differentiation, an increased percentage of apoptotic cells was observed in *Vps18* mutant Hoxb8 progenitor cells compared to CTRL cells, suggesting that *Vps18* mutant Hoxb8 cells underwent apoptosis which we defined as premature apoptosis. Moreover, an increased caspase 3 activation was detected in both *Vps18* mutant Hoxb8 cells compared to CTRL cells, which further confirmed that the cells underwent apoptosis. These findings were in line with previous reports for *Vps18* deficient neurons, where an elevated level of activated caspase 3 was observed (100). Active caspase 3 is a protease that plays a central role in cell apoptosis (187). Consequently, active caspase 3 has been considered as a reliable marker for apoptosis. However, Wang et al. reported that chemotherapy drugs treated Hela cells underwent GSDME-dependent pyroptosis, following the activation of caspase 3, suggesting that active caspase 3 was also involved in the pyroptosis pathway (188). Pyroptosis is a pro-inflammatory programmed cell death, which is characterized by pore formation in the plasma membrane but intact nucleus (189). In general, Annexin V and Sytox red staining is considered to be specific for detecting apoptotic cells (190). However, Annexin V also stains pyroptotic cells, while Sytox red does not. Thus, it is likely that *Vps18* mutant Hoxb8 cells died by apoptosis. In addition, premature apoptosis was absent when expression of VPS18 was rescued in VPS18 rescue cells, indicating that the observed premature apoptosis in *Vps18* mutants was specifically caused by a decreased VPS18 expression.

Previous studies have shown that in multiple cases of CN patients, their neutrophil progenitors underwent premature apoptosis (111, 177, 191, 192). One underlying mechanism was explained by persistent endoplasmic reticulum (ER) stress in these cells. Protein

folding by the ER is critical for protein biosynthesis. Abnormal folding or mislocating of proteins leads to ER stress (42). Unmitigated ER stress ultimately causes increased cell apoptosis. For instance, the upregulation of several ER stress markers, including X-box binding protein-1 (XBP1) splicing, binding immunoglobulin protein (Bip) and C/EBP homologous protein (CHOP) has been observed in *ELANE* mutant neutrophils, indicating the persistence of ER stress (38). These cells underwent premature apoptosis due to the unmitigated ER stress. Interestingly, premature apoptosis and disturbances of intracellular trafficking have been observed in *VPS45* mutant neutrophils (154, 193, 194). However, the potential increase in ER stress in these cells was not investigated. Whether mutations in *VPS18* induce ER stress is not known to date. Another underlying mechanism of premature apoptosis has been described through impaired mitochondrial function, as neutrophil differentiation is an energy-demanding process that requires proper mitochondrial function (185). As an anti-apoptotic protein which is predominantly located in mitochondria, HAX1 plays a fundamental role in maintenance of mitochondrial homeostasis (177). Deficiency of HAX1 leads to impaired mitochondrial function, leading to increased neutrophil premature apoptosis. Previous studies have shown that impaired autophagy led to impaired mitochondrial respiration (185). Moreover, impaired autophagy has been observed in *VPS18* mutant cells (100, 183). However, whether the function of mitochondria was influenced by *VPS18* mutations has not been studied. Taken together, the link between impaired vesicle trafficking and premature apoptosis in *Vps18* mutants needs to be further investigated.

4.5 *Vav-iCre*$^{+}$/*Vps18*$^{wt/flox}$ mouse model to study neutrophil maturation

To further explore the effect of VPS18 on neutrophil maturation *in vivo*, we generated a *Vps18* conditional mutant mouse line by crossing *Vav-iCre*$^{+/-}$ mice with *Vps18*$^{flox/flox}$ mice. The Vav-iCre transgenic line can drive Cre expression in all hematopoietic cells (195-198), thereby a downregulation of VPS18 was expected in *Vav-iCre*$^{+}$/*Vps18*$^{wt/flox}$ mice. However, in our case, the expression of VPS18 in hematopoietic cells was similar between *Vav-iCre*$^{-}$/*Vps18*$^{wt/flox}$ and *Vav-iCre*$^{+}$/*Vps18*$^{wt/flox}$ mice, indicating an inefficient reduction of VPS18 protein in hematopoietic cells in *Vav-iCre*$^{+}$/*Vps18*$^{wt/flox}$ mice. Thus, the *Vav-iCre*$^{+}$/*Vps18*$^{wt/flox}$ mice cannot be used to investigate the impact of *Vps18* mutations on neutrophil development. This is in accordance with Frey et al.'s recent findings that the inefficient deletion of VPS45 in the hematopoietic cells of *Vav-iCre*$^{+}$/*Vps45*$^{-/-}$ mice, suggesting that *Vav-iCre*$^{+}$/*Vps45*$^{-/-}$ mice cannot be used as an *in vivo* model to study the

function of VPS45 for neutrophil maturation (194). However, the reason for the inefficient deletion was not investigated. Nevertheless, one possible explanation for our case might be that a compensatory regulation of residual *Vps18* gene expression leads to normal protein levels of VPS18 in the hematopoietic cells of *Vav-iCre*$^{+}$/*Vps18*$^{wt/flox}$ mice. Interestingly, it has been reported that several mouse lines with neutropenia-associated genetic defects were not suitable as *in vivo* models for studying neutrophil maturation, as they cannot mimic the neutropenic phenotype observed in humans. (199-202). For instance, *Hax1* ko mice displayed a complete depletion of HAX1 but normal granulopoiesis (199, 200). Likewise, no NE protein was detected in *Elane* ko mice, but they showed normal granulopoiesis (201, 202). These findings indicate that the *in vivo* mouse model is not an appropriate model to study neutropenia.

4.6 Role of VPS18 for neutrophil development in zebrafish

In the past, zebrafish have been widely utilized as an *in vivo* model to investigate the impact of genetic mutations on neutrophil development (154, 199, 203). *Vps45* KO zebrafish larvae showed a significant decrease in neutrophil numbers, mirroring the observations in patients with mutations in *VPS45*. Consistent with the findings in *HAX1* mutant patients, the *hax1* KD zebrafish larvae exhibited impaired neutrophil development and disruption of the G-csf signaling pathway. Similarly, the phenotypes of the signal recognition particle *(srp)54*$^{+/-}$ zebrafish were also akin to the patients with mutations in *SRP54* who suffered from neutropenia and pancreatic insufficiency. In the present study, the total number of neutrophils was significantly diminished in both *vps18*$^{+/-}$ mutant Tg(*lyz:dsRed*, *vps18*$^{+/-}$ G26Δ) and Tg(*lyz:dsRed*, *vps18*$^{+/-}$ K464Δ) zebrafish lines compared to Tg(*lyz:dsRed*, *vps18*$^{+/+}$) zebrafish larvae, indicating that heterozygous mutations in *vps18* lead to reduced neutrophil numbers in zebrafish larvae. The *vps18*$^{+/-}$ mutant lines used in this study were generated by CRISPR/Cas9 technique. Here, both *vps18*$^{+/-}$ mutant lines showed reduced neutrophil numbers, indicating that this phenotype was not due to off-target effects of CRISPR/Cas9 gene editing technique.

Intriguingly, the father of the *VPS18* mutant patient also harbors the same mutation but remains clinically healthy. This led to the hypothesis that the patient might suffer from transient neutropenia with neutrophil counts improving with age (203). Unfortunately, the neutrophil counts of patient 1's father during his childhood were not available. Nevertheless, to verify the hypothesis, I quantified the neutrophil numbers from the WKM

(equivalent to hematopoietic BM in mammals) of two-year-old *vps18*$^{+/+}$ and *vps18*$^{+/-}$ adult zebrafish with flow cytometry analysis. Similar to the human situation, neutrophil counts of the adult zebrafish in both *vps18*$^{+/-}$ mutants were normal compared to *vps18*$^{+/+}$ zebrafish. However, the underlying mechanisms were not elucidated. It was reported that some children showed reduced neutrophil numbers during their childhood, but their neutrophil counts were resolved as they grew up (204). Another explanation why the father seems not to be affected, could be that the patient's neutropenia was gender related. However, the neutrophil counts between male and female *vps18*$^{+/-}$ adult zebrafish were similar (data not shown). Additionally, one could speculate that not every individual with mutations in *VPS18* develops neutropenia, which is known as incomplete penetrance. This has been reported before in paitents with mutation in *VPS33A,* another subunit of CORVET and HOPS complexes. Here, five patients carried the same mutation in *VPS33A*, yet one of them had normal neutrophil counts (78).

4.7 Function of Vps18 for neutrophil migration in zebrafish larvae

As highly motile phagocytes in the innate immune system, neutrophils play an essential role in host defense against pathogenic microorganisms (1). Patients with leukocyte adhesion deficiency (LAD) suffer from life-threatening recurrent bacterial infections owing to defective neutrophil recruitment (205). Patient 1 was also suffering from recurrent infections, suggesting that she had a defect in innate immunity. Thus, the recurrent infections might be due to impaired neutrophil functions, encompassing recruitment and bacterial killing. To analyze whether neutrophil recruitment to sites of inflammation and neutrophil migration in general were affected by mutations in *vps18*, neutrophil migration was analyzed in the zebrafish model. In general, *mpx* and *lyz* promoters are widely used to label neutrophil specifically in zebrafish (130, 144, 146, 147). Renshaw et al. initially established a transgenic zebrafish model that expresses GFP under the neutrophil specific *mpx* promoter (206). Hence, migration of neutrophils could be visualized in individual living zebrafish larvae using a fluorescent microscope. However, some groups reported that *mpx* might not be specific for neutrophils since a weak signal in macrophages has been observed in 3 dpf zebrafish larvae (147, 148). Hall et al. generated a transgenic zebrafish model in which the *lyz* promoter was used to drive expression of GFP or dsRed specifically in neutrophils (146). From 48 hpf onwards, the *lyz* promoter is active specifically in neutrophils (149, 150).

In the present study, we utilized the transgenic zebrafish line expressing dsRed under the *lyz* promoter to specifically label neutrophils to study the neutrophil migration behavior. Here, the migratory function of neutrophils in zebrafish larvae was not altered upon heterozygous mutations in *vps18*, neither at steady state nor during acute inflammation, suggesting that the residual Vps18 protein might be adequate to maintain a normal migratory capacity of mutant neutrophils. This is in line with data from *srp54*$^{+/-}$ neutropenic zebrafish larvae. Here, the residual Srp54 protein was sufficient to maintain the migratory function of neutrophils to sites of injury (203). The unaffected neutrophil migration in *vps18* mutant zebrafish larvae suggests that recurrent infections of patient 1 might be due to the overall low neutrophil numbers or other potentially affected neutrophil functions, such as the phagocytosis ability, ROS production, degranulation ability or NETs formation. In addition, as an essential process in neutrophil host defense, the release of granule components is tightly controlled by intracellular vesicle trafficking within neutrophils (207). Nonetheless, further analysis needs to be done to verify this hypothesis.

4.8 Conclusion

In summary, the role of VPS18 in neutrophil biology was studied. Both our *in vitro* and *in vivo* models showed reduced neutrophil numbers. These findings were consistent with the patient 1's phenotype. In addition, the neutrophil maturation defect and premature apoptosis in *Vps18* mutants suggest that these were the underlying mechanisms of neutropenia of the patient 1. Notably, the remaining expression of Vps18 seemed to be sufficient to sustain neutrophil migration either at steady state or during sterile inflammation. Moreover, the present study also indicates that the *Vav-iCre*$^{+}$/*Vps18*$^{+/-}$ mice might not be a suitable *in vivo* model to analyze the role of VPS18 in neutrophil development. Previous studies have identified impaired intracellular vesicle trafficking as a pathophysiological mechanism of neutropenia and neutrophil maturation arrest (41, 154, 179-182). As the importance of VPS18 in intracellular vesicle trafficking has been reported before (86, 90, 94-100), the phenotypes caused by *VPS18* mutations might be explained by the disruption of intracellular vesicle trafficking. In summary, deciphering the role of VPS18 in neutrophil biology provided novel molecular insights into the putative mechanisms of a novel congenital neutropenia syndrome.

References

1. Ley K, Laudanna C, Cybulsky MI, Nourshargh S. Getting to the site of inflammation: the leukocyte adhesion cascade updated. Nat Rev Immunol. 2007;7(9):678-89.

2. Lawrence SM, Corriden R, Nizet V. How Neutrophils Meet Their End. Trends Immunol. 2020;41(6):531-44.

3. Schymeinsky J, Sperandio M, Walzog B. The mammalian actin-binding protein 1 (mAbp1): a novel molecular player in leukocyte biology. Trends Cell Biol. 2011;21(4):247-55.

4. Blanter M, Gouwy M, Struyf S. Studying Neutrophil Function in vitro: Cell Models and Environmental Factors. J Inflamm Res. 2021;14:141-62.

5. Boeltz S, Amini P, Anders H-J, Andrade F, Bilyy R, Chatfield S, et al. To NET or not to NET:current opinions and state of the science regarding the formation of neutrophil extracellular traps. Cell Death Differ. 2019;26(3):395-408.

6. Kolaczkowska E, Kubes P. Neutrophil recruitment and function in health and inflammation. Nat Rev Immunol. 2013;13(3):159-75.

7. LeBert DC, Squirrell JM, Rindy J, Broadbridge E, Lui Y, Zakrzewska A, et al. Matrix metalloproteinase 9 modulates collagen matrices and wound repair. Development. 2015;142(12):2136-46.

8. Talukdar S, Oh DY, Bandyopadhyay G, Li D, Xu J, McNelis J, et al. Neutrophils mediate insulin resistance in mice fed a high-fat diet through secreted elastase. Nat Med. 2012;18(9):1407-12.

9. Shojaei F, Singh M, Thompson JD, Ferrara N. Role of Bv8 in neutrophil-dependent angiogenesis in a transgenic model of cancer progression. Proc Natl Acad Sci U S A. 2008;105(7):2640-5.

10. Nemeth T, Mocsai A. The role of neutrophils in autoimmune diseases. Immunol Lett. 2012;143(1):9-19.

11. Dixon G, Elks PM, Loynes CA, Whyte MK, Renshaw SA. A method for the in vivo measurement of zebrafish tissue neutrophil lifespan. ISRN Hematol. 2012;2012:915868.

12. Pillay J, den Braber I, Vrisekoop N, Kwast LM, de Boer RJ, Borghans JA, et al. In vivo labeling with 2H2O reveals a human neutrophil lifespan of 5.4 days. Blood. 2010;116(4):625-7.

13. Basu S, Hodgson G, Katz M, Dunn AR. Evaluation of role of G-CSF in the production, survival, and release of neutrophils from bone marrow into circulation. Blood. 2002;100(3):854-61.

14. Summers C, Rankin SM, Condliffe AM, Singh N, Peters AM, Chilvers ER. Neutrophil kinetics in health and disease. Trends Immunol. 2010;31(8):318-24.

15. Colotta F, Re F, Polentarutti N, Sozzani S, Mantovani A. Modulation of granulocyte survival and programmed cell death by cytokines and bacterial products. Blood. 1992;80(8):2012-20.

16. Kim MH, Granick JL, Kwok C, Walker NJ, Borjesson DL, Curry FR, et al. Neutrophil survival and c-kit(+)-progenitor proliferation in Staphylococcus aureus-infected skin wounds promote resolution. Blood. 2011;117(12):3343-52.

17. Borregaard N. Neutrophils, from marrow to microbes. Immunity. 2010;33(5):657-70.

18. Lawrence SM, Corriden R, Nizet V. The Ontogeny of a Neutrophil: Mechanisms of Granulopoiesis and Homeostasis. Microbiol Mol Biol Rev. 2018;82(1).

19. Yvan-Charvet L, Ng LG. Granulopoiesis and Neutrophil Homeostasis: A Metabolic, Daily Balancing Act. Trends Immunol. 2019;40(7):598-612.

20. Evrard M, Kwok IWH, Chong SZ, Teng KWW, Becht E, Chen J, et al. Developmental Analysis of Bone Marrow Neutrophils Reveals Populations Specialized in Expansion, Trafficking, and Effector Functions. Immunity. 2018;48(2):364-79 e8.

21. Kwok I, Becht E, Xia Y, Ng M, Teh YC, Tan L, et al. Combinatorial Single-Cell Analyses of Granulocyte-Monocyte Progenitor Heterogeneity Reveals an Early Uni-potent Neutrophil Progenitor. Immunity. 2020;53(2):303-18 e5.

22. Pillay J, Tak T, Kamp VM, Koenderman L. Immune suppression by neutrophils and granulocytic myeloid-derived suppressor cells: similarities and differences. Cell Mol Life Sci. 2013;70(20):3813-27.

23. Bjerregaard MD, Jurlander J, Klausen P, Borregaard N, Cowland JB. The in vivo profile of transcription factors during neutrophil differentiation in human bone marrow. Blood. 2003;101(11):4322-32.

24. Claus Hammer GK. Cytology in transplantation: Kempten Shulz; 1989.

25. Grindem CB, Neel JA, Juopperi TA. Cytology of bone marrow. Vet Clin North Am Small Anim Pract. 2002;32(6):1313-74, vi.

26. Cowland JB, Borregaard N. Granulopoiesis and granules of human neutrophils. Immunol Rev. 2016;273(1):11-28.

27. Faurschou M, Borregaard N. Neutrophil granules and secretory vesicles in inflammation. Microbes Infect. 2003;5(14):1317-27.

28. Martin C, Burdon PC, Bridger G, Gutierrez-Ramos JC, Williams TJ, Rankin SM. Chemokines acting via CXCR2 and CXCR4 control the release of neutrophils from the bone marrow and their return following senescence. Immunity. 2003;19(4):583-93.

29. Eash KJ, Greenbaum AM, Gopalan PK, Link DC. CXCR2 and CXCR4 antagonistically regulate neutrophil trafficking from murine bone marrow. J Clin Invest. 2010;120(7):2423-31.

30. Kaushansky K, Lichtman MA, Prchal JT, Levi MM, Press OW, Burns LJ, et al. Editors. Williams Hematology, 9e. New York, NY: McGraw-Hill Education; 2015.

31. Dale DC. How I diagnose and treat neutropenia. Curr Opin Hematol. 2016;23(1):1-4.

32. Segel GB, Halterman JS. Neutropenia in pediatric practice. Pediatr Rev. 2008;29(1):12-23; quiz 4.

33. Alexandropoulou O, Kossiva L, Haliotis F, Giannaki M, Tsolia M, Panagiotou IP, et al. Transient neutropenia in children with febrile illness and associated infectious agents: 2 years' follow-up. Eur J Pediatr. 2013;172(6):811-9.

34. Ku BC, Bailey C, Balamuth F. Neutropenia in the Febrile Child. Pediatr Emerg Care. 2016;32(5):329-34.

35. Skokowa J, Dale DC, Touw IP, Zeidler C, Welte K. Severe congenital neutropenias. Nat Rev Dis Primers. 2017;3:17032.

36. Belaaouaj A. Neutrophil elastase-mediated killing of bacteria: lessons from targeted mutagenesis. Microbes Infect. 2002;4(12):1259-64.

37. Papayannopoulos V, Metzler KD, Hakkim A, Zychlinsky A. Neutrophil elastase and myeloperoxidase regulate the formation of neutrophil extracellular traps. J Cell Biol. 2010;191(3):677-91.

38. Grenda DS, Murakami M, Ghatak J, Xia J, Boxer LA, Dale D, et al. Mutations of the ELA2 gene found in patients with severe congenital neutropenia induce the unfolded protein response and cellular apoptosis. Blood. 2007;110(13):4179-87.

39. Horwitz MS, Duan Z, Korkmaz B, Lee HH, Mealiffe ME, Salipante SJ. Neutrophil elastase in cyclic and severe congenital neutropenia. Blood. 2007;109(5):1817-24.

40. Kollner I, Sodeik B, Schreek S, Heyn H, von Neuhoff N, Germeshausen M, et al. Mutations in neutrophil elastase causing congenital neutropenia lead to cytoplasmic protein accumulation and induction of the unfolded protein response. Blood. 2006;108(2):493-500.

41. Horwitz M, Benson KF, Duan Z, Li FQ, Person RE. Hereditary neutropenia: dogs explain human neutrophil elastase mutations. Trends Mol Med. 2004;10(4):163-70.

42. Walter P, Ron D. The unfolded protein response: from stress pathway to homeostatic regulation. Science. 2011;334(6059):1081-6.

43. Dale DC, Makaryan V. ELANE-Related Neutropenia. In: Adam MP, Mirzaa GM, Pagon RA, Wallace SE, Bean LJH, Gripp KW, et al., editors. GeneReviews((R)). Seattle (WA)1993.

44. Carlsson G, Ahlin A, Dahllof G, Elinder G, Henter JI, Palmblad J. Efficacy and safety of two different rG-CSF preparations in the treatment of patients with severe congenital neutropenia. Br J Haematol. 2004;126(1):127-32.

45. Weston B, Todd RF, 3rd, Axtell R, Balazovich K, Stewart J, Locey BJ, et al. Severe congenital neutropenia: clinical effects and neutrophil function during treatment with granulocyte colony-stimulating factor. J Lab Clin Med. 1991;117(4):282-90.

46. Dale DC, Bonilla MA, Davis MW, Nakanishi AM, Hammond WP, Kurtzberg J, et al. A randomized controlled phase III trial of recombinant human granulocyte colony-stimulating factor (filgrastim) for treatment of severe chronic neutropenia. Blood. 1993;81(10):2496-502.

47. Donadieu J, Leblanc T, Bader Meunier B, Barkaoui M, Fenneteau O, Bertrand Y, et al. Analysis of risk factors for myelodysplasias, leukemias and death from infection among patients with congenital neutropenia. Experience of the French Severe Chronic Neutropenia Study Group. Haematologica. 2005;90(1):45-53.

48. Pinsk M, Burzynski J, Yhap M, Fraser RB, Cummings B, Ste-Marie M. Acute myelogenous leukemia and glycogen storage disease 1b. J Pediatr Hematol Oncol. 2002;24(9):756-8.

49. Rosenberg PS, Alter BP, Link DC, Stein S, Rodger E, Bolyard AA, et al. Neutrophil elastase mutations and risk of leukaemia in severe congenital neutropenia. Br J Haematol. 2008;140(2):210-3.

50. Schroeder T, Hildebrandt B, Mayatepek E, Germing U, Haas R. A patient with glycogen storage disease type Ib presenting with acute myeloid leukemia (AML) bearing

monosomy 7 and translocation t(3;8)(q26;q24) after 14 years of treatment with granulocyte colony-stimulating factor (G-CSF): a case report. J Med Case Rep. 2008;2:319.

51. Dror Y. Shwachman-Diamond syndrome. Pediatr Blood Cancer. 2005;45(7):892-901.

52. Yetgin S, Olcay L, Koc A, Germeshausen M. Transformation of severe congenital neutropenia to early acute lymphoblastic leukemia in a patient with HAX1 mutation and without G-CSF administration or receptor mutation. Leukemia. 2008;22(9):1797.

53. Cai H, Reinisch K, Ferro-Novick S. Coats, tethers, Rabs, and SNAREs work together to mediate the intracellular destination of a transport vesicle. Dev Cell. 2007;12(5):671-82.

54. Cui L, Li H, Xi Y, Hu Q, Liu H, Fan J, et al. Vesicle trafficking and vesicle fusion: mechanisms, biological functions, and their implications for potential disease therapy. Mol Biomed. 2022;3(1):29.

55. Gruenberg J. The endocytic pathway: a mosaic of domains. Nat Rev Mol Cell Biol. 2001;2(10):721-30.

56. Levine B, Kroemer G. Biological Functions of Autophagy Genes: A Disease Perspective. Cell. 2019;176(1-2):11-42.

57. Parzych KR, Klionsky DJ. An overview of autophagy: morphology, mechanism, and regulation. Antioxid Redox Signal. 2014;20(3):460-73.

58. Kawauchi T. Cell adhesion and its endocytic regulation in cell migration during neural development and cancer metastasis. Int J Mol Sci. 2012;13(4):4564-90.

59. Stenmark H. Rab GTPases as coordinators of vesicle traffic. Nat Rev Mol Cell Biol. 2009;10(8):513-25.

60. Bonifacino JS, Glick BS. The mechanisms of vesicle budding and fusion. Cell. 2004;116(2):153-66.

61. Wang T, Li L, Hong W. SNARE proteins in membrane trafficking. Traffic. 2017;18(12):767-75.

62. Chia PZ, Gleeson PA. Membrane tethering. F1000Prime Rep. 2014;6:74.

63. Ungermann C, Kummel D. Structure of membrane tethers and their role in fusion. Traffic. 2019;20(7):479-90.

64. Gillingham AK, Munro S. Long coiled-coil proteins and membrane traffic. Biochim Biophys Acta. 2003;1641(2-3):71-85.

65. Conibear E, Cleck JN, Stevens TH. Vps51p mediates the association of the GARP (Vps52/53/54) complex with the late Golgi t-SNARE Tlg1p. Mol Biol Cell. 2003;14(4):1610-23.

66. Lurick A, Kummel D, Ungermann C. Multisubunit tethers in membrane fusion. Curr Biol. 2018;28(8):R417-R20.

67. Suvorova ES, Duden R, Lupashin VV. The Sec34/Sec35p complex, a Ypt1p effector required for retrograde intra-Golgi trafficking, interacts with Golgi SNAREs and COPI vesicle coat proteins. J Cell Biol. 2002;157(4):631-43.

68. Boyd C, Hughes T, Pypaert M, Novick P. Vesicles carry most exocyst subunits to exocytic sites marked by the remaining two subunits, Sec3p and Exo70p. J Cell Biol. 2004;167(5):889-901.

69. Andag U, Neumann T, Schmitt HD. The coatomer-interacting protein Dsl1p is required for Golgi-to-endoplasmic reticulum retrieval in yeast. J Biol Chem. 2001;276(42):39150-60.

70. Nickerson DP, Brett CL, Merz AJ. Vps-C complexes: gatekeepers of endolysosomal traffic. Curr Opin Cell Biol. 2009;21(4):543-51.

71. Markgraf DF, Ahnert F, Arlt H, Mari M, Peplowska K, Epp N, et al. The CORVET subunit Vps8 cooperates with the Rab5 homolog Vps21 to induce clustering of late endosomal compartments. Mol Biol Cell. 2009;20(24):5276-89.

72. Perini ED, Schaefer R, Stoter M, Kalaidzidis Y, Zerial M. Mammalian CORVET is required for fusion and conversion of distinct early endosome subpopulations. Traffic. 2014;15(12):1366-89.

73. Ostrowicz CW, Brocker C, Ahnert F, Nordmann M, Lachmann J, Peplowska K, et al. Defined subunit arrangement and rab interactions are required for functionality of the HOPS tethering complex. Traffic. 2010;11(10):1334-46.

74. Zhang J, Lachance V, Schaffner A, Li X, Fedick A, Kaye LE, et al. A Founder Mutation in VPS11 Causes an Autosomal Recessive Leukoencephalopathy Linked to Autophagic Defects. PLoS Genet. 2016;12(4):e1005848.

75. Edvardson S, Gerhard F, Jalas C, Lachmann J, Golan D, Saada A, et al. Hypomyelination and developmental delay associated with VPS11 mutation in Ashkenazi-Jewish patients. J Med Genet. 2015;52(11):749-53.

76. Sofou K, Meier K, Sanderson LE, Kaminski D, Montoliu-Gaya L, Samuelsson E, et al. Bi-allelic VPS16 variants limit HOPS/CORVET levels and cause a mucopolysaccharidosis-like disease. EMBO Mol Med. 2021;13(5):e13376.

77. Yildiz Y, Kosukcu C, Aygun D, Akcaboy M, Oztek Celebi FZ, Tasci Yildiz Y, et al. Homozygous missense VPS16 variant is associated with a novel disease, resembling mucopolysaccharidosis-plus syndrome in two siblings. Clin Genet. 2021;100(3):308-17.

78. Pavlova EV, Shatunov A, Wartosch L, Moskvina AI, Nikolaeva LE, Bright NA, et al. The lysosomal disease caused by mutant VPS33A. Hum Mol Genet. 2019;28(15):2514-30.

79. Balderhaar HJ, Ungermann C. CORVET and HOPS tethering complexes - coordinators of endosome and lysosome fusion. J Cell Sci. 2013;126(Pt 6):1307-16.

80. Simon-Vecsei Z, Soth A, Lorincz P, Rubics A, Talas A, Kulcsar PI, et al. Identification of New Interactions between Endolysosomal Tethering Factors. J Mol Biol. 2021;433(13):166965.

81. Kim BY, Kramer H, Yamamoto A, Kominami E, Kohsaka S, Akazawa C. Molecular characterization of mammalian homologues of class C Vps proteins that interact with syntaxin-7. J Biol Chem. 2001;276(31):29393-402.

82. van der Kant R, Jonker CT, Wijdeven RH, Bakker J, Janssen L, Klumperman J, et al. Characterization of the Mammalian CORVET and HOPS Complexes and Their Modular Restructuring for Endosome Specificity. J Biol Chem. 2015;290(51):30280-90.

83. Guo Z, Johnston W, Kovtun O, Mureev S, Brocker C, Ungermann C, et al. Subunit organisation of in vitro reconstituted HOPS and CORVET multisubunit membrane tethering complexes. PLoS One. 2013;8(12):e81534.

84. Segala G, Bennesch MA, Ghahhari NM, Pandey DP, Echeverria PC, Karch F, et al. Vps11 and Vps18 of Vps-C membrane traffic complexes are E3 ubiquitin ligases and fine-tune signalling. Nat Commun. 2019;10(1):1833.

85. Hunter MR, Scourfield EJ, Emmott E, Graham SC. VPS18 recruits VPS41 to the human HOPS complex via a RING-RING interaction. Biochem J. 2017;474(21):3615-26.

86. Sadler KC, Amsterdam A, Soroka C, Boyer J, Hopkins N. A genetic screen in zebrafish identifies the mutants vps18, nf2 and foie gras as models of liver disease. Development. 2005;132(15):3561-72.

87. Behrmann H, Lurick A, Kuhlee A, Balderhaar HK, Brocker C, Kummel D, et al. Structural identification of the Vps18 beta-propeller reveals a critical role in the HOPS complex stability and function. J Biol Chem. 2014;289(48):33503-12.

88. Poupon V, Stewart A, Gray SR, Piper RC, Luzio JP. The role of mVps18p in clustering, fusion, and intracellular localization of late endocytic organelles. Mol Biol Cell. 2003;14(10):4015-27.

89. van der Beek J, Jonker C, van der Welle R, Liv N, Klumperman J. CORVET, CHEVI and HOPS - multisubunit tethers of the endo-lysosomal system in health and disease. J Cell Sci. 2019;132(10).

90. Rieder SE, Emr SD. A novel RING finger protein complex essential for a late step in protein transport to the yeast vacuole. Mol Biol Cell. 1997;8(11):2307-27.

91. Peterson MR, Emr SD. The class C Vps complex functions at multiple stages of the vacuolar transport pathway. Traffic. 2001;2(7):476-86.

92. Yogosawa S, Hatakeyama S, Nakayama KI, Miyoshi H, Kohsaka S, Akazawa C. Ubiquitylation and degradation of serum-inducible kinase by hVPS18, a RING-H2 type ubiquitin ligase. J Biol Chem. 2005;280(50):41619-27.

93. Yogosawa S, Kawasaki M, Wakatsuki S, Kominami E, Shiba Y, Nakayama K, et al. Monoubiquitylation of GGA3 by hVPS18 regulates its ubiquitin-binding ability. Biochem Biophys Res Commun. 2006;350(1):82-90.

94. Robinson JS, Graham TR, Emr SD. A putative zinc finger protein, Saccharomyces cerevisiae Vps18p, affects late Golgi functions required for vacuolar protein sorting and efficient alpha-factor prohormone maturation. Mol Cell Biol. 1991;11(12):5813-24.

95. Preston RA, Manolson MF, Becherer K, Weidenhammer E, Kirkpatrick D, Wright R, et al. Isolation and characterization of PEP3, a gene required for vacuolar biogenesis in Saccharomyces cerevisiae. Mol Cell Biol. 1991;11(12):5801-12.

96. Lindmo K, Simonsen A, Brech A, Finley K, Rusten TE, Stenmark H. A dual function for Deep orange in programmed autophagy in the Drosophila melanogaster fat body. Exp Cell Res. 2006;312(11):2018-27.

97. Sevrioukov EA, He JP, Moghrabi N, Sunio A, Kramer H. A role for the deep orange and carnation eye color genes in lysosomal delivery in Drosophila. Mol Cell. 1999;4(4):479-86.

98. Chi C, Zhu H, Han M, Zhuang Y, Wu X, Xu T. Disruption of lysosome function promotes tumor growth and metastasis in Drosophila. J Biol Chem. 2010;285(28):21817-23.

99. Maldonado E, Hernandez F, Lozano C, Castro ME, Navarro RE. The zebrafish mutant vps18 as a model for vesicle-traffic related hypopigmentation diseases. Pigment Cell Res. 2006;19(4):315-26.

100. Peng C, Ye J, Yan S, Kong S, Shen Y, Li C, et al. Ablation of vacuole protein sorting 18 (Vps18) gene leads to neurodegeneration and impaired neuronal migration by disrupting multiple vesicle transport pathways to lysosomes. J Biol Chem. 2012;287(39):32861-73.

101. Tucker KA, Lilly MB, Heck L, Jr., Rado TA. Characterization of a new human diploid myeloid leukemia cell line (PLB-985) with granulocytic and monocytic differentiating capacity. Blood. 1987;70(2):372-8.

102. Birnie GD. The HL60 cell line: a model system for studying human myeloid cell differentiation. Br J Cancer Suppl. 1988;9:41-5.

103. Allen LH. Closing the gap between murine neutrophils and neutrophil-like cell lines. J Leukoc Biol. 2023;114(3):199-201.

104. Pivot-Pajot C, Chouinard FC, El Azreq MA, Harbour D, Bourgoin SG. Characterisation of degranulation and phagocytic capacity of a human neutrophilic cellular model, PLB-985 cells. Immunobiology. 2010;215(1):38-52.

105. Wang GG, Calvo KR, Pasillas MP, Sykes DB, Hacker H, Kamps MP. Quantitative production of macrophages or neutrophils ex vivo using conditional Hoxb8. Nat Methods. 2006;3(4):287-93.

106. Knoepfler PS, Sykes DB, Pasillas M, Kamps MP. HoxB8 requires its Pbx-interaction motif to block differentiation of primary myeloid progenitors and of most cell line models of myeloid differentiation. Oncogene. 2001;20(39):5440-8.

107. Wang GG, Calvo KR, Pasillas MP, Sykes DB, Häcker H, Kamps MP. Quantitative production of macrophages or neutrophils ex vivo using conditional Hoxb8. Nat Methods. 2006;3(4):287-93.

108. Shannon JG, Hinnebusch BJ. Characterization and CRISPR/Cas9-mediated genetic manipulation of neutrophils derived from Hoxb8-ER-immortalized myeloid progenitors. J Leukoc Biol. 2023;114(1):42-52.

109. Liebermann DA, Hoffman B. Myeloid progenitors on demand. Nat Methods. 2006;3(4):248-9.

110. Chen CW, Sowden M, Zhao Q, Wiedmer T, Sims PJ. Nuclear phospholipid scramblase 1 prolongs the mitotic expansion of granulocyte precursors during G-CSF-induced granulopoiesis. J Leukoc Biol. 2011;90(2):221-33.

111. Gautam S, Kirschnek S, Gentle IE, Kopiniok C, Henneke P, Hacker H, et al. Survival and differentiation defects contribute to neutropenia in glucose-6-phosphatase-beta (G6PC3) deficiency in a model of mouse neutrophil granulocyte differentiation. Cell Death Differ. 2013;20(8):1068-79.

112. Chu JY, McCormick B, Mazelyte G, Michael M, Vermeren S. HoxB8 neutrophils replicate Fcgamma receptor and integrin-induced neutrophil signaling and functions. J Leukoc Biol. 2019;105(1):93-100.

113. Zehrer A, Pick R, Salvermoser M, Boda A, Miller M, Stark K, et al. A Fundamental Role of Myh9 for Neutrophil Migration in Innate Immunity. J Immunol. 2018;201(6):1748-64.

114. Saul S, Castelbou C, Fickentscher C, Demaurex N. Signaling and functional competency of neutrophils derived from bone-marrow cells expressing the ER-HOXB8 oncoprotein. J Leukoc Biol. 2019;106(5):1101-15.

115. Stojkov D, Amini P, Oberson K, Sokollik C, Duppenthaler A, Simon HU, et al. ROS and glutathionylation balance cytoskeletal dynamics in neutrophil extracellular trap formation. J Cell Biol. 2017;216(12):4073-90.

116. Kirschnek S, Vier J, Gautam S, Frankenberg T, Rangelova S, Eitz-Ferrer P, et al. Molecular analysis of neutrophil spontaneous apoptosis reveals a strong role for the pro-apoptotic BH3-only protein Noxa. Cell Death Differ. 2011;18(11):1805-14.

117. Bromberger T, Klapproth S, Sperandio M, Moser M. Humanized beta2 Integrin-Expressing Hoxb8 Cells Serve as Model to Study Integrin Activation. Cells. 2022;11(9).

118. Zhou Y, Hann J, Schenten V, Plancon S, Bueb JL, Tolle F, et al. Role of S100A8/A9 for Cytokine Secretion, Revealed in Neutrophils Derived from ER-Hoxb8 Progenitors. Int J Mol Sci. 2021;22(16).

119. Gran S, Honold L, Fehler O, Zenker S, Eligehausen S, Kuhlmann MT, et al. Imaging, myeloid precursor immortalization, and genome editing for defining mechanisms of leukocyte recruitment in vivo. Theranostics. 2018;8(9):2407-23.

120. Orosz A, Walzog B, Mocsai A. In Vivo Functions of Mouse Neutrophils Derived from HoxB8-Transduced Conditionally Immortalized Myeloid Progenitors. J Immunol. 2021;206(2):432-45.

121. Hickman DL, Johnson J, Vemulapalli TH, Crisler JR, Shepherd R. Chapter 7 - Commonly Used Animal Models. In: Suckow MA, Stewart KL, editors. Principles of Animal Research for Graduate and Undergraduate Students. Boston: Academic Press; 2017. p. 117-75.

122. Harvie EA, Huttenlocher A. Neutrophils in host defense: new insights from zebrafish. J Leukoc Biol. 2015;98(4):523-37.

123. Hoo JY, Kumari Y, Shaikh MF, Hue SM, Goh BH. Zebrafish: A Versatile Animal Model for Fertility Research. Biomed Res Int. 2016;2016:9732780.

124. Lieschke GJ, Currie PD. Animal models of human disease: zebrafish swim into view. Nat Rev Genet. 2007;8(5):353-67.

125. Howe K, Clark MD, Torroja CF, Torrance J, Berthelot C, Muffato M, et al. The zebrafish reference genome sequence and its relationship to the human genome. Nature. 2013;496(7446):498-503.

126. Hruscha A, Krawitz P, Rechenberg A, Heinrich V, Hecht J, Haass C, et al. Efficient CRISPR/Cas9 genome editing with low off-target effects in zebrafish. Development. 2013;140(24):4982-7.

127. Hruscha A, Schmid B. Generation of zebrafish models by CRISPR /Cas9 genome editing. Methods Mol Biol. 2015;1254:341-50.

128. Lieschke GJ, Trede NS. Fish immunology. Curr Biol. 2009;19(16):R678-82.

129. Renshaw SA, Trede NS. A model 450 million years in the making: zebrafish and vertebrate immunity. Dis Model Mech. 2012;5(1):38-47.

130. Lieschke GJ, Oates AC, Crowhurst MO, Ward AC, Layton JE. Morphologic and functional characterization of granulocytes and macrophages in embryonic and adult zebrafish. Blood. 2001;98(10):3087-96.

131. Colucci-Guyon E, Tinevez JY, Renshaw SA, Herbomel P. Strategies of professional phagocytes in vivo: unlike macrophages, neutrophils engulf only surface-associated microbes. J Cell Sci. 2011;124(Pt 18):3053-9.

132. Palic D, Andreasen CB, Ostojic J, Tell RM, Roth JA. Zebrafish (Danio rerio) whole kidney assays to measure neutrophil extracellular trap release and degranulation of primary granules. J Immunol Methods. 2007;319(1-2):87-97.

133. Davis JM, Clay H, Lewis JL, Ghori N, Herbomel P, Ramakrishnan L. Real-time visualization of mycobacterium-macrophage interactions leading to initiation of granuloma formation in zebrafish embryos. Immunity. 2002;17(6):693-702.

134. Lam SH, Chua HL, Gong Z, Lam TJ, Sin YM. Development and maturation of the immune system in zebrafish, Danio rerio: a gene expression profiling, in situ hybridization and immunological study. Dev Comp Immunol. 2004;28(1):9-28.

135. Miao KZ, Kim GY, Meara GK, Qin X, Feng H. Tipping the Scales With Zebrafish to Understand Adaptive Tumor Immunity. Front Cell Dev Biol. 2021;9:660969.

136. Bertrand JY, Traver D. Hematopoietic cell development in the zebrafish embryo. Curr Opin Hematol. 2009;16(4):243-8.

137. Berman JN, Kanki JP, Look AT. Zebrafish as a model for myelopoiesis during embryogenesis. Exp Hematol. 2005;33(9):997-1006.

138. de Jong JL, Zon LI. Use of the zebrafish system to study primitive and definitive hematopoiesis. Annu Rev Genet. 2005;39:481-501.

139. Le Guyader D, Redd MJ, Colucci-Guyon E, Murayama E, Kissa K, Briolat V, et al. Origins and unconventional behavior of neutrophils in developing zebrafish. Blood. 2008;111(1):132-41.

140. Jagannathan-Bogdan M, Zon LI. Hematopoiesis. Development. 2013;140(12):2463-7.

141. Bertrand JY, Kim AD, Violette EP, Stachura DL, Cisson JL, Traver D. Definitive hematopoiesis initiates through a committed erythromyeloid progenitor in the zebrafish embryo. Development. 2007;134(23):4147-56.

142. Murayama E, Kissa K, Zapata A, Mordelet E, Briolat V, Lin HF, et al. Tracing hematopoietic precursor migration to successive hematopoietic organs during zebrafish development. Immunity. 2006;25(6):963-75.

143. Willett CE, Cortes A, Zuasti A, Zapata AG. Early hematopoiesis and developing lymphoid organs in the zebrafish. Dev Dyn. 1999;214(4):323-36.

144. Bennett CM, Kanki JP, Rhodes J, Liu TX, Paw BH, Kieran MW, et al. Myelopoiesis in the zebrafish, Danio rerio. Blood. 2001;98(3):643-51.

145. Peters-Golden M, Brock TG. 5-lipoxygenase and FLAP. Prostaglandins Leukot Essent Fatty Acids. 2003;69(2-3):99-109.

146. Hall C, Flores MV, Storm T, Crosier K, Crosier P. The zebrafish lysozyme C promoter drives myeloid-specific expression in transgenic fish. BMC Dev Biol. 2007;7:42.

147. Ellett F, Pase L, Hayman JW, Andrianopoulos A, Lieschke GJ. mpeg1 promoter transgenes direct macrophage-lineage expression in zebrafish. Blood. 2011;117(4):e49-56.

148. Mathias JR, Dodd ME, Walters KB, Yoo SK, Ranheim EA, Huttenlocher A. Characterization of zebrafish larval inflammatory macrophages. Dev Comp Immunol. 2009;33(11):1212-7.

149. Meijer AH, van der Sar AM, Cunha C, Lamers GE, Laplante MA, Kikuta H, et al. Identification and real-time imaging of a myc-expressing neutrophil population involved in inflammation and mycobacterial granuloma formation in zebrafish. Dev Comp Immunol. 2008;32(1):36-49.

150. Yang CT, Cambier CJ, Davis JM, Hall CJ, Crosier PS, Ramakrishnan L. Neutrophils exert protection in the early tuberculous granuloma by oxidative killing of mycobacteria phagocytosed from infected macrophages. Cell Host Microbe. 2012;12(3):301-12.

151. Redd MJ, Kelly G, Dunn G, Way M, Martin P. Imaging macrophage chemotaxis in vivo: studies of microtubule function in zebrafish wound inflammation. Cell Motil Cytoskeleton. 2006;63(7):415-22.

152. Bader A, Gao J, Riviere T, Schmid B, Walzog B, Maier-Begandt D. Molecular Insights Into Neutrophil Biology From the Zebrafish Perspective: Lessons From CD18 Deficiency. Front Immunol. 2021;12:677994.

153. Ali S, Champagne DL, Spaink HP, Richardson MK. Zebrafish embryos and larvae: a new generation of disease models and drug screens. Birth Defects Res C Embryo Today. 2011;93(2):115-33.

154. Vilboux T, Lev A, Malicdan MC, Simon AJ, Jarvinen P, Racek T, et al. A congenital neutrophil defect syndrome associated with mutations in VPS45. N Engl J Med. 2013;369(1):54-65.

155. Kolehmainen J, Black GC, Saarinen A, Chandler K, Clayton-Smith J, Traskelin AL, et al. Cohen syndrome is caused by mutations in a novel gene, COH1, encoding a transmembrane protein with a presumed role in vesicle-mediated sorting and intracellular protein transport. Am J Hum Genet. 2003;72(6):1359-69.

156. Bradford YM, Van Slyke CE, Ruzicka L, Singer A, Eagle A, Fashena D, et al. Zebrafish information network, the knowledgebase for Danio rerio research. Genetics. 2022;220(4).

157. Gadbois T, Marcotte H, Rodrigue L, Coulombe C, Goyette N, Lavoie MC. Distribution of the Resident Oral Bacterial Populations in Different Strains of Mice. Microbial Ecology in Health and Disease. 2009;6(5):245-51.

158. Madeira F, Park YM, Lee J, Buso N, Gur T, Madhusoodanan N, et al. The EMBL-EBI search and sequence analysis tools APIs in 2019. Nucleic Acids Res. 2019;47(W1):W636-W41.

159. Stothard P. The sequence manipulation suite: JavaScript programs for analyzing and formatting protein and DNA sequences. Biotechniques. 2000;28(6):1102, 4.

160. Avdesh A, Chen M, Martin-Iverson MT, Mondal A, Ong D, Rainey-Smith S, et al. Regular care and maintenance of a zebrafish (Danio rerio) laboratory: an introduction. J Vis Exp. 2012(69):e4196.

161. Kimmel CB, Ballard WW, Kimmel SR, Ullmann B, Schilling TF. Stages of embryonic development of the zebrafish. Dev Dyn. 1995;203(3):253-310.

162. Westerfield M. A guide for the laboratory use of zebrafish (Danio rerio). The zebrafish book. 2000.

163. Karlsson J, von Hofsten J, Olsson PE. Generating transparent zebrafish: a refined method to improve detection of gene expression during embryonic development. Mar Biotechnol (NY). 2001;3(6):522-7.

164. Gerlach GF, Schrader LN, Wingert RA. Dissection of the adult zebrafish kidney. J Vis Exp. 2011(54).

165. Trede NS, Langenau DM, Traver D, Look AT, Zon LI. The use of zebrafish to understand immunity. Immunity. 2004;20(4):367-79.

166. Schindelin J, Arganda-Carreras I, Frise E, Kaynig V, Longair M, Pietzsch T, et al. Fiji: an open-source platform for biological-image analysis. Nat Methods. 2012;9(7):676-82.

167. Rozman S, Yousefi S, Oberson K, Kaufmann T, Benarafa C, Simon HU. The generation of neutrophils in the bone marrow is controlled by autophagy. Cell Death Differ. 2015;22(3):445-56.

168. Tait SW, Green DR. Mitochondria and cell death: outer membrane permeabilization and beyond. Nat Rev Mol Cell Biol. 2010;11(9):621-32.

169. Donadieu J, Beaupain B, Mahlaoui N, Bellanne-Chantelot C. Epidemiology of congenital neutropenia. Hematol Oncol Clin North Am. 2013;27(1):1-17, vii.

170. Hsieh MM, Everhart JE, Byrd-Holt DD, Tisdale JF, Rodgers GP. Prevalence of neutropenia in the U.S. population: age, sex, smoking status, and ethnic differences. Ann Intern Med. 2007;146(7):486-92.

171. Donadieu J, Fenneteau O, Beaupain B, Mahlaoui N, Chantelot CB. Congenital neutropenia: diagnosis, molecular bases and patient management. Orphanet J Rare Dis. 2011;6:26.

172. Zeidler C, Germeshausen M, Klein C, Welte K. Clinical implications of ELA2-, HAX1-, and G-CSF-receptor (CSF3R) mutations in severe congenital neutropenia. Br J Haematol. 2009;144(4):459-67.

173. Carlsson G, Fasth A, Berglof E, Lagerstedt-Robinson K, Nordenskjold M, Palmblad J, et al. Incidence of severe congenital neutropenia in Sweden and risk of evolution to myelodysplastic syndrome/leukaemia. Br J Haematol. 2012;158(3):363-9.

174. Horwitz M, Benson KF, Person RE, Aprikyan AG, Dale DC. Mutations in ELA2, encoding neutrophil elastase, define a 21-day biological clock in cyclic haematopoiesis. Nat Genet. 1999;23(4):433-6.

175. Bellanne-Chantelot C, Clauin S, Leblanc T, Cassinat B, Rodrigues-Lima F, Beaufils S, et al. Mutations in the ELA2 gene correlate with more severe expression of neutropenia: a study of 81 patients from the French Neutropenia Register. Blood. 2004;103(11):4119-25.

176. Boocock GR, Morrison JA, Popovic M, Richards N, Ellis L, Durie PR, et al. Mutations in SBDS are associated with Shwachman-Diamond syndrome. Nat Genet. 2003;33(1):97-101.

177. Klein C, Grudzien M, Appaswamy G, Germeshausen M, Sandrock I, Schaffer AA, et al. HAX1 deficiency causes autosomal recessive severe congenital neutropenia (Kostmann disease). Nat Genet. 2007;39(1):86-92.

178. Veiga-da-Cunha M, Gerin I, Chen YT, Lee PJ, Leonard JV, Maire I, et al. The putative glucose 6-phosphate translocase gene is mutated in essentially all cases of glycogen storage disease type I non-a. Eur J Hum Genet. 1999;7(6):717-23.

179. Jung J, Bohn G, Allroth A, Boztug K, Brandes G, Sandrock I, et al. Identification of a homozygous deletion in the AP3B1 gene causing Hermansky-Pudlak syndrome, type 2. Blood. 2006;108(1):362-9.

180. Enders A, Zieger B, Schwarz K, Yoshimi A, Speckmann C, Knoepfle EM, et al. Lethal hemophagocytic lymphohistiocytosis in Hermansky-Pudlak syndrome type II. Blood. 2006;108(1):81-7.

181. Introne W, Boissy RE, Gahl WA. Clinical, molecular, and cell biological aspects of Chediak-Higashi syndrome. Mol Genet Metab. 1999;68(2):283-303.

182. Nagle DL, Karim MA, Woolf EA, Holmgren L, Bork P, Misumi DJ, et al. Identification and mutation analysis of the complete gene for Chediak-Higashi syndrome. Nat Genet. 1996;14(3):307-11.

183. Wisner SR, Chlebowski M, Mandal A, Mai D, Stein C, Petralia RS, et al. An initial HOPS-mediated fusion event is critical for autophagosome transport initiation from the axon terminal. Autophagy. 2024:1-22.

184. Klapproth S, Moretti FA, Zeiler M, Ruppert R, Breithaupt U, Mueller S, et al. Minimal amounts of kindlin-3 suffice for basal platelet and leukocyte functions in mice. Blood. 2015;126(24):2592-600.

185. Riffelmacher T, Clarke A, Richter FC, Stranks A, Pandey S, Danielli S, et al. Autophagy-Dependent Generation of Free Fatty Acids Is Critical for Normal Neutrophil Differentiation. Immunity. 2017;47(3):466-80 e5.

186. Rao S, Yao Y, Soares de Brito J, Yao Q, Shen AH, Watkinson RE, et al. Dissecting ELANE neutropenia pathogenicity by human HSC gene editing. Cell Stem Cell. 2021;28(5):833-45 e5.

187. Porter AG, Janicke RU. Emerging roles of caspase-3 in apoptosis. Cell Death Differ. 1999;6(2):99-104.

188. Wang Y, Gao W, Shi X, Ding J, Liu W, He H, et al. Chemotherapy drugs induce pyroptosis through caspase-3 cleavage of a gasdermin. Nature. 2017;547(7661):99-103.

189. Yu P, Zhang X, Liu N, Tang L, Peng C, Chen X. Pyroptosis: mechanisms and diseases. Signal Transduct Target Ther. 2021;6(1):128.

190. Crowley LC, Marfell BJ, Scott AP, Waterhouse NJ. Quantitation of Apoptosis and Necrosis by Annexin V Binding, Propidium Iodide Uptake, and Flow Cytometry. Cold Spring Harb Protoc. 2016;2016(11).

191. Boztug K, Jarvinen PM, Salzer E, Racek T, Monch S, Garncarz W, et al. JAGN1 deficiency causes aberrant myeloid cell homeostasis and congenital neutropenia. Nat Genet. 2014;46(9):1021-7.

192. Massullo P, Druhan LJ, Bunnell BA, Hunter MG, Robinson JM, Marsh CB, et al. Aberrant subcellular targeting of the G185R neutrophil elastase mutant associated with severe congenital neutropenia induces premature apoptosis of differentiating promyelocytes. Blood. 2005;105(9):3397-404.

193. Stepensky P, Saada A, Cowan M, Tabib A, Fischer U, Berkun Y, et al. The Thr224Asn mutation in the VPS45 gene is associated with the congenital neutropenia and primary myelofibrosis of infancy. Blood. 2013;121(25):5078-87.

194. Frey L, Zietara N, Lyszkiewicz M, Marquardt B, Mizoguchi Y, Linder MI, et al. Mammalian VPS45 orchestrates trafficking through the endosomal system. Blood. 2021;137(14):1932-44.

195. de Boer J, Williams A, Skavdis G, Harker N, Coles M, Tolaini M, et al. Transgenic mice with hematopoietic and lymphoid specific expression of Cre. Eur J Immunol. 2003;33(2):314-25.

196. Shimshek DR, Kim J, Hubner MR, Spergel DJ, Buchholz F, Casanova E, et al. Codon-improved Cre recombinase (iCre) expression in the mouse. Genesis. 2002;32(1):19-26.

197. Ogilvy S, Metcalf D, Gibson L, Bath ML, Harris AW, Adams JM. Promoter elements of vav drive transgene expression in vivo throughout the hematopoietic compartment. Blood. 1999;94(6):1855-63.

198. Ogilvy S, Elefanty AG, Visvader J, Bath ML, Harris AW, Adams JM. Transcriptional regulation of vav, a gene expressed throughout the hematopoietic compartment. Blood. 1998;91(2):419-30.

199. Doll L, Aghaallaei N, Dick AM, Welte K, Skokowa J, Bajoghli B. A zebrafish model for HAX1-associated congenital neutropenia. Haematologica. 2021;106(5):1311-20.

200. Chao JR, Parganas E, Boyd K, Hong CY, Opferman JT, Ihle JN. Hax1-mediated processing of HtrA2 by Parl allows survival of lymphocytes and neurons. Nature. 2008;452(7183):98-102.

201. Nanua S, Murakami M, Xia J, Grenda DS, Woloszynek J, Strand M, et al. Activation of the unfolded protein response is associated with impaired granulopoiesis in transgenic mice expressing mutant Elane. Blood. 2011;117(13):3539-47.

202. Grenda DS, Johnson SE, Mayer JR, McLemore ML, Benson KF, Horwitz M, et al. Mice expressing a neutrophil elastase mutation derived from patients with severe congenital neutropenia have normal granulopoiesis. Blood. 2002;100(9):3221-8.

203. Schurch C, Schaefer T, Muller JS, Hanns P, Arnone M, Dumlin A, et al. SRP54 mutations induce congenital neutropenia via dominant-negative effects on XBP1 splicing. Blood. 2021;137(10):1340-52.

204. Dale DC. How I manage children with neutropenia. Br J Haematol. 2017;178(3):351-63.

205. Anderson DC, Schmalsteig FC, Finegold MJ, Hughes BJ, Rothlein R, Miller LJ, et al. The severe and moderate phenotypes of heritable Mac-1, LFA-1 deficiency: their quantitative definition and relation to leukocyte dysfunction and clinical features. J Infect Dis. 1985;152(4):668-89.

206. Renshaw SA, Loynes CA, Trushell DM, Elworthy S, Ingham PW, Whyte MK. A transgenic zebrafish model of neutrophilic inflammation. Blood. 2006;108(13):3976-8.

207. Masgrau-Alsina S, Sperandio M, Rohwedder I. Neutrophil recruitment and intracellular vesicle transport: A short overview. Eur J Clin Invest. 2020;50(6):e13237.

Apendix:

Acknowledgements

First and foremost, I would like to express my deep appreciation to my supervisors, Prof. Dr. Barbara Walzog and Dr. Daniela Maier-Begandt, for giving me the opportunity to work on such an exciting project. Especially, Daniela, for her invaluable guidance, mentorship, and unwavering support throughout my PhD journey. Without her, I cannot have traversed my PhD path and gain numerous knowledge. Moreover, she also helped me become a good researcher and present this thesis in the best possible way. Additionally, I thank her for generating the *vps18* mutant zebrafish lines allowing me to work on this exciting model. Furthermore, I thank Dr. Annette Zehrer for generating and providing the CTRL and *Vps18* mutant Hoxb8 cell lines for the study.

I also extend my appreciation to my TAC committee members, Prof. Dr. Christian Schulz, Prof. Dr. Jörg Renkawitz and Prof. Dr. Markus Sperandio. Their insights and expertise have enriched the quality of my research.

Gratitude is also owed to my research collaborators, Prof. Dr. Christoph Klein and Dr. Monika Linder, for sharing the patient's information. I thank Prof. Dr. Oliver Soehnlein and Mathis Richter on their support on the neutrophil maturation assay. I also thank Dr. Bettina Schmid for her advice regarding the zebrafish experiments and Sabine Schlink for technical assistance and zebrafish care. Furthermore, I would like to thank Dr. Lisa Richter and Pardis Khosravani from BMC Core Facility Flow Cytometry of LMU Munich for their support with flow cytometry analysis. I thank Dr. Steffen Dietzel from BMC Core Facility Bioimaging of LMU Munich for the support with the bright field microscopy.

I really appreciate the financial support from SFB914, TRR332 and China Scholarship Council fellowship. It is a great honor that I was a member of the SFB914 and IRTG914, as I benefited so much from the workshops, lectures, seminars, annual retreats. A special thank you must go to Dr. Verena Kochan who always encouraged and helped me during my PhD life.

Special thanks to my fellow lab mates of Walzog group. Particularly to Dr. Almke Bader for consistently answering my "stupid" questions and helping me to resolving all challenges. I am grateful for having Thibaud Rivière in the laboratory and he was always willing to help me when I had questions. Also, I would like to thank Tanja Weisser for supporting me with my experiments and encouraging me a lot. Moreover, I would like to thank Jennifer Truong and Ulrike Wilhelm-Forster for the technical assistance and Dr.

Ingrid Hepper for the administrative support. Without them, my PhD journey would not have been as joyful.

A special acknowledgment goes to my parents for their unwavering support, unconditional love, and belief in my abilities. Of course, I would also like to thank all my friends for their support during my PhD journey.

Affidavit

Affidavit

Gao, Jincheng

Surname, first name

Street

Zip code, town, country

I hereby declare, that the submitted thesis entitled:

The role of vacuolar protein sorting-associated protein 18 homolog (VPS18) in neutrophil biology

……

is my own work. I have only used the sources indicated and have not made unauthorised use of services of a third party. Where the work of others has been quoted or reproduced, the source is always given.

I further declare that the dissertation presented here has not been submitted in the same or similar form to any other institution for the purpose of obtaining an academic degree.

Chongqing, 27.02.2025
place, date

Jincheng Gao
Signature doctoral candidate

Confirmation of congruency

Confirmation of congruency between printed and electronic version of the doctoral thesis

Gao, Jincheng

Surname, first name

Street

Zip code, town, country

I hereby declare, that the submitted thesis entitled:

The role of vacuolar protein sorting-associated protein 18 homolog (VPS18) in neutrophil biology

……

is congruent with the printed version both in content and format.

Chongqing, 27.02.2025 Jincheng Gao

place, date Signature doctoral candidate

List of publications

Bader A, **Gao J**, Rivière T, Schmid B, Walzog B, Maier-Begandt D. Molecular Insights Into Neutrophil Biology From the Zebrafish Perspective: Lessons From CD18 Deficiency. Front Immunol. 2021 Sep 7;12:677994.